The Vertical City Weather Generator (VCWG v1.1.0)

Response to Reviewers

Moradi et al.

March 6, 2020

Dear Dr. Wolfgang Kurtz

Thank you for processing our manuscript and we appreciate the effort of reviewers in providing detailed feedback toward the improvement of our manuscript. We have addressed all of the comments below in a point by point response letter. We are pleased to inform you that all of their suggestions have been implemented.

In brief, we have replaced the rural model, which originally had too many unjustified constants, with a well-established surface layer model, i.e. the Monin-Obukhov Similarity Theory (MOST). This fundamental change has resulted in improved performance of the VCWG model. We have extended our model evaluation from a one-day comparison with field observation to a two-week comparison with field observations. We are now calculating model hourly BIAS and Root Mean Square Error (RMSE) for all model variables, including potential temperature, wind speed, and specific humidity. We are also calculating the model hourly mean and standard deviation for Urban Heat Island (UHI) over two weeks. We have extended the model exploration to include testing all four sub models of VCWG including the building energy model and the radiation model. Our seasonal exploration is now extended to an entire year.

We hope that you find this version of the manuscript satisfactory and in compliance with the journal's high standards. Please do not hesitate to inquire any further information. We will be happy to include any further suggestions toward the improvement of the manuscript.

Regards,

Amir A. Aliabadi

On behalf of all co-authors

1 Reviewer 1

General: The paper introduces a computational platform for the simulation of urban microclimate that is composed of four sub-models (all together named VCWG). The introduced model is a vertical diffusion urban microclimate model that communicates with and receives its boundary conditions from a rural model, a building energy model, and a radiation model. While the idea of generating a computationally efficient model that considers the effect of the main microclimate contributors (buildings, trees, etc.) is useful for practical applications, the model fails (fundamentally) in representing the true physics. The level of simplification in the modeling assumptions, together with the use of too many 'unjustified' parameterization is overwhelming. Major revision in modeling is required before making it open to the public. I'll try to mention some of the major issues:

Response: We thank the reviewer, and we agree that parameterizations and the physics can be represented in a more justified manner, without overwhelming use of 'unjustified' or 'oversimplified' parameterizations. We have benefited from the reviewer comments to examine our choices of formulations for physical processes. Where possible we have considered and examined alternative established models or reduced the number of fitted parameters needed. Nevertheless, it is the nature of the model to use simplifying assumptions and fitted parameters because the model considers numerous physical processes.

1.1 Comments

1. In the rural model, the authors mention that a mixing length based on Obukhov length may fail in some condition, but what is the justification for the use of eq 3?

Response: Thank you. We have now reformulated the rural model entirely based on the Monin-Obukhov Similarity Theory (MOST). The specific models used are [Businger et al., 1971] and [Dyer, 1974]. Here the stability parameter is defined as $\zeta = z/L$, where z is height above ground and L is the Obukhov length. The rural model takes surface sensible heat flux from the energy balance equations at the surface, aerodynamic roughness length scale z_0, wind speed at 10 m, and temperature at 2 m as input variables. It subsequently calculates friction velocity u_* and the vertical profile of the potential temperature according to the MOST formulation. It subsequently forces the top potential temperature on the urban model as fixed boundary condition. It also parameterizes the horizontal pressure gradient in the urban model as a function of friction velocity. Please see section 2.1.2 of the revised manuscript for the complete explanation of using MOST.

2. In the mixing length equation (eq. 3), how Ccrur, which is a scaling correction factor, is optimized? It is mentioned that it is 'optimized' to 1 during unstable conditions and 1.5 during stable conditions (line 31, page 8). Why and how C* is optimized to 1?

Response: Thank you. This equation is now entirely removed from the new rural model parameterization.

3. Looking into Aliabadi et al. 2019, it does not seem that the condition for eq. 4 is relevant for the rural model in this work. If it does, it is not mentioned/justified by the authors. In addition, it is not clear how this equation is found from Aliabadi et al. 2019.

Response: Thank you. This equation is now entirely removed from the new rural model parameterization.

4. What is the reference for equation 10? Why does it need a scaling factor and why is it fixed to a value of 10? Based on which reasoning this equation is also scaled with Hbl=2000m?

Response: Thank you. The scaling factor and the associated equation is now entirely removed from the new rural model parameterization.

5. What is the reference for the convective heat transfer equation (eq. 7)? What are the assumptions behind this model? How is it found, and for which condition it is valid?

Response: This equation is extracted from [Palyvos, 2008], which was determined from wind tunnel measurements for parallel flow condition. It has been used for the same purpose in a previous study [Bueno et al., 2012] which introduces the Urban Weather Generator (UWG) model. UWG is the predecessor model used and integrated into VCWG. We acknowledge that this formulation does not consider aerodynamic roughness length and the thermal stability condition. The authors are not aware of a better formulation for the convective heat transfer coefficient considering these effects.

6. The same questions (regarding the justification, validity, references in the literature) is also valid for the parametrization/equations of the pressure gradient and density equations.

Response: Thank you. This equation has been used extensively to force the momentum equation in the urban vertical diffusion model [Krayenhoff et al., 2015, Nazarian et al., 2019]. We can derive this equation below. We can apply the law of the wall for the Navier-Stokes momentum equation based on the following assumptions [Bredberg, 2000]:

- One dimensional flow with variation only in the vertical direction
- Fully-developed flow with zero gradients in the streamwise direction, apart from a pressure gradient
- Negligible convection

So, streamwise and vertical momentum equations are reduced to

$$0 = -\frac{\partial P}{\partial x} + \frac{d}{dz}\left(\mu\frac{dU}{dz} - \rho\overline{u'w'}\right) \tag{S.1}$$

$$0 = -\frac{\partial P}{\partial z} - \frac{d}{dz}(\rho\overline{w'w'}). \tag{S.2}$$

Eq. S.2 can be integrated to determine pressure $P(x,z) = -\rho\overline{w'w'} + P_{wall}(x)$. Inserting the latter into eq. S.1 and assuming that $\partial\rho\overline{w'w'}/\partial x = 0$, then the integration yields

$$0 = -\frac{dP_{wall}}{dx}z + \mu\frac{dU}{dz} - \rho\overline{u'w'} - \tau_{wall}. \tag{S.3}$$

At $z = H_{top}$, where H_{top} is the height of the top of the domain, the shear stress, $\rho\overline{u'w'}$, and the

velocity gradient $\partial U/\partial z$, are zero and the pressure gradient can be determined as

$$\frac{dP_{wall}}{dx} = -\frac{1}{H_{top}}\tau_{wall}, \tag{S.4}$$

where τ_{wall} is shear stress at the wall. Meanwhile, shear stress at a distance away from the wall within the logarithmic layer, is ρu_*^2, while this value approximates shear stress at the wall [Aliabadi, 2018]. Finally, the absolute pressure gradient can be determined as:

$$\frac{dP_{wall}}{dx} = -\frac{\rho u_*^2}{H_{top}}. \tag{S.5}$$

7. Equations 1 to 9 that are used in rural model contain too many random/unjustified scaling parameters that are just simply mentioned as optimized parameters. This allows the existence of too many free knobs that can be fixed/switched freely to fit the results to desired ones.

Response: Thank you. The entire rural model is now formulated based on well-established Monin-Obukhov Similarity Theory (MOST), which eliminates the need for use of too many unjustified free parameters.

8. A detailed uncertainty quantification analysis for all parameters used in the model is required to show the robustness of the model and to avoid over-fitting.

Response: Thank you. The number of unjustified parameters and scaling factors are now reduced by replacing the diffusion model in the rural area with MOST. The critical bulk Richardson number is set to be 0.25, which is widely recommended by other studies [Louis, 1979, Jeričević and Grisogono, 2006]. As mentioned in Sec. 2.1.3., the diffusion coefficient and the corresponding parameters are based on [Krayenhoff, 2014] and [Nazarian et al., 2019].

9. The whole rural model (that is based on several models, which are not physically justified) can be replaced by simple day and nighttime potential temperature profiles that are widely exist in the literature (even text books, e.g. Stull's book) based on several field studies. Even an assumption of constant profile in the mixed and SBL is a more reliable approach.

Response: Thank you. The entire rural model is now formulated based on well-established Monin-Obukhov Similarity Theory (MOST), which eliminates the need for use of too many unjustified free parameters.

10. Equations 10 and 11 (and rest of the equations in section 2.1.2) provided for the urban vertical diffusion model are based on the assumption of horizontal homogeneity together with a zero mean vertical velocity. Both these assumptions are strongly non-valid inside an urban area that makes the use of these equations, which are inappropriate and wrong. Santiago and Martilli (2010) are referenced for the use of these equations. However, this reference uses this formulation for a mesoscale model over an urban area. Horizontal homogeneity and zero mean vertical velocity could be valid for a mesoscale model, but there is no way to justify these assumptions for an urban area.

Response: Thank you. We updated the reference list. The assumption here is not horizontal homogeneity, because recent vertical diffusion models developed for urban climate simulations

account for and parameterize dispersive terms, which are determined from Reynolds-Averaged Navier Stokes (RANS) or Large Eddy Simulations (LES) of turbulent flows. In fact, dispersive terms account for horizontal and vertical exchanges arising from non-horizontal homogeneity [Santiago and Martilli, 2010, Krayenhoff, 2014, Krayenhoff et al., 2015, Simón-Moral et al., 2017, Nazarian et al., 2019, Krayenhoff et al., 2020].

11. Based on what I mentioned above, the validation study in Sect. 3 is not reliable. However, for future references, a complete validation study is desired for all aspects of the model. The model is composed of four sub-models that their combined performance should be tested (especially when they have a feedback interaction with each other). The validation study does not provide any information regarding the building energy and radiation models.

Response: Thank you. We agree with the reviewer. We have extended the model 'evaluation' and 'exploration' analyses to consider all four sub-models. In addition, where possible, we perform evaluation over a longer period of time (i.e. two weeks or an entire year).

For evaluation, we test aspects of the model for which we have observation data. For the entire VCWG model we provide statistical measures of model performance. Specifically, we provide the hourly BIAS and Root Mean Squre Error (RMSE) statistics for model-predicted potential temperature, wind speed, and specific humidity against observations calculated for running the model for two weeks. In addition, we calculate the hourly mean and standard deviation for prediction of UHI, and we compare this prediction with observations of UHI.

For exploration, we test other aspects of the model separately. For the urban vertical diffusion model, we run VCWG for two weeks in Vancouver, Canada, while investigating the effects of changing plan area density, frontal area density, and leaf area density on vertical profiles of potential temperature and horizontal wind speed. Please see sections 3.2.1 and 3.2.2 in the revised manuscript.

For the building energy model, we run VCWG for two weeks in Vancouver, Canada, to study the effects of building type, cooling system Coefficient Of Performance (COP), and heating system thermal efficiency η_{heat} on cooling/heating waste heat, dehumidification waste heat, gas combustion waste heat, water heating waste heat, and UHI. Figures S.1 and S.2 provide the time series of waste heat fluxes and UHI associated with running VCWG under the above building energy configurations. As far as building type is concerned, it is noted that a school substantially increases the waste heat fluxes and UHI compared to a small office. As far as building COP and η_{heat} are concerned, it is noted that low-energy-efficient buildings increase the waste heat fluxes and UHI compared to energy-efficient buildings. In section 3.2.3 of the revised manuscript we provide hourly mean and standard deviation of the waste heat fluxes and UHI calculated for running the model for two weeks along with a detailed discussion of this investigation.

For radiation model, we run VCWG for two weeks in Vancouver, Canada, to study the effects of canyon aspect ratio and street canyon axis angle (with respect to the north axis) on direct solar radiation flux, diffusive solar radiation flux, and net longwave and shortwave radiation fluxes. Please see section 3.2.4 in the revised manuscript.

For the entire model, we test its performance in different seasons and different climate zones.

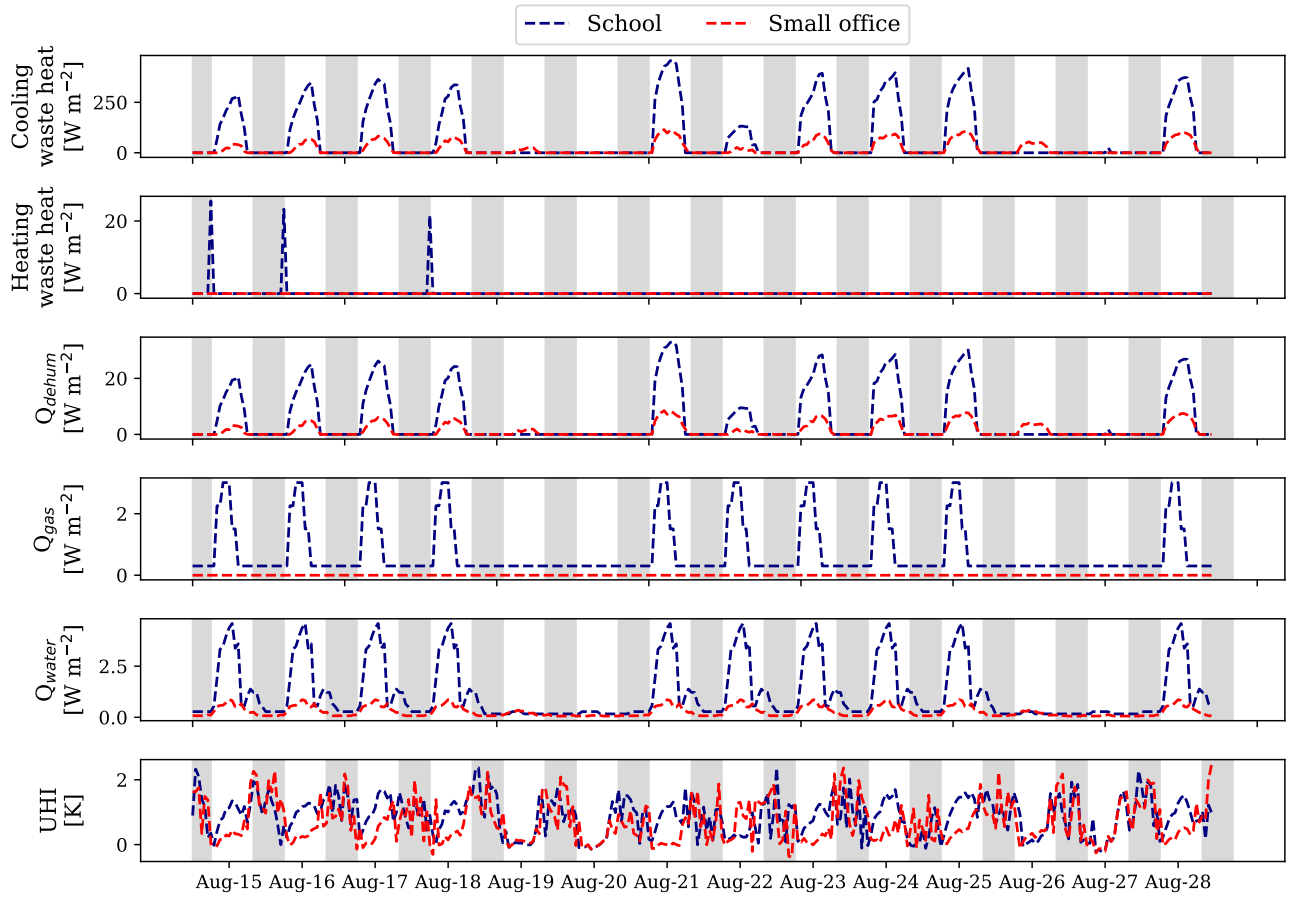

Figure S.1: Effect of building type on cooling/heating waste heat, dehumidification waste heat, gas combustion waste heat, water heating waste heat, and UHI; heat flux units specified per building footprint area.

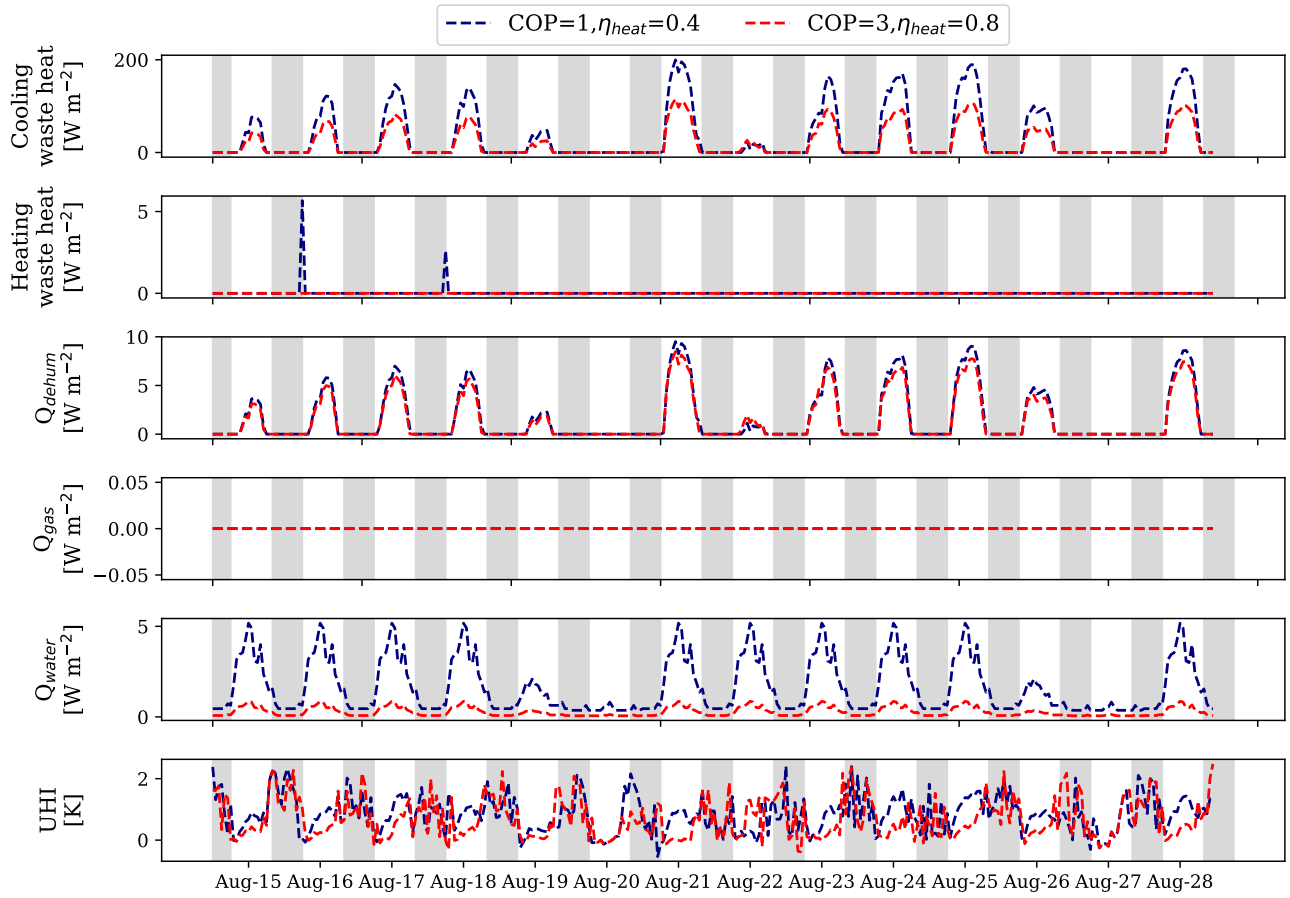

Figure S.2: Effect of building cooling system Coefficient Of Performance (COP) and heating system thermal efficiency (η_{heat}) on cooling/heating waste heat, dehumidification waste heat, gas combustion waste heat, water heating waste heat, and UHI; heat flux units specified per building footprint area.

Section 3.2.5 in the revised manuscript shows the VCWG results for the daily and seasonal variation of the UHI in Vancouver, Canada. We also run VCWG for different cities with different climate zones including Buenos Aires, Phoenix, Vancouver, Osaka, and Copenhagen. Please see section 3.2.6 in the revised manuscript.

12. I noticed that the contribution of two of the authors is described as 'have improved the one-dimensional vertical diffusion model for the urban climate based on large-eddy simulations'. Based on the scope of the work, it is not clear how this improvement is done.

Response: Thank you. We specified the contribution of these two authors in the author contribution section as

NN and ESK provided their code for the one-dimensional vertical diffusion model for the urban climate that were integrated into VCWG.

2 Reviewer 2

The objective of this work, i.e. creating a detailed urban canopy model as an extension to simpler models (Bueno et al. model) is worthwile. The advantage of the proposed approach is that it can be used in standalone mode, not requiring a host mesoscale model, and thus constituting a very computationally efficient way of simulating urban climate. However, I have several objections to the manuscript:

Response: We thank the reviewer for the constructive comments. All reviewer comments have been incorporated and addressed.

2.1 Comments

1. The approach makes very strong assumptions (e.g. regarding the establishment of the vertical profiles); while sometimes this could work I am not convinced it does in this case, as I am not convinced by the validation results.

Response: Thank you. We have improved the model given these comments. The rural model is now parameterized based on well-established Monin-Obukhov Similarity Theory (MOST) [Businger et al., 197 Dyer, 1974] to provide the vertical profile of potential temperature and friction velocity (at 10 m elevation) to force the urban model. The urban vertical diffusion model is obtained from [Santiago and Martilli, 2010, Krayenhoff, 2014, Krayenhoff et al., 2015, Simón-Moral et al., 2017, Krayenhoff et al., 2020]. It is also updated with the most recent refinements proposed by [Nazarian et al., 2019 In this study, the urban vertical diffusion model is also rigorously tested using a two-week observation field campaign where the model performance is assessed by consideration of BIAS and RMSE error statistics for potential temperature, wind speed, and specific humidity as well as mean and standard deviation of UHI. In addition, the model is tested further under exploration mode to assess its sub-model performance. We hope that the new approach taken provides convincing results demonstrating that the model is fit for purpose.

2. the manuscript contains dubious parameterizations (see detailed comments below). the manuscript

contains odd data (e.g. extremely high saturation vapour pressure in Fig 5)

Response: Thank you. We fixed the very high saturation vapour pressure. As mentioned earlier, new well-established parameterizations are considered. Most notably we are now using the MOST formulation for the rural model. In the rural model, it is assumed that the specific humidity is constant in the vertical direction. This assumption is valid so long as the water vapour pressure is less than the saturation water vapour pressure for a given altitude. This condition must be checked to confirm the adequacy of this assumption. The specific humidity can be calculated from the ratio of water vapour density to the air density, which can be simplified using ideal gas law $Q = 0.622 P_v / P_a$, where P_v is water vapor pressure and P_a is the air pressure. We can calculate the saturation pressure (P_{sat}) using the Clausius-Clapeyron equation

$$P_{sat} = 0.61094 \exp\left(\frac{17.625 T_{rur}}{T_{rur} + 243.04}\right). \tag{S.6}$$

where P_{sat} is in kPa. A density profile is required to convert the real temperature profile in the rural area (T_{rur}) to potential temperature profile and vice versa. Using a reference density (ρ_0), reference temperature (T_0), and reference pressure (P_0) at the surface level from the weather station at 2 m elevation, and considering a lapse rate of -0.000133 kg m^{-3} m^{-1} for density within the surface layer, the density profile can be simplistically parameterized by

$$\rho = \rho_0 - 0.000133(z - z_0). \tag{S.7}$$

Fig. S.3 shows the time series of P_{sat} and P_v on the top of the domain for two weeks run in the rural area. Vapour pressure is always less than saturation pressure. So, Assuming constant specific humidity up to the height of five times of average building height in the rural area does not violate the requirement for constancy of the water vapour pressure with height

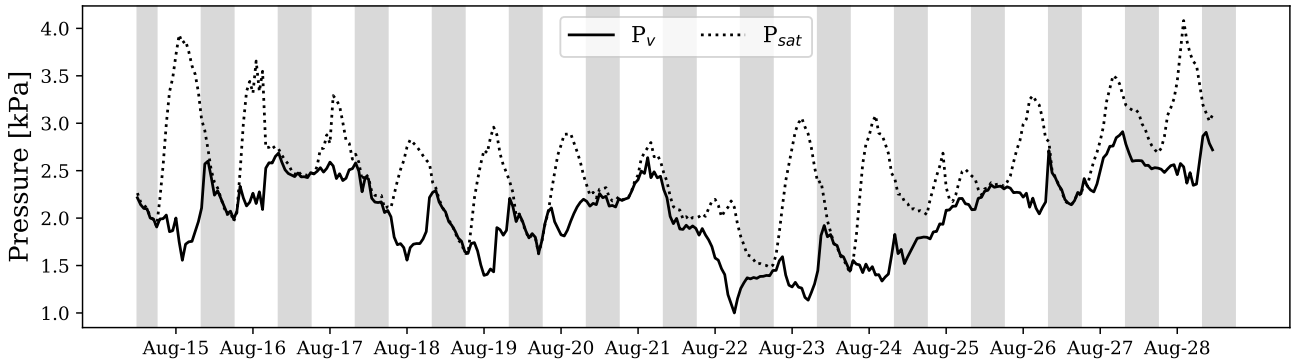

Figure S.3: variation of water vapour pressure and saturation vapour pressure on the top of the domain for the rural model

3. I noticed odd model behaviour (city cooler than rural area during the night in Fig 7)

Response: Thank you. By visiting the individual formulations in the model. We can now reproduce the well-known diurnal variation of Urban Heat Island (UHI) in figure 15 of the revised manuscript in section 3.2.6.

4. Too often clarity leaves to be desired; at several instances I couldn't figure out the meaning of a sentence, even after multiple readings. (examples in the detailed comments below). A less important remark is perhaps that the authors do not refer to work by Erell and Williamson (2006), who were perhaps the first to implement the approach of the present manuscript, i.e. forcing an urban canopy model with rural data. (see https://rmets.onlinelibrary.wiley.com/doi/abs/10.1002/joc.1469)

Response: Thank you. We have checked and improved the clarity and meaning of sentences throughout. The work by [Erell and Williamson, 2006] has been cited as follows in section 1.1

Another bulk flow (single-layer) model is Canyon Air Temperature (CAT) model, which utilizes standard data from a meteorological station to estimate air temperature in a street canyon [Erell and Williamson, 2006].

2.2 Detailed comments

5. Introduction, p2 l10: (C. S. B. Grimmond, 2009) => (Grimmond, 2009)

Response: Thank you. We have fixed it.

6. p2 l31: "paucity of microscale models" - what about the widely used ENVI-met model?

Response: Thank you. We have now reviewed high fidelity models based on Computational Fluid Dynamics (CFD) with high spatiotemporal flow resolution in more detail and provided some examples. ENVI-met is included in this review. Section 1.1 is now revised as follows:

Some example Computational Fluid Dynamics (CFD) models of this kind include Open-source Field Operation And Manipulation (OpenFOAM) [Aliabadi et al., 2017, Aliabadi et al., 2018], Parallelized Large-Eddy Simulation Model (PALM) [Maronga et al., 2015, Resler et al., 2017], and ENVI-met [Crank et al., 2018].

7. p3 l25: Trees have a similar albedo than the urban surface, so have little potential for reducing the overall albedo. The authors should revise their statement on this or else demonstrate its validity.

Response: Thank you. We have revised the statement in section 1 as follows

Urban trees can potentially provide shade and shelter, and, therefore, change the energy balance of the individual buildings as well as the entire city [Akbari et al., 2001].

8. p.4: The authors state that urban canopy models (UCMs) "are not coupled to the surrounding rural area". This is only partially correct, since UCMs generally are part of a mesoscale model and therefore are connected to the rural areas surrounding a city.

Response: Thank you. We have made more clarifications. In our approach VCWG is forced with meteorological variables *measured* near the surface outside a city without the need to use forcing variables from a mesoscale model. We made the following revisions in the manuscript under section 1.1.

More recently TUF-3D was coupled to an Indoor-Outdoor Building Energy Simulator (TUF-3D-IOBES), but still this model adopted a bulk flow (single-layer) parameterization [Yaghoobian and Kleissl, 2012

More recently, the BEP model has been coupled to a Building Energy Model (BEP+BEM) but it is forced with meteorological variables from higher altitudes above a city using mesoscale models, instead of near surface meteorological variables measured outside the city (rural areas).

An overview of the literature reveals an apparent paucity of an independent urban microclimate model that accounts for some spatiotemporal variation of meteorological parameters in the urban environment and considers the effects of trees, building energy, radiation, and the connection to the near-surface rural meteorological conditions measured outside a city, without the need for mesoscale modeling, computationally efficiently and is operationally simple for practical applications.

9. p.4 l28: Change 'the direction that turbulent...' to 'the direction in which turbulent...'

Response: Thank you. We have corrected it.

10. General comment: the Introduction is (too) long; at the same time there are many references to rather old papers. The authors should consider reducing the length of the Introduction, preferably in those paragraphs that refer to the older papers.

Response: Thank you. We have removed the general-knowledge information from the introduction with the associated references. Instead, we have focused on the review of the literature that pertains to urban climate modelling, which is the main focus of this study. We have also reduced the length of the objective section by moving material to the methodology section. Overall, the introduction section is now one page shorter.

11. p6 l27: what is 'horizontal infrared radiation intensity' (I am puzzled by the 'horizontal' is this about radiation on a horizontal surface?)

Response: Thank you. We removed the variables from the EPW file that were not used by VCWG. Section 2.1.2 now has the following statement.

The Rural Model (RM) takes latitude, longitude, dry bulb temperature, relative humidity, dew point temperature, and pressure at 2 m elevation, wind speed and direction at 10 m elevation, down-welling direct radiation, and down-welling diffuse radiation from an Energy Plus Weather (EPW) file.

12. p6 l28: same question for 'diffuse horizontal radiation' is this perhaps radiation falling onto a horizontal plane?)

Response: Thank you. Please see our response to the previous comment.

13. p6 l28: the Energy Plus Weather file is introduced a bit haphazardly, with just an Internet link as reference (while the data taken from it are crucially important for the method). I, for one, have no clue really what these data are, how good they are, what precisely is contained (hourly?, which location exactly?, ...). Why not employ, for instance, hourly ERA5 data from ECMWF?

Or, for that matter, why not directly take vertical profiles from ERA5 or a similar data source?

Response: Thank you. We agree that in addition to rural data from EPW, the VCWG model can also be forced with weather or even climate models. This can be achieved by forcing the model with near-surface rural meteorological variables, or by forcing the model on top of the surface layer over an urban area. However, EPW files are easy to work with and accessible to a more general user, while ECMWF data products are not convenient, requiring advanced knowledge in meteorology. Nevertheless, the use of ECMWF data products can be made optional to the user in future versions of VCWG. We have added a description of the EPW dataset in section 2.1.1 as follows

Building energy and solar radiation simulations are typically carried out with standardized weather files. Energy Plus Weather (EPW) files include recent weather data for 2100 locations and are saved in the standard EnrgyPlus format, developed by US department of energy.[1] The data is available for most North American cities, European cities, and other regions around the World. The weather data are arranged by World Meteorological Organization (WMO) based on region and country. An EPW file contains typical hourly-based data of meteorological variables. The meteorological variables are dry bulb temperature, dew point temperature, relative humidity, incoming direct and diffusive solar radiation fluxes from sky, wind direction, wind speed, sky condition, precipitation, and general information about field logistics and soil properties. Precipitation data is often missing in the EPW files, which affects calculation of latent heat in the rural area.

14. p6 l30: how is the horizontal pressure gradient calculated from (I presume) a single pressure observation?

Response: Thank you. The derivation for the calculation of the horizontal pressure gradient is given in the response to reviewer 1 comment 6. This methodology uses the 'law of the wall concept' and 'scaling' of the momentum transport equation to reduce the Navier-Stokes equation to obtain the horizontal pressure gradient as a function of friction velocity and height of the top of the domain.

15. p7 l31: authors refer to Fig.4, but that is still several pages away. Please move this Figure closer to where it is referred to first.

Response: Thank you. We have moved the figure to section 2.1.

16. p8 l2: 'The atmospheric variation...': I am puzzled by the use of 'atmospheric'; do the authors perhaps mean to say 'the vertical variation...'?

Response: Thank you. The whole rural model has been revised.

17. p8 l7: why repeat the Internet link to the EPW? (appears on p.6 already)

Response: Thank you. We now avoid repeating the link.

18. p8 l25: 'In this study, the thermal stability condition is roughly approximated based on the

[1] https://energyplus.net/weather

available incoming solar radiation in the way that presence or absence of incoming solar radiation on the surface indicate unstable and stable conditions, respectively.' I have no clue what this is supposed to mean concretely. I do understand that surface solar radiation affects stability, but from reading this sentence I cannot imagine how this is done concretely in the model.

Response: Thank you. Please see our response to reviewer 1 comment 1. In the revised manuscript, we formulate the rural model using the Monin-Obukhov Similarity Theory (MOST). In this approach the thermal stability is given using the stability parameter $\zeta = z/L$, where z is height above the ground (10 m), and L is Obukhov length, which is a function of friction velocity and sensible heat flux at 10 m. Sensible heat flux at 10 m is calculated using energy balance near the surface.

19. p9 eq4: the parameterization for u_* appears very (too) simple: no effect of surface roughness, no effect of atmospheric stability. I am sure that this expression works well for Guelph, Canada, but how well does this work elsewhere?

Response: Thank you. Please see our response to reviewer 1 comment 1. Now we are using MOST which fully accounts for surface aerodynamics roughness lengthscale z_0 and thermal stability $\zeta = z/L$.

20. p9 l6: 'When the surface is warmer than air, upward heat flux released into the atmosphere creates a thermally unstable condition.' Expressions like this are too obvious and belong rather to text books than scientific papers. As a general comment: the authors could considerably shorten their paper by removing statements like this one, which do not really contribute to the paper.

Response: Thank you. We have removed generic and textbook-type statements.

21. p9 l13: 'sensible heat flux from biogenic activity of vegetation'. What is this? I am puzzled by 'biogenic', which I know in the context of e.g. emissions of - biogenic - chemical compounds, but not when related to the sensible heat flux. Is this sensible energy released because of chemical activity associated with biogenic emissions? I suppose not, but that is what it looks like...

Response: Thank you. It has been observed that energy balance of vegetation is crucial for the development of accurate weather forecasting [Ciccioli et al., 1997]. Chemical and physiological processes inside plants can alter vegetation temperature and consequently the global energy circulation of soil–vegetation–atmosphere [van der Kooi et al., 2019].

22. p9 eq7: cfr my remark on eq4: the parameterization of the transfer coeffient for the calculation of sensible heat flux appears too simple, not accounting for stability, roughness, ...

Response: Thank You. Please see our response to reviewer 1 comment 5. We acknowledge this limitation of our model. At the moment, the authors are not aware of a better formulation for the convective heat transfer coefficient considering effects of stability and surface roughness.

23. p9 l23: 'The rural model also outputs a horizontal pressure gradient based on friction velocity calculation...'. Justify this.

Response: Thank you. This approach has been used extensively to force the momentum equa-

tion in the urban vertical diffusion model [Krayenhoff et al., 2015, Nazarian et al., 2019], which can be determined by applying the law of the wall for the Navier-Stokes momentum equation [Bredberg, 2000]. For more details, please see our responses to reviewer 1 comment 6 and reviewer 2 comment 19.

24. p9 l25: what is the basis for the parameterisation for the pressure gradient (rho u*ˆ2 / Havg)? Please add a reference to justify this.

Response: Thank you. Please see our response to reviewer 1 comment 6 and reviewer 2 comments 19 and 23.

25. p9 l25: what is Havg? Later in the manuscript Havg represents average building height... (does the horizontal pressure gradient depend on the building height??)

Response: Thank you. As explained in our response to reviewer 1 comment 6, that height is the height of the top of the domain, which is now replaced with H_{top} for clarity.

26. p9 l27: the specific humidity does not vary with height in the model. This is a heavy assumption, but I can imagine that with only surface data there is no way to actually do otherwise. But the authors justify this by saying 'This assumption is valid so long as the water vapour pressure is less than the saturation water vapour pressure for a given altitude.' I disagree, as you can very well have a vertically variable profile of specific humidity even when 'the water vapour pressure is less than the saturation water vapour pressure'.

Response: Thank you. We agree, and we removed the statement. Ideally, one may use the Monin-Obukhov Similarity Theory (MOST) to infer vertical variation of specific humidity in the surface layer if latent heat near the surface is available. However, latent heat is not an input to the model and it is not available in the EPW dataset. So our assumption to not consider variation of specific humidity with height is made for lack of a better assumption. Section 2.1.2 now contains the following statement.

This assumption is made, for lack of a better assumption, because with only surface data and lack of latent heat flux, it is not practical to calculate variation of specific humidity with height in the surface layer.

27. p11 eq15: how is waste heat (QHVAC) estimated?

Response: Thank you. Waste heat is calculated differently under cooling and heating modes. Under cooling mode it is calculated by adding the cooling demand (Q_{cool}), consisting of surface cooling demand, ventilation demand, infiltration (or exfiltration) demand, and internal energy demand (lighting, equipment, and occupants), energy consumption of the cooling system (W_{cool}), dehumidification demand (Q_{dehum}), energy consumption by gas combustion (e.g. cooking) (Q_{gas}), and energy consumption for water heating (Q_{water}).

$$Q_{HVAC} = \underbrace{\underbrace{Q_{surf} + Q_{ven} + Q_{inf} + Q_{int}}_{Q_{cool}} + W_{cool}}_{\text{Cooling waste heat}} + Q_{dehum} + Q_{gas} + Q_{water} \quad \text{(S.8)}$$

Under heating mode, total waste heat is calculated by adding the heating waste heat (Q_{heat}), consisting of surface heating demand, ventilation demand, infiltration (or exfiltration) demand, and internal energy demand (lighting, equipment, and occupants) (accounting for thermal efficiency of the heating system (η_{heat})), dehumidification demand (Q_{dehum}), energy consumption by gas combustion (e.g. cooking) (Q_{gas}), and energy consumption for water heating (Q_{water}).

$$Q_{HVAC} = \underbrace{\underbrace{(Q_{surf} + Q_{ven} + Q_{inf} + Q_{int})}_{Q_{heat}}/\eta_{heat}}_{\text{Heating waste heat}} + Q_{dehum} + Q_{gas} + Q_{water} \quad \text{(S.9)}$$

Detailed mathematical definitions for each term are provided in the manuscript and in [Bueno Unzeta, 2010] detailed.

28. Fig.4: upper right quadrant: correct 'Hdomian' (suppose this should be Hdomain instead)

Response: Thank you. To be consistent with the revised manuscript, we have replaced H_{domain} with H_{top}.

29. p15 l12: same remark as above regarding this parameterization of the pressure gradient

Response: Thank you. Please see our response to reviewer 1 comment 6.

30. p16 l6: the authors (again) state that specific humidity can well be constant with height; in a situation with a non-zero surface latent heat flux this assumption will certainly not be correct.

Response: Thank you. We agree and acknowledge this as a limitation of our assumption. Please see our response to reviewer 2 comment 26.

31. p17 Fig5: is it possible that the saturation vapour pressure (blue curve) is hugely overestimated? see eg https://en.wikipedia.org/wiki/Vapour-pressure-of-water for some values: at 25 °C the saturation vapour pressure is approx 3.17 kPa, while Fig5 shows values around 20 kPa (which would imply temperatures of 60 °C). Is it possible that the authors have made a conversion error between different units (mbar vs hPa / mbar vs kPa / ...)?

Response: Thank you. We have checked the equation for saturation pressure and there was a unit conversion mistake. Please see our response to reviewer 2 comment 2. As shown in Fig. S.3, at all hours and all altitudes (considered at the top of the domain) the vapor pressure is below saturation pressure.

32. p20 Fig7: the caption should say which line corresponds to the model and which the observations. I can of course guess which line is either of these, but still it should be included.

Response: Thank you. We have replaced that figure with Fig. 5 in the revised manuscript, which shows the evaluation of temperature at three specific heights, where field measurements are available.

33. p20 Fig7: I am not convinced at all that the graphs confirm a good model performance. The simulated profile (I assume the solid black line corresponds to model results - see remark above) deviates substantially from the observed one. Also, the observations (dash/dot line) almost appear not to change throughout the day, while the simulation result does vary between stable/unstable atmospheric profiles.

Response: Thank you. Please see our response to reviewer 1 comment 11. We have extended the model 'evaluation' and 'exploration' analyses to consider all four sub-models: rural model, urban vertical diffusion model, radiation model, and building energy model. In addition, where possible, we perform evaluation over a longer period of time (e.g. two weeks). In the new comparison, we plot diurnal variation of BIAS and RMSE, as measured over two weeks in Guelph, for wind speed, temperature, and specific humidity. Please see figures 5 and 6 in the new version of the manuscript. For wind speed and temperature, the error statistics are reported at three heights. Any differences in the model performance under thermally stable versus thermally unstable conditions would be apparent in these plots. For instance we can see that the BIAS for predicting the potential temperature is higher at night (thermally stable condition), while the BIAS for predicting wind speed is higher during the day (thermally unstable condition). Overall, the model produces a realistic diurnal and seasonal pattern for UHI as is evidenced in figures 14 and 15 of the revised manuscript.

34. p20 Fig7: in the lower graph: the urban temperature goes below the rural value between (say) 0200 LST and 1000 LST. This is counter to anything I have seen in model results and observations. Surprisingly, in the the late afternoon / early night this is reversed (urban temperature > rural value). Could this issue be related to a spin-up effect? When considering Fig 15 (p30) I would think the negative UHI in the first night of the simulation might be a spin-up effect.

Response: Thank you. This error has been fixed in the revised manuscript. Figures 14 and 15 in the revised manuscript show the well-known diurnal pattern for UHI, showing higher UHI values during nighttime and lower UHI values during daytime. Also, for Guelph, the average VCWG-predicted mean and standard deviation for UHI are +1.20 and 1.53 K, respectively. These values are in reasonable agreement with observations reporting mean and standard deviation for UHI of +1.08 and 1.23 K, respectively.

35. p21 Fig9: this validation for Q is not convincing

Response: Thank you. We agree. Now we have calculated BIAS and RMSE of the model for predicting Q over two weeks. Please see section 3.1 and figure 5 in the revised manuscript.

36. p22 Table2: using fractional bias or percentage error (cfr abstract) for temperature is not appropriate, because in that case the error depends on the units employed. A bias on temperature expressed in °C or in K gives completely different outcomes. So, a statement such as 'the overall model bias on potential temperature is 5%' (abstract) has no meaning unless you specify the units employed, and even then it is better to avoid it.

Response: Thank you. We agree. Throughout the new revision of the manuscript we have strictly forbidden any relative calculation of error, i.e. normalized bias or normalized root mean square error, or other statistics, i.e. mean and standard deviation.

References

[Akbari et al., 2001] Akbari, H., Pomerantz, M., and Taha, H. (2001). Cool surfaces and shade trees to reduce energy use and improve air quality in urban areas. *Sol. Energy*, 70(3):295–310.

[Aliabadi, 2018] Aliabadi, A. A. (2018). *Theory and applications of turbulence: A fundamental approach for scientists and engineers*. Amir A. Aliabadi Publications, Guelph, Ontario, Canada.

[Aliabadi et al., 2017] Aliabadi, A. A., Krayenhoff, E. S., Nazarian, N., Chew, L. W., Armstrong, P. R., Afshari, A., and Norford, L. K. (2017). Effects of roof-edge roughness on air temperature and pollutant concentration in urban canyons. *Bound.-Lay. Meteorol.*, 164(2):249–279.

[Aliabadi et al., 2018] Aliabadi, A. A., Veriotes, N., and Pedro, G. (2018). A very large-eddy simulation (VLES) model for the investigation of the neutral atmospheric boundary layer. *Journal of Wind Engineering and Industrial Aerodynamics*, 183:152–171.

[Bredberg, 2000] Bredberg, J. (2000). On the wall boundary condition for turbulence models. Internal report 00/4, Department of Thermo and Fluid Dynamics, Chalmers University of Technology, Göteborg, Sweden.

[Bueno et al., 2012] Bueno, B., Norford, L. K., Hidalgo, J., and Pigeon, G. (2012). The urban weather generator. *J. Build. Perf. Simulat.*, 6(4):269–281.

[Bueno Unzeta, 2010] Bueno Unzeta, B. (2010). *An urban weather generator coupling a building simulation program with an urban canopy model*. PhD thesis, Massachusetts Institute of Technology.

[Businger et al., 1971] Businger, J. A., Wyngaard, J. C., Izumi, Y., and Bradley, E. F. (1971). Flux-profile relationships in the atmospheric surface layer. *J. Atmos. Sci.*, 28(2):181–189.

[Ciccioli et al., 1997] Ciccioli, P., Fabozzi, C., Brancaleoni, E., Cecinato, A., Frattoni, M., Cieslik, S., Kotzias, D., Seufert, G., Foster, P., and Steinbrecher, R. (1997). Biogenic emission from the mediterranean pseudosteppe ecosystem present in castelporziano. *Atmos. Environ.*, 31:167–175.

[Crank et al., 2018] Crank, P. J., Sailor, D. J., Ban-Weiss, G., and Taleghani, M. (2018). Evaluating the ENVI-met microscale model for suitability in analysis of targeted urban heat mitigation strategies. *Urban climate*, 26:188–197.

[Dyer, 1974] Dyer, A. (1974). A review of flux-profile relationships. *Bound.-Lay. Meteorol.*, 7(3):363–372.

[Erell and Williamson, 2006] Erell, E. and Williamson, T. (2006). Simulating air temperature in an urban street canyon in all weather conditions using measured data at a reference meteorological station. *Int. J. Climatol.*, 26(12):1671–1694.

[Jeričević and Grisogono, 2006] Jeričević, A. and Grisogono, B. (2006). The critical bulk richardson number in urban areas: verification and application in a numerical weather prediction model. *Tellus A*, 58(1):19–27.

[Krayenhoff, 2014] Krayenhoff, E. S. (2014). *A multi-layer urban canopy model for neighbourhoods with trees*. PhD thesis, University of British Columbia.

[Krayenhoff et al., 2020] Krayenhoff, E. S., Jiang, T., Christen, A., Martilli, A., Oke, T. R., Bailey, B. N., Nazarian, N., Voogt, J. A., Giometto, M. G., Stastny, A., et al. (2020). A multi-layer urban canopy meteorological model with trees (BEP-Tree): Street tree impacts on pedestrian-level climate. *Urban Climate*, 32:100590.

[Krayenhoff et al., 2015] Krayenhoff, E. S., Santiago, J.-L., Martilli, A., Christen, A., and Oke, T. R. (2015). Parametrization of Drag and Turbulence for Urban Neighbourhoods with Trees. *Bound.-Lay. Meteorol.*, 156(2):157–189.

[Louis, 1979] Louis, J.-F. (1979). A parametric model of vertical eddy fluxes in the atmosphere. *Bound.-Lay. Meteorol.*, 17(2):187–202.

[Maronga et al., 2015] Maronga, B., Gryschka, M., Heinze, R., Hoffmann, F., Kanani-Sühring, F., Keck, M., Ketelsen, K., Letzel, M. O., Sühring, M., and Raasch, S. (2015). The Parallelized Large-Eddy Simulation Model (PALM) version 4.0 for atmospheric and oceanic flows: model formulation, recent developments, and future perspectives. *Geosci. Model Dev.*, 8(8):2515–2551.

[Nazarian et al., 2019] Nazarian, N., Krayenhoff, E. S., and Martilli, A. (2019). A one-dimensional model of turbulent flow through 'urban' canopies: Updates based on large-eddy simulation. *Geosci. Model Dev. Discussions*, 2019:1–24.

[Palyvos, 2008] Palyvos, J. (2008). A survey of wind convection coefficient correlations for building envelope energy systems' modeling. *Appl. Therm Eng.*, 28(8-9):801–808.

[Resler et al., 2017] Resler, J., Krč, P., Belda, M., Juruš, P., Benešová, N., Lopata, J., Vlček, O., Damašková, D., Eben, K., Derbek, P., Maronga, B., and Kanani-Sühring, F. (2017). Palm-usm v1. 0: A new urban surface model integrated into the palm large-eddy simulation model. *Geosci. Model Dev.*, 10(10):3635–3659.

[Santiago and Martilli, 2010] Santiago, J. L. and Martilli, A. (2010). A Dynamic Urban Canopy Parameterization for Mesoscale Models Based on Computational Fluid Dynamics Reynolds-Averaged Navier-Stokes Microscale Simulations. *Bound.-Lay. Meteorol.*, 137(3):417–439.

[Simón-Moral et al., 2017] Simón-Moral, A., Santiago, J. L., and Martilli, A. (2017). Effects of unstable thermal stratification on vertical fluxes of heat and momentum in urban areas. *Bound.-Lay. Meteorol.*, 163(1):103–121.

[van der Kooi et al., 2019] van der Kooi, C. J., Kevan, P. G., and Koski, M. H. (2019). The thermal ecology of flowers. *Ann. Bot-London*, 124(3):343–353.

[Yaghoobian and Kleissl, 2012] Yaghoobian, N. and Kleissl, J. (2012). Effect of reflective pavements on building energy use. *Urban Climate*, 2:25–42.

The Vertical City Weather Generator (VCWG v1.1.0.0)

Mohsen Moradi[1], Benjamin Dyer[2], Amir Nazem[1], Manoj K. Nambiar[1], M. Rafsan Nahian[1], Bruno Bueno[5], Chris Mackey[7], Saeran Vasanthakumar[8], Negin Nazarian[3], E. Scott Krayenhoff[4], Leslie K. Norford[6], and Amir A. Aliabadi[1]

[1]School of Engineering, University of Guelph, Guelph, Canada
[2]Department of Physics and Astronomy, McMaster University, Hamilton, Canada
[3]Built Environment, University of New South Wales, Sydney, Australia
[4]School of Environmental Sciences, University of Guelph, Guelph, Canada
[5]Fraunhofer Institute for Solar Energy Systems ISE, Freiburg, Germany
[6]Department of Architecture, Massachusetts Institute of Technology, Cambridge, USA
[7]Ladybug Tools LLC, Boston, USA
[8]Kieran Timberlake Research Group, Philadelphia, USA

Correspondence: Amir A. Aliabadi (aliabadi@uoguelph.ca)

Abstract. The Vertical City Weather Generator (VCWG) is a computationally efficient urban microclimate model developed to predict temporal and vertical variation of temperature, wind speed, and specific humidity. It is composed of various sub models: a rural model, an urban microclimate model, and a building energy model. In a nearby rural site, ~~a rural model is forced with weather data to solve a vertical diffusion equation to calculate vertical potential temperature profiles using a novel parameterization~~the Monin-Obukhov Similarity Theory (MOST) is used to solve for the vertical profile of potential temperature and friction velocity at 10 m elevation, which is forced with weather data. The rural model also calculates a horizontal pressure gradient. The rural model outputs are then forced on a vertical diffusion urban microclimate model that solves vertical transport equations for momentum, temperature, and specific humidity. The urban microclimate model is also coupled to a building energy model using ~~feedback~~ two-way interaction. The aerodynamic and thermal effects of urban elements and vegetation are considered in VCWG. To evaluate the VCWG model, a microclimate field campaign was held in Guelph, Canada, from 15 July 2018 to 5 September 2018. The meteorological measurements were carried out under a comprehensive set of wind directions, wind speeds, and thermal stability conditions in both the rural and the nearby urban areas. The model evaluation ~~indicated~~ indicates that the VCWG ~~predicted~~ predicts vertical profiles of meteorological variables in reasonable agreement with field measurements~~for selected days. In comparison to measurements, the overall model biases for potential temperature,~~ . The average BIAS for wind speed, temperature and specific humidity ~~were within 5%, 11%, and 7%~~is 1.06 ms^{-1}, -1.43 K, and 0.005 kgkg^{-1}, respectively. The modeled and observed Urban Heat Island (UHI) values are in agreement. VCWG-predicted mean and standard deviation for UHI are +1.20 and 1.53 K, respectively, in reasonable agreement with observations reporting a mean and deviation for UHI of +1.08 and 1.23 K, respectively. The performance of the model ~~was~~ is further explored to investigate the effects of urban configurations such as plan and frontal area densities, varying levels of vegetation, building energy configuration, radiation configuration, seasonal variations, different climate zones, and time series analysis on the model

predictions. The results obtained from the explorations ~~were~~ are reasonably consistent with previous studies in the literature, justifying the reliability and computational efficiency of VCWG for operational urban development projects.

1 Introduction

Urban areas interact with the atmosphere through various exchange processes of heat, momentum, and mass, which substantially impact the human comfort, air quality, and urban energy consumption. Such complex interactions are observable from the Urban Canopy Layer (UCL) to a few hundred meters within the Atmospheric Boundary Layer (ABL) (Britter and Hanna, 2003). ~~Much of the urban climate research has focused on UCL, characterized by a heterogeneous urban structure, variety of human activities, and pollution sources. There is evidence that urban development can modify the urban climate by changing the atmosphere-earth surface interactions (Oke, 1982). It can noticeably affect atmospheric stability, dispersion of pollutants, and the Urban Heat Island (UHI), creating warmer cities than the surrounding undeveloped areas . The latter can often have significant negative influences on building energy performance and human health (Akbari, 2005). The UHI is mainly attributed to the reduction in loss of longwave radiation within the urban area, increased heat storage, anthropogenic heat released from human activities, urban greenhouse effect, inter-reflections of radiation within the surfaces of urban elements, and loss of evaporation from surfaces compared to vegetated surfaces (Oke et al., 1991), all of which affect energy performance of buildings (C. S. B. Grimmond, 2009).~~

~~UHI can be viewed as a primarily nighttime phenomenon, but it can also be occasionally observed during daytime. It has been suggested that the UHI pattern is strongly influenced by wind speed, wind direction, and the daily maximum air temperature at a rural site nearby a city (Founda and Santamouris, 2017). During extremely high temperatures, which may be accompanied by high humidity and higher absorption and storage of heat in urban areas, as opposed to rural areas, urban surfaces exhibit higher temperatures and, therefore, the sensible heat released from urban surfaces amplify (Li and Bou-Zeid, 2013; Founda and Santamouris, 2017 . Daytime UHI has been reported in Hong Kong (Siu and Hart, 2013), where UHI was detected in the early afternoon and at its peak just before sunset. Most commonly during nighttime, urban areas cool down at a lower rate than the surrounding rural areas due to radiation trapping and reduced convection so that the UHI is at its maximum at nights. In addition, excessive heat gain during a heat wave will be released into the~~ Modeling enables a deeper understanding of interactions between urban areas and the atmosphere and can possibly offer solutions toward mitigating adverse effects of urban ~~environment at nights with noticeable UHI (Oke, 1982; Founda and Santamouris, 2017). Nevertheless, the UHI phenomenon is more complicated to be easily generalized because it depends on multiple factors such as built density, ventilation rate, shading, radiation heat transfer, evaporation, and more, where occasionally an Urban Cool Island (UCI) can also be observed in the same climate zone (Yang et al., 2017).~~ development on the climate. A brief review of modeling efforts is essential toward more accurate model development for the understanding of urban areas-atmosphere interactions.

Mesoscale models incorporating the urban climate were initially aimed to resolve weather features with grid resolutions of at best few hundred meters horizontally and a few meters vertically, without the functionality to resolve ~~micro-scale~~ microscale three-dimensional flows or to account for atmospheric interactions with specific urban elements such as roads, roofs, and walls

(Bornstein, 1975). These models usually consider the effect of built-up areas by introducing an urban aerodynamic roughness length (Grimmond and Oke, 1999) or adding source or sink terms in the momentum (drag) and energy (anthropogenic heat) equations (Dupont et al., 2004). Therefore, if higher grid resolutions less than ten meters (horizontal and vertical) are desired (Moeng et al., 2007; Wang et al., 2009; Talbot et al., 2012), microscale climate models should be deployed. Some efforts also have begun to develop ~~multi-scale~~ multiscale climate models by coupling mesoscale and microscale models (Chen et al., 2011; Conry et al., 2014; Kochanski et al., 2015; Mauree et al., 2018). ~~All efforts considered, there is a paucity of robust and computationally efficient urban microclimate models that are capable of resolving spatial distribution of climate indicators such as wind, temperature, and humidity, while they are coupled to a nearby rural meteorological conditions as well as a building energy model.~~ Numerous studies have used Computational Fluid Dynamics (CFD) to investigate the urban microclimate taking into account interactions between the atmosphere and the urban elements with full three-dimensional flow analysis (Saneinejad et al., 2012; Blocken, 2015; Nazarian and Kleissl, 2016; Aliabadi et al., 2017; Nazarian et al., 2018). Despite accurate predictions, CFD models are not computationally efficient, particularly for weather forecasting at larger scales and for a long period of time, and they usually do not represent many processes in the real atmosphere such as clouds and precipitation. As an alternative, UCMs require understanding of the interactions between the atmosphere and urban elements to parameterize various exchange processes of radiation, momentum, heat, and moisture within and just above the canopy, based on experimental data (Masson, 2000; Kusaka et al., 2001; Chin et al., 2005; Aliabadi et al., 2019), three-dimensional simulations, or simplified urban configurations (Martilli et al., 2002; Coceal and Belcher, 2004; Krayenhoff et al., 2014, 2015; Nazarian and Kleissl, 2016). These urban canopy models are more computationally efficient than CFD models. They are designed to provide more details on heat storage and radiation exchange, while they employ less detailed flow calculations.

Urban microclimate models must account for a few unique features of the urban environment. Urban obstacles such as trees and buildings contribute substantially to the changing of flow and turbulence patterns in cities (Kastner-Klein et al., 2004). Difficulties arise when the spatially inhomogeneous urban areas create highly three-dimensional wind patterns that result in the difficulty of parameterizations (Roth, 2000; Resler et al., 2017). For example, the surfaces of urban obstacles exert form and skin drag and consequently alter flow direction and produce eddies at different spatiotemporal scales. This can lead to the formation of shear layers at roof level with variable oscillation frequencies (Tseng et al., 2006; Masson et al., 2008; Zajic et al., 2011), all of such phenomena should be properly approximated in parameterizations.

Heat exchanges between the indoor and outdoor environments significantly influence the urban microclimate. Various studies have attempted to parametrize heat sources and sinks caused by buildings such as heat fluxes due to infiltration, exfiltration, ventilation, walls, roofs, roads, windows, and building energy systems (Kikegawa et al., 2003; Salamanca et al., 2010; Yaghoobian and Kleissl, 2012). Therefore, a Building Energy Model (BEM) is required to be properly integrated in an urban microclimate model to take account of the impact of building energy performance on the urban microclimate (Bueno et al., 2011, 2012b; Gros et al., 2014). This ~~feedback~~ two-way interaction between the urban microclimate and indoor environment can significantly affect ~~UHI~~ Urban Heat Island (UHI) and energy consumption of buildings (Adnot et al., 2003; Salamanca et al., 2014).

Urban vegetation can substantially reduce the adverse effects of UHI, particularly during heat waves, resulting in more thermal comfort (Grimmond et al., 1996; Akbari et al., 2001; Armson et al., 2012). Urban trees can potentially ~~increase the overall albedo of a city,~~ provide shade and shelter, and, therefore, change the energy balance of the individual buildings as well as the entire city (Akbari et al., 2001). A study of the local-scale surface energy balance revealed that the amount of energy dissipated due to the cooling effect of trees is not negligible and should be parameterized properly (Grimmond et al., 1996). In addition, the interaction between urban elements, most importantly trees and buildings, is evident in radiation trapping within the canyon and most importantly shading impact of trees (Krayenhoff et al., 2014; Redon et al., 2017; Broadbent et al., 2019). Buildings and trees obstruct the sky with implications in long and shortwave radiation fluxes downward and upward that may create unpredictable diurnal and seasonal changes in UHI (Futcher, 2008; Kleerekoper et al., 2012; Yang and Li, 2015). Also, it has been shown that not only trees but also the fractional vegetation coverage on urban surfaces can alter urban temperatures with implications in UHI (Armson et al., 2012). Trees, particularly those which are shorter than buildings, also exert drag and alter flow patterns within the canopy, however, this effect is not as significant as that drag induced by buildings (Krayenhoff et al., 2015). Such complex interactions must be accounted for in successful urban microclimate models.

1.1 Research Gaps

Numerous studies have focused on high fidelity urban microclimate models with high spatiotemporal flow resolution, capturing important features of the urban microclimate with acceptable accuracy (Gowardhan et al., 2011; Soulhac et al., 2011; Blocken, 2015; Nazarian et al., 2018). Some example Computational Fluid Dynamics (CFD) models of this kind include Open-source Field Operation And Manipulation (OpenFOAM) (Aliabadi et al., 2017, 2018), Parallelized Large-Eddy Simulation Model (PALM) (Maronga et al., 2015; Resler et al., 2017), and ENVI-met (Crank et al., 2018). Despite the advances, however, high fidelity models capable of resolving three-dimensional flows ~~, such as CFD or those extending to mesoscale weather forecasting,~~ at microscale are not computationally efficient and they are complex to implement for operational applications. As a remedy, lower-dimensional flow urban microclimate models have been developed with many practical applications in city planning, architecture, and engineering consulting. For example, bulk flow (single-layer) models such as Urban Weather Generator (UWG) calculate the flow dynamics in one point, usually the centre of a hypothetical urban canyon, which is representative of all locations (Mills, 1997; Kusaka et al., 2001; Salamanca et al., 2010; Ryu et al., 2011; Bueno et al., 2012a, 2014). Another bulk flow (single-layer) model is Canyon Air Temperature (CAT) model, which utilizes standard data from a meteorological station to estimate air temperature in a street canyon (Erell and Williamson, 2006). The Town Energy Balance (TEB) calculates energy balances for urban surfaces, which is forced by meteorological data and incoming solar radiation in the urban site with no connection to rural meteorological conditions (Masson et al., 2002). The Temperatures of Urban Facets - 3D (TUF-3D) model calculates urban surface temperatures with the main focus on three-dimensional radiation exchange, but it adopts bulk flow (single-layer) ~~modelling~~ modeling without a connection to the surrounding rural area (Krayenhoff and Voogt, 2007). More recently ~~TUF~~ TUF-3D was coupled to an Indoor-Outdoor Building Energy Simulator (~~TUF-IOBES~~TUF-3D-IOBES), but still this model adopted a bulk flow (single-layer) parameterization ~~with no connection to the surrounding rural area~~ (Yaghoobian and Kleissl, 2012). The multi-layer Building Effect ~~Parametrization (BEP) model or its next generation BEP-Tree~~

~~model include~~ Parametrization-Tree (BEP-Tree) model includes variable building heights, the vertical variation of climate variables and the effects of trees, but ~~they are~~ it is not linked to a building energy model ~~(Martilli et al., 2002; Krayenhoff, 2014)~~ (Martilli et al., 2002; Krayenhoff, 2014; Krayenhoff et al., 2020). More recently, the BEP model has been coupled to a Building Energy Model (BEP+BEM) but ~~without a connection to the rural meteorological conditions~~it is forced with meteorological variables from higher altitudes above a city using mesoscale models, instead of near surface meteorological variables measured outside the city (rural areas). An overview of the literature reveals an apparent paucity of an independent urban microclimate model that accounts for some spatiotemporal variation of meteorological parameters in the urban environment and considers the effects of trees, building energy, radiation, and the connection to the near-surface rural meteorological conditions measured outside a city, without the need for mesoscale modeling, computationally efficiently and is operationally simple for practical applications.

1.2 Objectives

In this study, we present a new urban microclimate model, called the Vertical City Weather Generator (VCWG), which attempts to overcome some of the limitations mentioned in the previous section. It resolves vertical profiles (the direction ~~that~~ in which turbulent transport is significant) of climate parameters, such as temperature, wind, and humidity, in relation to urban design parameters. VCWG also includes a building energy model. It allows parametric investigation of design options on urban climate control at multiple heights, particularly if high density and high-rise urban design options are considered. This is a significant advantage over the bulk flow (single-layer) models such as UWG, which only consider one point for flow dynamics inside a hypothetical canyon (Masson, 2000; Kusaka et al., 2001; Dupont et al., 2004; Krayenhoff and Voogt, 2007; Lee and Park, 2008; Bueno et al., 2012a, 2014). The VCWG is designed to cycle through different atmospheric stability conditions that could be observed over the course of a day, but it is very computationally efficient with the capability to be run up to and beyond an entire year. The advantages of VCWG are as follows. 1) It does not need to be coupled to a mesoscale weather model because it functions standalone as a microclimate model. 2) Unlike many UCMs that are forced with climate variables above the urban roughness sublayer (e.g. TUF-3D), VCWG is forced with rural climate variables measured at 2m (temperature and humidity) and 10m (wind) elevation that are widely accessible and available around the world, making VCWG highly practical for urban design investigations ~~at~~ in different climates. 3) VCWG provides urban climate information in one dimension, i.e. resolved vertically. This is advantageous over bulk flow (single-layer) models because vertical transport of momentum, heat, and atmospheric species is significantly important. 4) VCWG is coupled with the building energy model using ~~feedback~~ two-way interaction.

~~VCWG is based on a predecessor bulk flow (single-layer) Urban Canopy Model (UCM), titled the Urban Weather Generator (UWG), which predicts the urban air temperature by assuming a relationship between urban and rural climates (Bueno et al., 2012a) . UWG was used because it contains simple parameterizations of heat exchange processes between the key urban elements, particularly the building energy systems, and the atmosphere. It also imposes a low computational cost, enabling its usage to predict the urban microclimate on many spatial locations and over long periods of time (Bueno et al., 2014). UWG accounts for vegetation, but in rudimentary ways, only considering surface covered vegetation. So, it was extended in this study to~~

include the effect of trees on the urban microclimate in more realistic ways with a predefined leaf area density profile. It is also extended to predict vertical profiles of temperature, specific humidity, wind in the urban environment based on models by Santiago and Martilli (2010), Krayenhoff et al. (2015), and Simón-Moral et al. (2017). The inclusion of trees in VCWG necessitated the implementation of new long and shortwave radiation models from Lee and Park (2008) and Redon et al. (2017) , which calculate radiation heat heat fluxes in and out of a simplified infinite urban canyon. The remaining parameterizations within VCWG are extracted from other experimental field campaigns that particularly attempt to estimate the turbulent statistics (friction velocity and convective velocity scale), exchange velocity, and aerodynamic roughness lengths, in the rural and urban environments (Rotach et al., 2005; Balogun et al., 2010; Zajic et al., 2011; Roth et al., 2015; Aliabadi et al., 2019).

To evaluate the model, a microclimate field campaign in a representative urban area and a surrounding rural area was held in Guelph, Canada, during the Summer of 2018. Three components of wind velocity, temperature, relative humidity, and solar radiation were rigorously measured in this field campaign at different locations and under a comprehensive set of wind speeds, wind directions, and atmospheric stability conditions. To explore the model, the VCWG is set to run to investigate the effect effects of building dimensions, urban vegetations, and seasonal changes vegetation, building energy configuration, radiation configuration, seasonal variations, other climates, and time series analysis on the model outcome. The VCWG is also set to run for different climate zones for cities of Guelph, Buenos Aires, Tucson, Vancouver, Osaka, and Copenhagen.

1.3 Organization of the Article

The paper is structured as follows. Section 2 describes the methodology. In Sect. 2.1, all components of the VCWG and the way that they are integrated are presented. Firstly, the First, the Energy Plus Weather (EPW) dataset is introduced, which is the background rural weather data used to force VCWG. Next, the Rural Model (RM), used to determine the potential temperature profile, friction velocity, and the horizontal pressure gradient in the rural area, is described. Then, details are discussed for the one-dimensional vertical diffusion model for the urban environment, the building energy model, and the radiation model, which are forced by the RM to predict the vertical profiles of meteorological quantities in the urban area. Sect. Section 2.2 describes the location and details of the field campaign, including meteorological instruments used. Section 3 provides the results and discussion. It starts with the evaluation of VCWG by comparing simulation results with those of the field measurements in Sect. ??3.1. Then, results from other explorations including effects of building dimensions, foliage density, building energy configuration, radiation configuration, seasonal variation, different climate zones, and time series analysis on urban climate are presented in Sect. ??3.2. Finally, Sect. 4 is devoted to conclusions and future work. Additional information about the equations used in the model and the details about the VCWG software are provided in the appendix.

2 Methodology

2.1 Vertical City Weather Generator (VCWG)

In this section, the Vertical City Weather Generator (VCWG) is introduced.

Figure 1 shows the VCWG model schematic. VCWG consists of four integrated sub models~~including~~. 1) a Rural Model (RM) (Sect. 2.1.2) ~~that~~ forces meteorological boundary conditions on VCWG ~~, a~~ based on Monin-Obukhov similarity theory (Businger et al., 1971; Dyer, 1974) and a soil heat transfer model (Bueno et al., 2012a, 2014). 2) a one-dimensional vertical diffusion model (Sect. 2.1.3) is used for calculation of the urban potential temperature, wind speed, turbulence kinetic energy, and specific humidity profiles, considering the effect of trees. This model was initially developed by Santiago and Martilli (2010) and Simón-Moral et al. (2017), while it was later ingested into another model called the Building Effect Parametrization with Trees (BEP-Tree), considering the effects of trees (Krayenhoff, 2014; Krayenhoff et al., 2015, 2020). 3) a Building Energy Model (BEM) (Sect. 2.1.4) ~~, and a radiation model with vegetation (Sect. 2.1.5). VCWG is based on the following predecessor models: a well-parameterized one-dimensional vertical diffusion model for urban microclimate variables known as the Building Effect Parametrization with Trees (BEP-Tree) model (Santiago and Martilli, 2010; Krayenhoff et al., 2014, 2015; Simón-Moral et al., 2017 , an urban microclimate model with bulk flow (single-layer) and building energy parameterization known as~~ is used to determine the sensible and latent waste heats of buildings imposed on the urban environment. This model is a component of the Urban Weather Generator (UWG) ~~(Bueno et al., 2014), and~~ model (Bueno et al., 2012a, 2014). 4) a radiation model ~~characterizing longwave (Lee and Park, 2008)~~ with vegetation (Sect. 2.1.5) is used to compute the longwave (Loughner et al., 2012) and shortwave (Redon et al., 2017) ~~radiation heat transfer in and out a two-dimensional urban canyon~~ heat exchanges between the urban canyon and the atmosphere/sky.

The sub models are integrated to predict vertical variation of urban microclimate parameters including potential temperature, wind speed, specific humidity, and turbulence kinetic energy as influenced by aerodynamic and thermal ~~effect~~ effects of urban elements including longwave and shortwave radiation exchanges, sensible heat fluxes released from urban elements, cooling effect of trees, and the induced drag by urban obstacles. ~~Fig. 1 depicts the sub models in the VCWG and their relationship with each other.~~ The Rural Model (RM) takes latitude, longitude, dry bulb temperature, relative humidity, dew point temperature, and pressure at 2 m elevation, wind speed and direction at 10 m elevation, ~~horizontal infrared radiation intensity, global horizontal radiation, direct normal~~ down-welling direct radiation, and ~~diffuse horizontal~~ down-welling diffuse radiation from an Energy Plus Weather (EPW) file[1]. For every time step, and forced with the set of weather data, the RM then computes a potential temperature profile, a constant specific humidity profile, and a horizontal pressure gradient, all of which are forced as boundary conditions to the one-dimensional vertical diffusion model in the urban area. The potential temperature and specific humidity are forced as fixed values on top of the domain for the urban vertical diffusion model in the temperature and specific humidity equations, respectively. The horizontal pressure gradient is forced as a source term for the urban vertical diffusion model in the momentum equation. While forced by the RM, the urban one-dimensional vertical diffusion model is also coupled with a building energy model and the two-dimensional radiation model. The three models have feedback interaction and converge to a ~~solution (temperature and wind speed)~~ potential temperature solution iteratively. The urban one-dimensional vertical diffusion model calculates the flow quantities at the centre of control volumes, which are generated by splitting the urban computational domain into multiple layers within an above the urban canyon (see Fig. 2). The urban domain extends to five times building height that conservatively includes the entire ~~roughness sublayer within the atmospheric~~

[1] ~~https://energyplus.net/weather~~

~~boundary layer~~ atmospheric roughness sublayer (Santiago and Martilli, 2010; Aliabadi et al., 2017). The feedback interaction coupling scheme among the building energy model, radiation model, and the urban one-dimensional vertical diffusion model is designed to update the boundary conditions, surfaces temperatures, and the source/sink terms in the transport equations. For each time step, the iterative ~~calculation~~ calculations for all the sub models ~~continues~~ continue until the convergence criterion of ~~temperature and wind speed~~ potential temperature in the canyon are fulfilled. More details about the sub models are provided in the subsequent sections and the appendix.

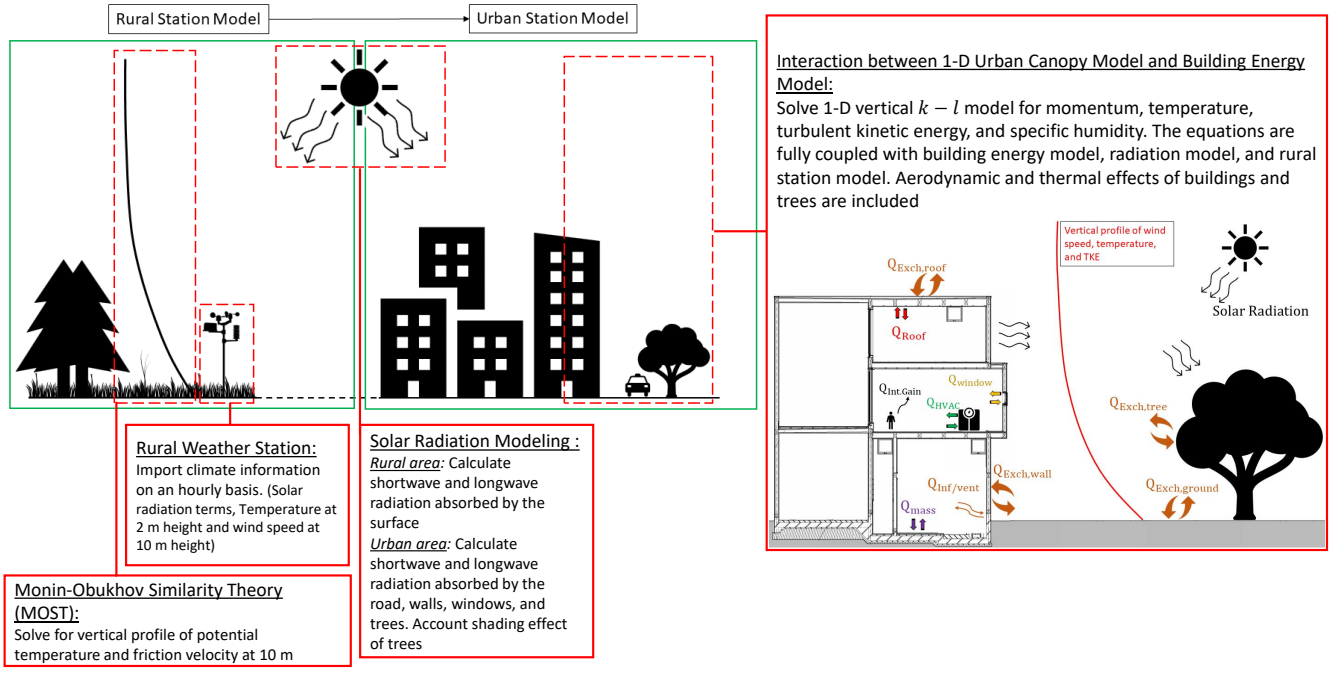

Figure 1. The schematic of Vertical City Weather Generator (VCWG).

2.1.1 ~~Rural Model~~Energy Plus Weather Data

Building energy and solar radiation simulations are typically carried out with standardized weather files. Energy Plus Weather (EPW) files include recent weather data for 2100 locations and are saved in the standard EnrgyPlus format, developed by US department of energy.[1] The data is available for most North American cities, European cities, and other regions around the World. The weather data are arranged by World Meteorological Organization (WMO) based on region and country. An EPW file contains typical hourly-based data of meteorological variables. The meteorological variables are dry bulb temperature, dew point temperature, relative humidity, incoming direct and diffusive solar radiation fluxes from sky, wind direction, wind speed,

[1] https://energyplus.net/weather

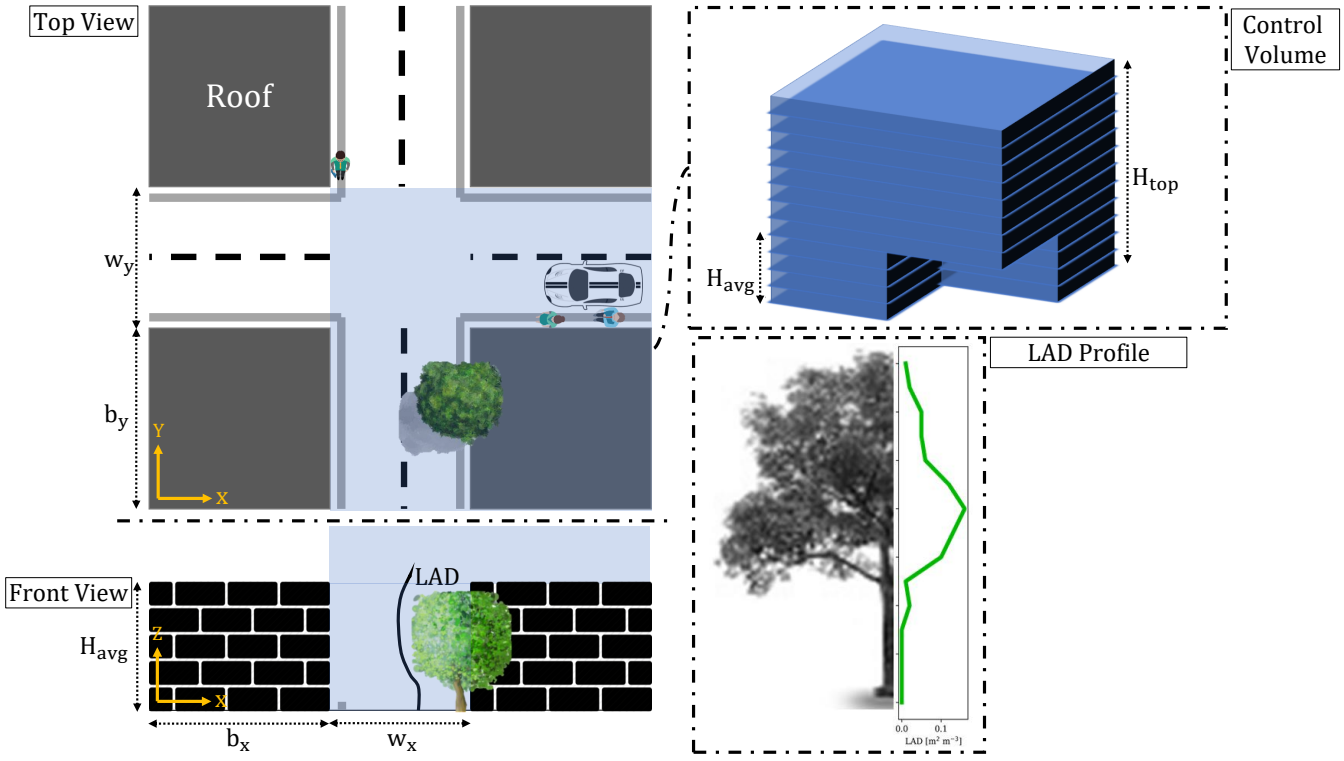

Figure 2. Simplified urban area used in VCWG and corresponding layers of control volumes within and above the canyon. The height of the domain is five times of the average building height.

sky condition, precipitation, and general information about field logistics and soil properties. Precipitation data is often missing in the EPW files, which affects calculation of latent heat in the rural area.

2.1.2 Rural Model

~~Throughout the VCWG development, Reynolds averaging is used for meteorological variables so the instantaneous variable is the sum of the time-averaged part plus the turbulent fluctuating part, i.e. , where represents the instantaneous variable of interest, is the time-averaged variable, and is the fluctuating part of the variable.~~

In the rural model~~(see Fig. 1), a Vertical Diffusion Model (VDM) calculates~~ , the Monin–Obukhov Similarity Theory (MOST) is used to solve for the vertical profile of potential temperature ~~in the rural site using meteorological information measured at the weather station. The atmospheric variation of potential temperature in the vertical direction is assumed to be quasi-steady. At every time step of the model, the temperature at the lowest level is forced by rural measurements at~~ and friction velocity at 10 m ~~, i.e. from a weather file, then the VDM predicts the vertical structure of~~ elevation using meteorological measurements near the surface. MOST is usually applied to the atmospheric surface layer over flat and homogeneous lands

to describe the vertical profiles of wind speed, potential temperature, and specific humidity as functions of momentum flux, sensible heat flux, and latent heat flux measured near the surface, respectively. Using MOST the gradient of potential temperature ~~using the forced temperature and other parameters such as a source/sink term, diffusion coefficient, and mixing length. It is also assumed that the rural area is horizontally homogeneous and very flat. The combination of input parameters are sourced from an Energy Plus Weather (EPW) database[2]. The mean potential temperature~~ is ~~parameterized using the gradient-diffusion hypothesis,~~ given by

$$0 = \frac{\partial}{\partial z}\left(-\frac{K_m}{Pr_t}\frac{\partial \overline{\Theta}_{rur}}{\partial z}\right) + \gamma = \frac{Q_{net,rur}}{\rho C_p \kappa u_* z}\Phi_H\left(\frac{z}{L}\right), \tag{1}$$

where $\overline{\Theta}_{\mathrm{rur}}$ is mean potential temperature in the rural ~~site, is turbulent diffusivity for momentum, is turbulent Prandtl number, is heat source/sink term, and is the vertical coordinate. It has been suggested that turbulent Prandtl number varies between to depending on atmospheric stability and scale of analysis and decreases under more unstable conditions (Raupach et al., 1996; Grachev et al. . In this study, for simplicity, is set to be , but it can be changed as the input of the model.~~

~~Two approaches have been suggested to formulate , based on uniform turbulent viscosity and the mixing-length model (Pope, 2000). The former considers a constant turbulent viscosity that is suitable only for simple shear flows. In the mixing length model, which is more applicable in boundary layer flows, is proportional to the mixing-length () and the gradient of mean horizontal wind speed ()~~

$$K_m = \ell^2 \frac{\partial \overline{S}_{rur}}{\partial z}.$$

area, $\mathrm{Q_{net,rur}}$ is net rural sensible heat flux, ρ is air density near the rural surface, $\mathrm{C_p}$ is air specific heat capacity, $\mathrm{u_*}$ is friction velocity, and κ is the von Kármán constant. Φ_{H} is known as the universal dimensionless temperature gradient. This terms was estimated for different thermal stability conditions based on experimental data by (Businger et al., 1971; Dyer, 1974)

$$\Phi_H\left(\frac{z}{L}\right) = \begin{cases} 0.74 + 4.7\frac{z}{L}, & \frac{z}{L} > 0 (\text{Stable}) \\ 0.74, & \frac{z}{L} = 0 (\text{Neutral}) \\ 0.74\left(1 - \frac{9z}{L}\right)^{-1/4}, & \frac{z}{L} < 0 (\text{Unstable}). \end{cases} \tag{2}$$

~~A log-law is assumed for wind profile given an aerodynamic roughness length and wind measurement at . From the corresponding log-law the vertical gradient of wind speed is calculated analytically by simple differentiation of the log-law and then used to determine momentum diffusivity. Numerous studies have attempted to parameterize mixing-length based on the well-known Obukhov length (Peña et al., 2010; Sun, 2011; Keck et al., 2014; Sun et al., 2016), which is the ratio of shearing to buoyancy effects representing the atmospheric stability condition.~~

[2] ~~https://energyplus.net/weather~~

In the dimensionless stability parameter z/L, z is height above ground and L is Obukhov-Length given by

$$L = \frac{-\overline{\Theta}_{rur,z=2m} u_*^3}{g\kappa \frac{Q_{net,rur}}{\rho C_p}}. \tag{3}$$

It has been shown that such models break down in neutral or weakly stable conditions, when the vertical turbulent heat flux approaches zero (Grachev et al., 2013; Aliabadi et al., 2016a; Optis et al., 2016; Sun et al., 2016). In this study, the thermal stability condition is roughly approximated based on the available incoming solar radiation in the way that presence or absence of incoming solar radiation on the surface indicate unstable and stable conditions, respectively. The mixing length can be obtained by (Gryning et al., 2007) observed that there is a monotonic reduction in friction velocity with increasing stratification (Joffre et al., 2001). So, friction velocity in Eq. 1 is estimated from momentum flux generalization (Monin and Obukhov, 1957)

$$\frac{1}{\ell}\frac{\partial \overline{S}_{rur}}{\partial z} = \frac{1}{C_{crur}}\left(\frac{1}{\kappa z} + \frac{1}{C_* u_*}\right)\frac{u_*}{\kappa z}\Phi_M\left(\frac{z}{L}\right), \tag{4}$$

where the first term on the right-hand side indicates a linear relationship with height near the surface, while the second term restricts the value of length scale in the upper part of the atmospheric surface layer asymptotically. is a scaling correction factor, which is optimized to during unstable conditions and during stable conditions, is a model constant optimized to be , and is von Kármán constant. Friction velocity was parameterized based on field data from a previous microclimate field campaign in rural and urban areas located in Guelph, Canada (Aliabadi et al., 2019) $\overline{\mathrm{S}}_{\mathrm{rur}}$ is the mean horizontal wind speed in the rural area and Φ_{M} is the universal dimensionless wind shear and is estimated for different thermal stability conditions based on experimental data (Businger et al., 1971; Dyer, 1974)

$$u_*\Phi_M\left(\frac{z}{L}\right) = 0.07_{rur} + 0.12.\begin{cases} 1 + 4.7\frac{z}{L}, & \frac{z}{L} > 0(\text{Stable}) \\ 1, & \frac{z}{L} = 0(\text{Neutral}) \\ \left(1 - \frac{15z}{L}\right)^{-1/4}, & \frac{z}{L} < 0(\text{Unstable}). \end{cases} \tag{5}$$

It is suggested that thermal exchange processes within the atmospheric surface layer are tightly coupled to heat transfer with the earth surface (Stull, 1988). When the surface is warmer than air, upward heat flux released into the atmosphere creates a thermally unstable condition. On the other hand, downward heat flux, mostly observed over night when the surface is cooling, creates a thermally stable condition. Sensible heat fluxes are required to estimate . Friction velocity can be determined by numerically integrating Eq. 4 from the elevation of the rural aerodynamic roughness length z_0 to 10 m in an iterative process. This method provides a friction velocity that is corrected for thermal stability effects. The potential temperature profiles are also obtained by numerical integration of Eq. 1.

Meteorological information obtained from the weather station including direct and diffuse solar radiation, temperature at the height of 2 m elevation, and wind speed at the height of 10 m elevation are used to calculate the net sensible heat flux at the

surface

$$Q_{net,rur} = \underbrace{Q_{Hveg,rur} + h_{conv}(T_{0,rur} - T_{air,rur}) + Q_{rad,rur}}_{\text{sensible heat flux}}, \quad (6)$$

where $Q_{net,rur}$ is the net sensible heat flux (positive upward from the surface into the atmosphere at the rural site), $Q_{Hveg,rur}$ is the sensible heat flux from biogenic activity of vegetation (Ciccioli et al., 1997; van der Kooi et al., 2019), h_{conv} is the convection heat transfer coefficient at the surface, $T_{0,rur}$ is the rural surface temperature calculated by the rural model, $T_{air,rur}$ is the air temperature at ~~the height of~~ 2 m elevation, and $Q_{rad,rur}$ is the longwave and shortwave radiation absorbed by rural surface (for more details see Appendix A). ~~Therefore, the heat sink/source term in Eq. ?? can be parameterized as~~

~~$$\gamma = C_\gamma \left(\frac{Q_{net,rur}}{\rho C_p}\right) \frac{1}{H_{bl}},$$~~

~~where is air density near the rural surface, is air specific heat capacity, is a scaling factor for heat sink/source term equal to , and is the diurnally-averaged boundary-layer height.~~ Numerous studies have focused on parameterization of convection heat transfer coefficient reviewed by Palyvos (2008). In this study, the following boundary-layer type correlation between h_{conv} and mean wind speed ($\overline{S}_{rur,z=10m}$) is used

$$h_{conv} = 3.7\overline{S}_{rur} + 5.8. \quad (7)$$

The rural model also outputs a horizontal pressure gradient based ~~on~~ the friction velocity calculation that is later used as a source term for the urban one-dimensional vertical diffusion momentum equation. The pressure gradient is parameterized as ~~.~~ ~~This choice does not necessitate a need for solving a vertical diffusion equation for momentum in the rural area~~ $\rho u_*^2/H_{top}$, where H_{top} is the height of the top of the domain, here five times the average building height (Krayenhoff et al., 2015; Nazarian et al., 2019) .

Another assumption made in the rural model is that the specific humidity is constant in the vertical direction, i.e. invariant with height, for the lowest range of the atmospheric surface layer. This assumption is ~~valid so long as the water vapour pressure is less than the saturation water vapour pressure for a given altitude. This condition must be checked to confirm the adequacy of this assumption. The specific humidity can be calculated from the ratio of water vapour density to the air density, which can be simplified using ideal gas law , where is water vapor pressure and is the air pressure. We can calculate the saturation pressure () using the Clausius-Clapeyron equation~~

~~$$P_{sat} = 6.1094 \exp\left(\frac{17.625 T_{rur}}{T_{rur} + 243.04}\right).$$~~

made, for lack of a better assumption, because with only surface data and lack of latent heat flux, it is not practical to calculate variation of specific humidity with height in the surface layer.

A density profile is required to convert the real temperature profile in the rural area (T_{rur}) to potential temperature profile and vice versa, which is used in the Eq. ~~??~~1. Using a reference density (ρ_0), reference temperature (T_0), and reference pressure

(P_0) at the surface level from the weather station at 2 m elevation, and considering a lapse rate of $-0.000133\ \mathrm{kg\ m^{-3}\ m^{-1}}$ for density within the surface layer, the density profile can be simplistically parameterized by

$\rho = \rho_0 - 0.000133(z - z_0).$

$\rho = \rho_0 - 0.000133(z - z_0).$

After ~~checking that the condition is met for constancy of specific humidity with height, the specific humidity calculated~~ calculating potential temperature and specific humidity at the top of the domain by the rural model, these values can be applied as ~~a fixed value~~ fixed-value boundary condition at the top of the domain in the urban one-dimensional vertical diffusion model in the energy and specific humidity transport ~~equation~~equations.

2.1.3 Urban Vertical Diffusion Model

Numerous studies have attempted to parameterize the interaction between urban elements and the atmosphere in terms of dynamical and thermal effects, from very simple models based on ~~Monin-Obukhov similarity theory~~ MOST (Stull, 1988), to the bulk flow (single-layer) parameterizations (Krayenhoff and Voogt, 2007; Masson, 2000; Kusaka et al., 2001; Bueno et al., 2014), to multi-layer models ~~(Hamdi and Masson, 2008; Santiago and Martilli, 2010; Krayenhoff et al., 2015)~~ (Hamdi and Masson, 2008; with different levels of complexity. The multi-layer models usually treat aerodynamic and thermal effects of urban elements as sink or source terms in momentum, heat, specific humidity, and turbulence kinetic energy equations. Parameterization of the exchange processes between the urban elements and the atmosphere can be accomplished using either experimental data or CFD simulations (Martilli et al., 2002; Dupont et al., 2004; Kondo et al., 2005; Kono et al., 2010; Lundquist et al., 2010; Santiago and Martilli, 2010; Krayenhoff et al., 2015; Aliabadi et al., 2019). CFD-based parameterizations proposed by Martilli and Santiago (2007), Santiago and Martilli (2010), ~~and Krayenhoff et al. (2015)~~Krayenhoff et al. (2015), Nazarian et al. (2019) use results from Reynolds-Averaged Navier-Stokes (RANS) ~~simulations~~ or Large-Eddy Simulations (LES) including effects of trees and buildings. These parameterizations consider the CFD results at different elevations after being temporally and horizontally averaged.

For the one-dimensional vertical diffusion model, any variable such as cross- and along-canyon wind velocities (U and V, respectively), potential temperature (Θ), and specific humidity (Q) is presented using Reynolds averaging. The one-dimensional time-averaged momentum equations in the cross- and along-canyon components ~~, which are originally developed by Santiago and Martilli (2010),~~ can be shown as (Santiago and Martilli, 2010; Krayenhoff, 2014; Krayenhoff et al., 2015; Simón-Moral et

$$\frac{\partial \overline{U}}{\partial t} = \underbrace{-\frac{\partial \overline{uw}}{\partial z}}_{I} \underbrace{-\frac{1}{\rho}\frac{\partial \overline{P}}{\partial x}}_{II} \underbrace{-D_x}_{III}, \tag{8}$$

$$\frac{\partial \overline{V}}{\partial t} = \underbrace{-\frac{\partial \overline{vw}}{\partial z}}_{I} \underbrace{-\frac{1}{\rho}\frac{\partial \overline{P}}{\partial y}}_{II} \underbrace{-D_y}_{III}, \tag{9}$$

where $\overline{P}$ is time-averaged pressure. The terms on the right hand side of Eqs. 8 and 9 are the vertical gradient of turbulent flux of momentum (I), acceleration due to the large-scale pressure gradient (II), and the sum of pressure, building form, building skin, and vegetation drag terms (III). The parameterization of the latter term is detailed in Appendix A ~~based on studies by Santiago and Martilli (2010) and Krayenhoff et al. (2015) and~~ and is not reported here for brevity. K-theory was used to parameterize the vertical momentum fluxes, i.e. $\partial\overline{uw}/\partial z = -K_m \partial\overline{U}/\partial z$ and $\partial\overline{vw}/\partial z = -K_m \partial\overline{V}/\partial z$ (the same approach will be used in energy and humidity equations), where the diffusion coefficient is calculated using a k$-\ell$ model

$$K_m = C_k \ell_k k^{1/2}, \tag{10}$$

where C_k is a constant and ℓ_k is a length scale optimized using ~~CFD~~sensitivity analysis based on CFD (Nazarian et al., 2019). C_k can be obtained based on the bulk Richardson number $Ri_b = g H_{avg} \Delta\overline{\Theta} / (\Delta\overline{S}^2 \overline{\Theta}_{avg})$, where g is gravitational acceleration, H_{avg} is average building height, $\Delta\overline{\Theta}$ and $\Delta\overline{S}$ are the variation of temperature and horizontal wind speed over vertical distance H_{avg} (i.e. roof level minus street level), and $\overline{\Theta}_{avg}$ is the mean temperature in the canyon. ~~After performing an optimization procedure the best value of~~ C_k was determined depending on a critical bulk Richardson number, which is set to ~~,~~ 0.25. The value C_k=2 is used for unstable condition (~~) and~~ $Ri_b > 0.25$) and C_k=1 is used for stable condition ($Ri_b < 0.25$). More details on C_k and ℓ_k are provided in Krayenhoff (2014) and Nazarian et al. (2019). The turbulence kinetic energy k can be calculated using a prognostic equation ~~(Stull, 1988)~~ (Krayenhoff et al., 2015)

$$\frac{\partial k}{\partial t} = \underbrace{K_m \left[\left(\frac{\partial \overline{U}}{\partial z} \right)^2 + \left(\frac{\partial \overline{V}}{\partial z} \right)^2 \right]}_{I} + \underbrace{\frac{\partial}{\partial z} \left(\frac{K_m}{\sigma_k} \frac{\partial k}{\partial z} \right)}_{II} - \underbrace{\frac{g}{\Theta_0} \frac{K_m}{Pr_t} \frac{\partial \overline{\Theta}}{\partial z}}_{III} + \underbrace{S_{wake}}_{IV} - \underbrace{\varepsilon}_{V}, \tag{11}$$

where g is acceleration due to gravity and Θ_0 is a reference potential temperature. The terms on the right hand side of Eq. 11 are shear production (I), turbulent transport of kinetic energy parameterized based on K-theory (II), buoyant production/dissipation (III), wake production by urban obstacles (IV), and dissipation (V). Parameterization of the last two terms is presented in more ~~details~~ detail in Appendix A and Krayenhoff (2014) and not reported here for brevity. σ_k is turbulent Prandtl number for kinetic energy, which is generally suggested to be σ_k=1 (Pope, 2000).

To calculate vertical profile of potential temperature in the urban area, the transport equation can be derived as

$$\frac{\partial \overline{\Theta}}{\partial t} = \underbrace{\frac{\partial}{\partial z} \left(\frac{K_m}{Pr_t} \frac{\partial \overline{\Theta}}{\partial z} \right)}_{I} + \underbrace{S_{\Theta R} + S_{\Theta G} + S_{\Theta W} + S_{\Theta V} + S_{\Theta A} + S_{\Theta waste}}_{II}, \tag{12}$$

where the first term on the right hand side is turbulent transport of heat (I) and the heat sink/source terms (II) correspond to sensible heat exchanges with roof ($S_{\Theta R}$), ground ($S_{\Theta G}$), wall ($S_{\Theta W}$), urban vegetation $S_{\Theta V}$, and radiative divergence $S_{\Theta A}$ detailed in appendix A and by ~~Krayenhoff et al. (2014)~~ Krayenhoff (2014) and not reported here for brevity (see Fig. 1). Contribution of the waste heat emissions from building heating ventilation and air conditioning (HVAC) system $S_{\Theta waste}$ is parameterized by

$$S_{\Theta waste} = F_{st} \frac{1}{\rho C_p \Delta z} Q_{HVAC}, \tag{13}$$

where Q_{HVAC} is total sensible waste heat released into the urban atmosphere per building footprint area, F_{st} is the fraction of waste heat released at street level, while the remainder fraction $1-F_{st}$ is released at roof level, and Δz is grid discretization in the vertical direction. Depending on the type of building, waste heat emissions can be released partially at street level and the rest at roof level, which can be adjusted by changing F_{st} from 0 to 1. In this study, it is set to ~~.~~0.3. Term Q_{HVAC} is calculated by the building energy model as

$$Q_{HVAC} = \underbrace{\underbrace{Q_{surf} + Q_{ven} + Q_{inf} + Q_{int}}_{Q_{cool}} + W_{cool}}_{\text{Cooling waste heat}} + Q_{dehum} + Q_{gas} + Q_{water}, \tag{14}$$

$$Q_{HVAC} = \underbrace{\underbrace{(Q_{surf} + Q_{ven} + Q_{inf} + Q_{int})/\eta_{heat}}_{Q_{heat}}}_{\text{Heating waste heat}} + Q_{dehum} + Q_{gas} + Q_{water}, \tag{15}$$

under cooling and heating mode, respectively. Under cooling mode Q_{HVAC} is calculated by adding the cooling demand (Q_{cool}), consisting of surface cooling demand, ventilation demand, infiltration (or exfiltration) demand, and internal energy demand (lighting, equipment, and occupants), energy consumption of the cooling system (W_{cool}), dehumidification demand (Q_{dehum}), energy consumption by gas combustion (e.g. cooking) (Q_{gas}), and energy consumption for water heating (Q_{water}). Under heating mode, Q_{HVAC} is calculated by adding the heating waste heat (Q_{heat}), consisting of surface heating demand, ventilation demand, infiltration (or exfiltration) demand, and internal energy demand (lighting, equipment, and occupants) (accounting for thermal efficiency of the heating system (η_{heat})), dehumidification demand (Q_{dehum}), energy consumption by gas combustion (e.g. cooking) (Q_{gas}), and energy consumption for water heating (Q_{water}).

To complete the urban one-dimensional vertical diffusion model (see Fig. 1), the transport equation for specific humidity is

$$\frac{\partial \overline{Q}}{\partial t} = \underbrace{\frac{\partial}{\partial z}\left(\frac{K_m}{Sc_t}\frac{\partial \overline{Q}}{\partial z}\right)}_{I} + \underbrace{S_{QV}}_{II}, \tag{16}$$

where $\overline{Q}$ is time-averaged specific humidity. The turbulent transport of specific humidity (I) is parameterized based on K-theory, Sc_t is turbulent Schmidt number set to 1 in this study, and source term S_{QV} (II) is caused by latent heat from vegetation detailed in appendix A and by Krayenhoff (2014) but not reported here for brevity.

2.1.4 Building Energy Model

~~Building energy consumption due to HVAC systems and the associated interaction with the urban atmosphere can alter the urban microclimate. It has been reported that such interaction can change UHI depending on the region and climate of interest (De Munck et al., 2013; Schoetter et al., 2017).~~ In this study, the balance equation for convection, conduction, and radiation

heat fluxes is applied to all building elements (wall, roof, floor, windows, ceiling, and internal mass) to calculate the indoor air temperature. Then, a sensible heat balance equation, between convective heat fluxes released from indoor surfaces and internal heat ~~gain~~ gains and sensible heat fluxes from HVAC system and infiltration (or exfiltration), is solved to obtain the time evolution of indoor temperature as

$$\forall \rho C_p \frac{dT_{in}}{dt} = \Sigma Q_{cv,i} + Q_{gain} + Q_{inf/exf} + Q_{sys} Q_{surf} + Q_{ven} + Q_{inf} + Q_{int} Q_{cool/heat}, \quad (17)$$

where $\forall$ is indoor volume, T_{in} is indoor air temperature, ~~is heat conduction from the building elements, is internal heat gain, is heat associated with infiltration or exfiltration, and is heat released from the air conditioning system~~and $Q_{cool/heat}$ is cooling or heating demand as specified in Eqs. 14 and 15. More details on parameterization of the terms in Eq. 17 can be found in appendix A and Bueno et al. (2012b) but are not reported here for brevity.

~~The same~~ A similar balance equation can be derived for latent heat to determine the time evolution of the indoor air specific humidity

$$\forall \rho L_v \frac{dQ_{in}}{dt} = Q_{gain} + Q_{inf} + Q_{sys},$$

~~which is composed of latent heat gain , infiltration latent heat , and latent heat from the air conditioning system . The terms on the right hand side of Eq. ?? are~~ as well as the dehumidification load Q_{dehum}, which is parameterized in Bueno et al. (2012b) but ~~are~~ is not detailed here for brevity. Note that energy consumption by gas combustion (e.g. cooking) Q_{gas} and water heating Q_{water} does not influence indoor air temperature or specific humidity, but such energy consumption sources appear in the waste heat Eqs. 14 and 15. These terms are determined from schedules (Bueno et al., 2012b).

2.1.5 Radiation Model with Vegetation

~~Urban trees provide shade to buildings and ground and reduce the amount of shortwave radiation within the urban canyon by reflection and transmission. It has been shown that a fraction of shortwave and longwave radiation is reflected or transmitted by leaves, variable depending on species of trees (Kong et al., 2017).As a result, trees can reduce surface temperatures significantly and consequently improve thermal comfort during the Summer. On the other hand, trees can induce drag and lower the wind speed within the urban area that can potentially contribute to reduced ventilation rates within the urban canyon (Krayenhoff et al., 2015) . Therefore, interactions between building and vegetation and their impact on the urban environments should be understood and modelled in detail. Only few studies have included such interactions in the urban microclimate models (Lee and Park, 2008; Krayenhoff et a~~

In VCWG, there are two types of vegetation: ~~surface covered vegetation~~ ground vegetation cover and trees. ~~Surface covered vegetation~~ Ground vegetation cover fraction is specified by ~~surface fraction covered by vegetation~~δ_s. Tree vegetation is specified by ~~three~~ four parameters: Leaf Area Index (~~LAI~~LAI), Leaf Area Density (~~LAD~~LAD) profile, cover fraction of tree canopy δ_t, and trunk height h_t. Both types of vegetation are specified with the same albedo α_V and emissivity ε_V. The VCWG user can change these input parameters for different vegetation structures. The parameterization of shortwave radiation accounts for the incoming direct and diffuse components of solar radiation, and it is used in this study to account for the shading effects of trees

on vertical and horizontal urban surfaces as well as the shading effect of buildings on trees. The total amount of shortwave radiation absorbed by each urban element S_i is calculated by adding the before-reflection absorption of shortwave radiation to the sum of multiple ~~infinite~~ reflections within the canyon (Redon et al., 2017). Parameterization of the longwave radiation received and emitted by the urban elements ~~is based on two assumptions that the surfaces are Lambertian and that only one reflection is allowed (Lee and Park, 2008)~~L_i assumes Lambertian surfaces. Again the total amount of longwave radiation absorbed by each urban element is calculated by adding the before-reflection absorption of longwave radiation to the sum of multiple reflections within the canyon (Loughner et al., 2012). Both shortwave and longwave radiation models are coupled to the vertical diffusion and the building energy models using feedback interaction. Detailed formulations are not provided here for brevity, but the reader is referred to the appendix A and original studies by Redon et al. (2017) and ~~Lee and Park (2008)~~Loughner et al. (2012) .

2.2 Experimental Field Campaign

2.2.1 Logistics

To evaluate results from VCWG, comprehensive microclimate field measurements were conducted from 15 July 2018 to 5 September 2018, in Guelph, Canada, which is detailed below. Guelph is located in southwestern Ontario, Canada, with cold Winters and humid Summers. The urban microclimate field measurements were conducted in the Reek Walk, a typical quasi two-dimensional urban canyon, located at the University of Guelph (43.5323°N and 80.2253°W). The rural microclimate field measurements were conducted in the Guelph Turfgrass Institute, a research green space area located at 43.5473°N and 80.2149°W, about 2 km northeast of the Reek Walk ~~.~~ (see Fig. 3). The average building height for the urban area is H_{avg}=20 m, and the plan area density is λ_p=0.55. The road, Reek Walk, where meteorological instruments ~~are~~ were installed, is covered by grass and asphalt in equal fractions. As shown in Fig. 3, urban trees are distributed across the neighbourhood.

The urban canyon axis is oriented in the northwest-southeast direction and x and y directions are set to be cross- and the along-canyon, respectively (see Fig. 4). The frontal area density λ_f varies from 0.31 to 0.51 when the approaching wind direction changes from along- to cross-canyon, respectively. Figure 4 shows that the predominant wind directions were from west and southwest, roughly perpendicular to the canyon axis, for the field campaign duration. Based on studies aimed to characterize the wind flow pattern within a built-up area (Zajic et al., 2011; Grimmond and Oke, 1999), the observed flow configuration alternates between skimming flow and wake interface regimes. However, the flow within the urban site is more complicated than the simple regimes and the associated parametrizations.

2.2.2 Instruments

In the rural site, wind speed, wind direction (at 10 m elevation), relative humidity, and temperature (at 2 m elevation) are collected on an hourly basis by the Guelph Turfgrass Institute meteorological station, which bears World Meteorological Organization (WMO) identifier 71833. ~~As shown in Fig. 3c, A Doppler mini SOnic Detection And Ranging (miniSODAR)~~

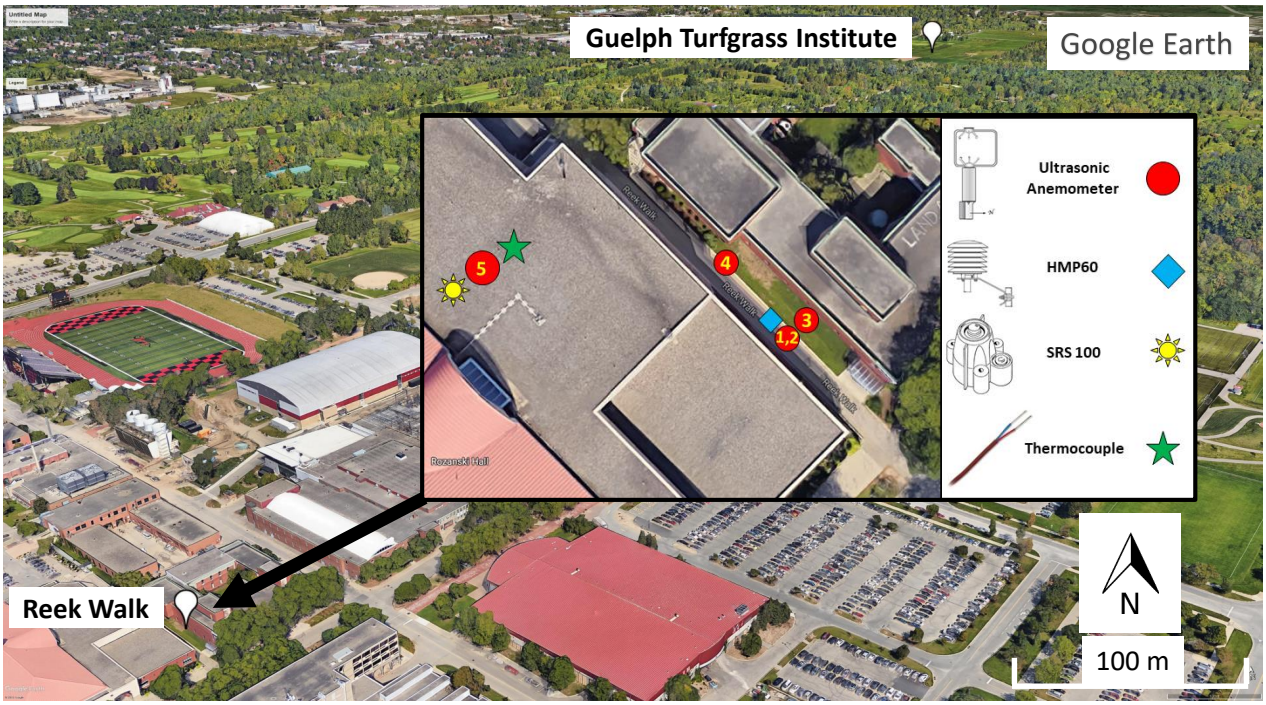

Figure 3. ~~(a) Top view~~ View of the rural weather station (Guelph Turfgrass Institute) and the urban site (Reek Walk, University of Guelph) ~~weather stations~~used for the microclimate field campaign; ~~(b)~~ inset map shows the location of the meteorological instruments in the urban site; ~~(c) rural weather station and the Doppler miniSoDAR instrument operated in the rural area;~~ images were obtained from Google Earth.

~~instrument from Atmospheric Systems Corporation (ASC)~~[2] ~~was also operated to measure wind speed and wind direction from 30 to 200 altitude at 10-vertical resolution, which output averaged data every 30 minutes. The miniSODAR data is not reported for brevity, but it was used to evaluate the reported WMO meteorological measurements.~~

Data from this station and those of EPW for London, Ontario, were combined to create an EPW dataset for model evaluation.

In the urban site, meteorological ~~information~~ data was collected within and above the canyon using five 81000 R. M. Young ultrasonic anemometers from Young U.S.A.[2] distributed horizontally and vertically. The accuracy and resolution of measurements for wind speed were $\pm 1\%$ and 0.01 $\mathrm{m\,s^{-1}}$, respectively, and for temperature were ± 2 K and 0.01 K, respectively. Four anemometers were deployed within the canyon, two were placed on a pole at heights of 2.4 m and 5.5 m elevation from the ground and the other two anemometers were located 4 m and 30 m away from the pole in the cross- and along-canyon directions, respectively. The fifth anemometer was deployed on a tripod on the roof at 2.5 m ~~height~~ elevation from roof level (see Fig. 3~~b~~). Three of these anemometers located at different elevations were used for comparison to VCWG model results. It has been

[2] ~~http://www.minisodar.com/sodar/~~

[2] http://youngusa.com/

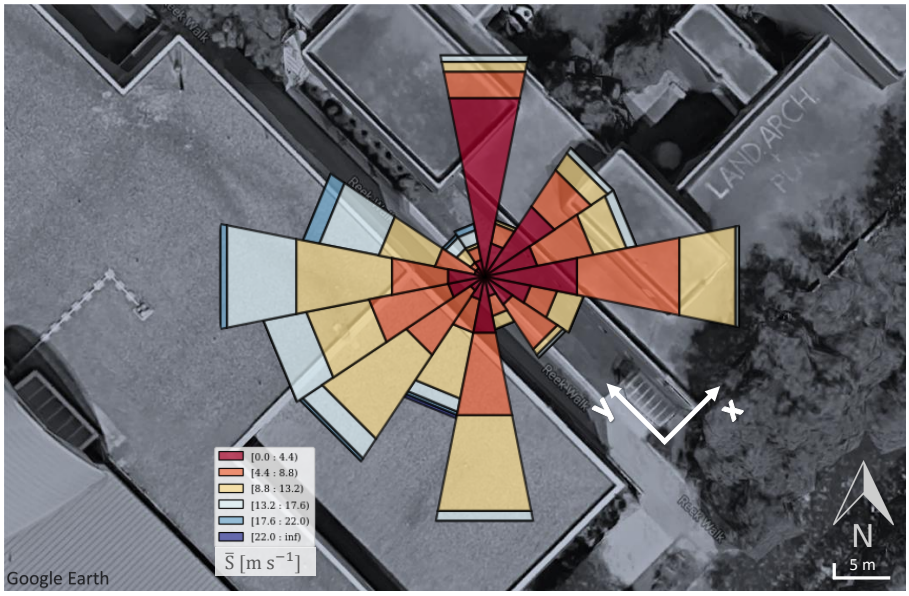

Figure 4. Wind rose plot above the urban site (Reek Walk, University of Guelph) between 15 July 2018 and 5 September 2018; image was obtained from Google Earth.

suggested that the sampling frequency should be at least 10 Hz to measure ~~turbulence (Balogun et al., 2010; Giometto et al., 2016)~~ atmospheric turbulence (Balogun et al., 2010; Giometto et al., 2016; Aliabadi et al., 2019). The anemometers were adjusted to sample three components of wind speed and air temperature at a frequency of 20 Hz using Campbell Scientific[3] CR6 data loggers. ~~A Pace SRS-100 solar radiation sensor from Pace Scientific[4] was placed at the roof to measure solar irradiance every minute with a resolution of 1 . Type E thermocouples from Omega[4] were also used near the surfaces at street and roof levels to measure temperature every minute. Data from the thermocouple sensors are not reported for brevity.~~ As shown in Fig. 3~~b~~, a Campbell Scientific HMP60 sensor was deployed at ~~the street level~~1 m elevation, which measured minute-averaged relative humidity with an accuracy of $\pm 3\%$ and temperature with an accuracy of ± 0.6K.

Wind tunnel tests were conducted to calibrate the wind speeds measured by the ultrasonic anemometers against a reference pitot tube (No figures are shown for this calibration). The HMP60 sensor was used as the reference measurement to calibrate all other temperatures and relative humidities measured, including those of the WMO station.

~~Wind rose plot above the urban site (Reek Walk, University of Guelph) between 15 July 2018 and 5 September 2018; ; image was obtained from Google Earth.~~

[3]https://www.campbellsci.ca

[4]~~https://www.pace-sci.com~~

[4]~~https://www.omega.ca~~

3 Results and Discussion

In this section, the VCWG model results are compared to the microclimate field measurements. We also explored the capability of the model to predict urban climate for ~~various urban configurations and in different climate conditions~~investigations of the effects of building dimensions, urban vegetation, building energy configuration, radiation configuration, seasonal variations, and other climates. The simplified urban neighbourhood is depicted in Fig. 2. In VCWG, buildings with uniformly-distributed height, equal width, and equal spacing from one another, represent the urban area. The computational domain height is five times the average building height, which makes it suitable for microclimate analysis (Santiago and Martilli, 2010; Aliabadi et al., 2017). A uniform Cartesian grid with $2\ \mathrm{m}$ vertical resolution is used, where buildings are removed from control volumes (see Fig. 2). The flow is assumed to be pressure-driven with the pressure gradient of $\rho \mathrm{u}_*^2/\mathrm{H}_{\mathrm{top}}$, which is decomposed into the x and y directions based on the wind angle. In this equation, the adjustment for wind angle is made based on canyon orientation and the incoming wind angle at the top of the domain. This pressure gradient is forced as source terms on the momentum Eqs. 8 and 9. The boundary condition for potential temperature and humidity equations (Eqs. 12 and 16) are determined from the rural model (see Fig. 1). Thus, the VCWG is aimed to calculate momentum and energy exchanges for the centre of each cell in the vertical direction based on the boundary conditions obtained from the rural model, the building energy model, and the radiation model.

~~Simplified urban area used in VCWG and corresponding layers of control volumes within and above the canyon. The height of the domain is five times of the average building height.~~

~~Fig. **??** shows the time series of and on the top of the domain over the course of a day in the rural area. Vapour pressure is always less than saturation pressure. However, vapour pressure tends closer to the saturation pressure under strongly stable condition from Local Solar Time () to . Assuming constant specific humidity up to the height of five times of average building height in the rural area does not violate the requirement for constancy of the water vapour pressure with height. Note, however, that this assumption does not apply to high altitudes where condensation may occur due to water vapour pressure exceeding saturation vapour pressure.~~

~~Diurnal variation of water vapour pressure and saturation vapour pressure on the top of the domain for the rural model.~~

3.1 Model-Observation Comparison

~~Temperature observations from Aircraft Meteorological Data Reports (AMDAR) in the Kansas City International airport (MCI) for 15 August 2018 was used to evaluate the results of the VCWG in the rural area. The commercial aircraft, mostly in North America, measure planetary boundary layer profiles of meteorological variables during climb and descent. The data are archived by National Oceanic and Atmospheric Administration (NOAA) and are freely available, which is accessed via the Meteorological Assimilation Data Ingest System (MADIS) portal [4]. These measurements are widely used to evaluate weather forecasting models and to understand climate under different conditions (Moninger et al., 2010; Zhang et al., 2019). AMDAR data report pressure altitude as the vertical position of the aircraft, which can be converted to pressure using the equation~~

[4] ~~https://amdar.noaa.gov/~~

proposed by WMO (2003)

$$P = 1013.25\left(1 - \frac{0.3048 z_p}{145366.45}\right)^{5.2553},$$

where is pressure in and is pressure altitude in . Then, the hypsometric equation can be used to determine the actual vertical position of the aircraft (Stull, 2016). Figure ?? shows the comparison between aircraft measured data and the rural model prediction of potential temperature profiles. The rural model is in reasonable agreement with the measured data and it can capture the atmospheric stability conditions and diurnal variation in potential temperature over a course of the day.

Comparison between the AMDAR data and the VCWG prediction of potential temperature profiles in the rural site.

The results of the VCWG are now compared to the measured data in collected during the microclimate field campaign. The actual weather data in the rural area including wind speed and wind direction at 10 m heightelevation, temperature and relative humidity at 2 m heightelevation, atmospheric pressure, and terms describing radiative components fluxes are used from the WMO and the field campaign datasetsassembled EPW dataset. The input parameters representing the urban area are listed in Table ??1. The simulations were run for two days starting from 19 weeks starting from 15 August 2018 with the first 24 hours treated as model spin-up period. For such analysis, the run time is approximately 15 minutes, however it can vary slightly depending on the grid sizespacing and time step.

Vertical profiles of potential temperature To compare VCWG results with measured meteorological variables from field campaign, the hourly BIAS and Root Mean Square Error (RMSE) are calculated over an entire diurnal cycle by considering the model results and measurements over a two-week period. These statistics are calculated for potential temperature at different heights, wind speed at different heights, mean horizontal wind speed , and specific humidity at street level are compared with the measurements at three heights in the urban area (see Figs. ??-??) . Additionally, normalized mean square error () and fractional bias () are calculatedto perform a quantitative error analysis near the ground. For the Urban Heat Island (UHI) the overall mean and standard deviation is calculated. BIAS and RMSE are defined as

$$NMSEBIAS = \frac{\sum_{i=1}^{n}(O_i - M_i)^2}{(\sum_{i=1}^{n} O_i)(\sum_{i=1}^{n} M_i)} \frac{\sum_{i=1}^{n}(M_i - O_i)}{n}, \tag{18}$$

$$FBRMSE = \frac{\sum_{i=1}^{n} O_i - \sum_{i=1}^{n} M_i}{0.5(\sum_{i=1}^{n} O_i + \sum_{i=1}^{n} M_i)} \sqrt{\frac{\sum_{i=1}^{n}(M_i - O_i)^2}{n}}, \tag{19}$$

where O_i and M_i are the field observations and results from the VCWG model, respectively (see Table ??) . While is a measure of the shift between the observed and predicted quantities, is a measure of the spread between observed and predicted quantities. For a perfect model, and are both equal to zero. As shown in Fig. ??, the potential temperature profiles show a typical diurnal cycle of atmospheric stability, starting with strongly stable condition after midnight () and persisting until just before the sunrise. Subsequently, the potential temperature profiles tend to neutral and unstable conditions as the sun rises (). During the daytime, the urban surfaces are absorbing solar radiation causing the atmosphere at the lower levels to rise in temperature resulting in strongly unstable conditions (and). As the sun sets in the late afternoon, the urban surfaces are cooled,

Table 1. List of input parameters used to ~~evaluate the~~ run VCWG ~~(The profile used~~ for ~~validation is shown in Fig~~model evaluation.~~2).~~

Parameter	Symbol	Value
Latitude °N	lat	43.53
Longitude °W	lon	80.22
Season	-	Summer
Plan area density	λ_p	0.44
Frontal area density	λ_f	0.55
Average buildings height [m]	H_{avg}	20
Average of leaf area density profile [m^2m^{-3}]	LAD	~~0.048~~ 0.28
~~Building Type~~ Trunk height [m]	h_t	4
Cover fraction of tree canopy	δ_t	0.48
Ground vegetation cover fraction	δ_s	0.5
Building type	-	Office
Urban ~~Albedos~~ albedos (roof, ground, wall, vegetation)	$\alpha_R, \alpha_G, \alpha_W, \alpha_V$	~~0.13, 0.1~~0.22, 0.08, 0.2, ~~0.25~~ 0.2
Urban ~~Emissivities~~ emissivities (roof, ground, wall, vegetation)	$\varepsilon_R, \varepsilon_G, \varepsilon_W, \varepsilon_V$	0.9, ~~0.93, 0.92, 0.96~~ 0.94, 0.9, 0.95
Rural ~~Overall Albedo~~ overall albedo	α_{rur}	~~0.1~~ 0.2
Rural ~~Emissivity~~ overall emissivity	ε_{rur}	0.93
Rural ~~Aerodynamic Roughness Length~~ aerodynamic roughness length [m]	z_{0rur}	0.1
~~Average boundary layer height~~ Ground aerodynamic roughness length [m]	z_{0G}	~~2000~~ 0.02
Roof aerodynamic roughness length [m]	z_{0R}	0.02
Vertical resolution [m]	Δz	2
Time step [s]	Δt	60
Canyon axis orientation °N	θ_{can}	−45

~~which result in weakly unstable and then again stable conditions for the following day. The temperature difference between the urban (inside canyon) and rural areas, which is known as Urban Heat Island (UHI), shows that UHI hits a peak in the late afternoon for the day of interest with an average of , which is in reasonable agreement with the study by Aliabadi et al. (2019) predicting an average UHI of in August 2017. The VCWG follows the trend of the measured potential temperature within and above the canyon, particularly during the daytime. The error analysis shows that the average and are quantified as and , respectively.~~ M_i and O_i are modelled and measured (observed) quantities. Here n is 14 because each hourly model-observation comparison is conduced over two weeks.

~~As shown in Fig. **??**, the vertical profile of mean horizontal wind speed obtained from the VCWG shows reasonable agreement with the field data and it is always within the error bar (5th and 95th hourly percentiles) at different heights. The~~ The error statistics are shown in Figs. 5 and 6. The average BIAS and RMSE for temperature are −1.43 and 1.56 K, respectively. It can be seen that the hourly BIAS is within 2 K and the model exhibits a cold BIAS most of the time with

~~Comparison between the field measurements and the VCWG prediction of potential temperature profiles in the urban site; diurnal variation~~

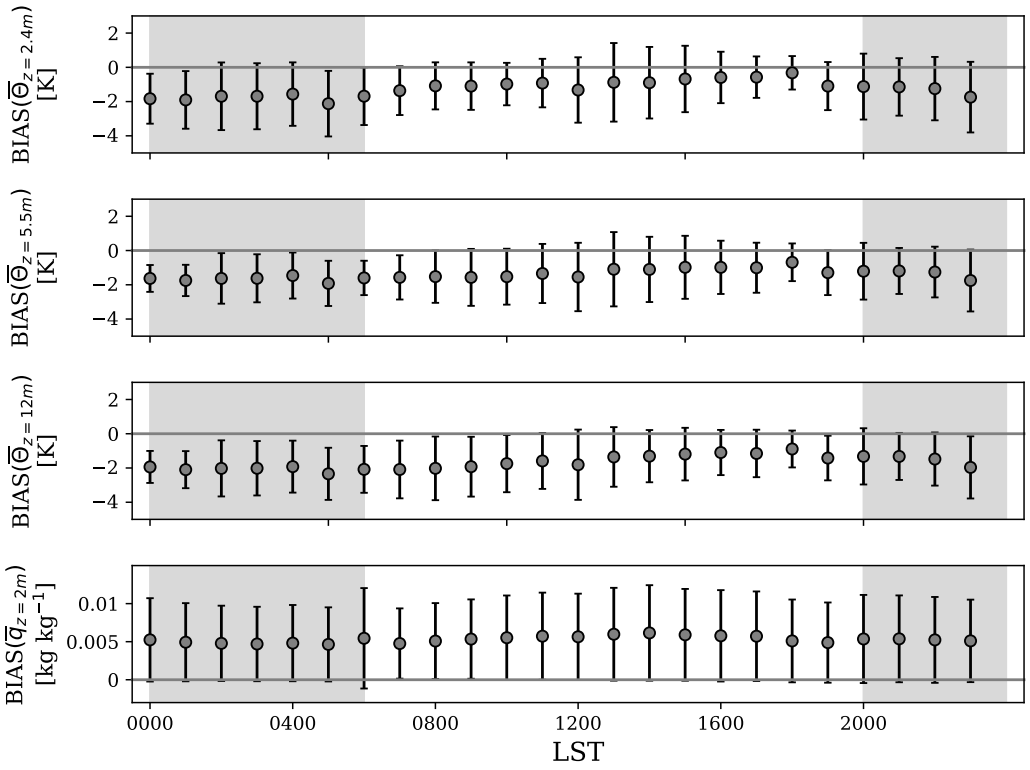

~~of UHI.~~

Figure 5. Comparison between the field measurements and the VCWG prediction of potential temperature (at various elevations) and specific humidity near the ground in the urban site; diurnal variation of BIAS and RMSE (error bar) are shown using data obtained over a two-week period; nighttime is shown with shaded regions; times in Local Standard Time (LST).

respect to the observations. The average BIAS and RMSE for specific humidity are 0.005 and 0.006 kgkg^{-1}, respectively. It can be seen that the hourly BIAS is within 0.005 kgkg^{-1} and the model exhibits a positive BIAS most of the time with respect to the observations.

The average BIAS and RMSE for wind speed are 1.06 and 1.32 ms^{-1}, respectively. It can be seen that the hourly BIAS is within 0.5 ms^{-1} at 2 and 5.5 m elevations, which indicates that at these elevations the effects of urban obstacles ~~, which induce drag and substantially reduce~~ inducing drag and reducing wind speed within the built-up area ~~, are captured~~ are captured well by the model. However, the BIAS is higher at 12 m elevation. Here VCWG exhibits a positive hourly BIAS up to 5 ms^{-1} during windy conditions in the mid afternoon period. It has been proposed that the oncoming boundary layer and the shear layer developing at the roof level significantly contribute in mass and momentum exchange between the in-canyon and above-canyon atmosphere (Kang and Sung, 2009; Perret and Savory, 2013). This shear layer is characterized by highly turbulent flow making ~~the measurements and simulations~~ realistic modeling more challenging (Salizzoni et al., 2011; Perret and Savory,

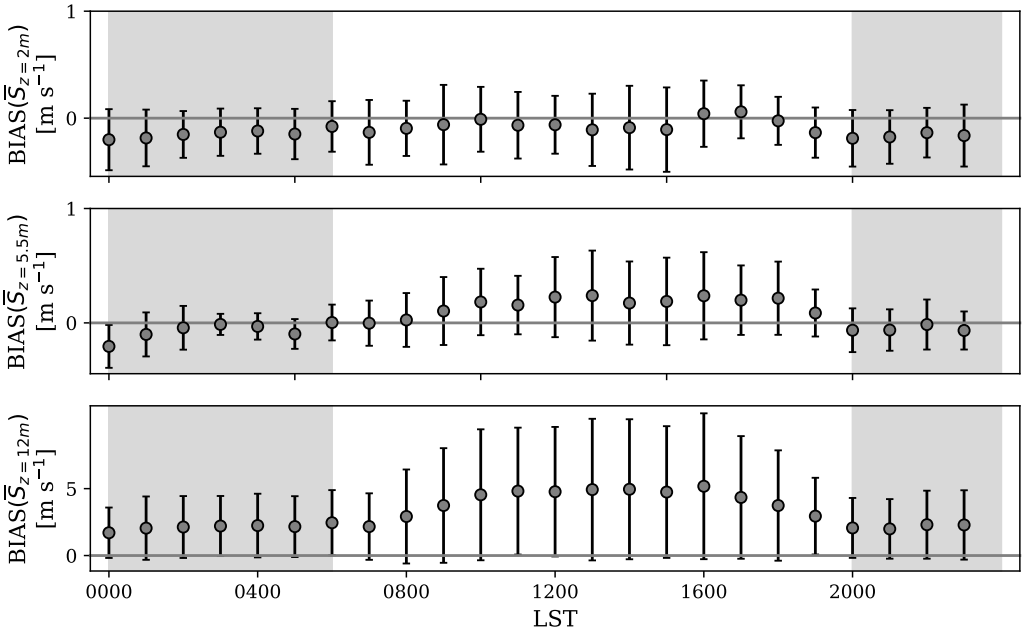

Figure 6. Comparison between the field measurements and the VCWG prediction of wind speed (at various elevations) in the urban site; diurnal variation of BIAS and RMSE (error bar) are shown using data obtained over a two-week period; nighttime is shown with shaded regions; times in Local Standard Time (LST).

2013) . Figure **??** exhibits that the VCWG deviates predicting the average wind speeds at this height, but there is an overall reasonable agreement with the measurements, with an average and of and , respectively (see Table **??**). thus explaining the model deviation from the observations at higher elevations closer to the shear layer.

Comparison between the field measurements and the VCWG prediction of mean horizontal wind speed profiles in the urban site.

As discussed in Sect. 2.2, the relative humidity was only measured at the street level. Figure **??** compares the 30-min average specific humidity measured in the field with the mean specific humidity within the canyon obtained from the VCWG. The vertical variation of in the canyon is not significant (not shown here). From error analysis, small average values of both and , 0.012 and 0.074 respectively, show an acceptable agreement with the experimental dataUHI for the observation is computed by considering the difference between the average temperature measurements inside the canyon and those temperatures provided by the EPW dataset. For VCWG, UHI is calculated by considering the difference between the average temperature prediction in the canyon from 2 m to average building height elevation and the average temperature prediction using the rural model for the same range of elevations. The average VCWG-predicted mean and standard deviation for UHI are $+1.20$ and 1.53 K,

respectively. These values are in reasonable agreement with observations reporting mean and standard deviation for UHI of +1.08 and 1.23 K, respectively.

Comparison between the field measurements and the VCWG prediction of specific humidity in the urban site.

Normalized Mean Square Error () and Fractional Bias () for potential temperature, mean horizontal wind speed, and specific humidity in the urban site. Parameter → ↓ 0000 0.002 −0.071 0.024 0.221 - - 0400 0.003 0.085 0.010 0.144 - - 0800 0.003 0.097 0.094 0.468 0.002 −0.045 1200 0.000 0.025 0.007 0.043 0.007 0.085 1600 0.003 0.096 0.047 0.327 0.006 0.080 2000 0.002 0.075 0.191 −0.532 0.031 0.175 Overall 0.002 0.051 0.062 0.112 0.012 0.074

3.2 Model Exploration

The VCWG performance is assessed by evaluating the model performance as a function of the urban configurations (λ_p, λ_f, LAD), different seasons (), different climate zones ()building energy configuration (building type, thermal efficiency, and coefficient of performance), radiation configuration (canyon aspect ratio and canyon axis angle), different seasons, different climate zones, and time series analysis. Except for the analysis of different seasons and climate zones, all explorations were performed by running VCWG to simulate the urban microclimate in Vancouver, Canada, for two weeks in August 2011. For exploration of different seasons, VCWG was run to simulate the urban microclimate in Vancouver, Canada, for an entire year in 2011. For different climate zones, VCWG was run to simulate the urban microclimate in other cities. More details on the explorations are provided in the subsequent sectionsand Tables ?? and ??. Such analyses will provide more information on spatiotemporal variation of the atmospheric meteorological states variables and reveal the complexity of urban microclimate modellingmodeling. Additionally, the potentials and limitations of VCWG will be discussed.

List of input parameters for the simulations designed to explore various urban configurations (The average foliage density of , , options are presented.). The latitude, longitude, aerodynamic roughness length scale, albedos, emissivities, building type, vertical resolution, and canyon axis orientation for these explorations are the same as in Table ??. Case Studies → Vegetation Seasons Input Parameters ↓ Season Summer Summer Summer Summer,Winter 0.25, 0.36, 0.44 0.44 0.44 0.44 0.55 0.42, 0.55, 0.69 0.55 0.55 20 15, 20, 25 20 20 Average of Leaf Area Density (LAD) profile 0.048 0.048 0.039, 0.048, 0.104 0.048

3.2.1 Urban Plan and Frontal Area Densities

In urban canopy modellingmodeling, two parameters often used to describe building and canyon geometries are plan area density (λ_p), which is the ratio of the total plan area of the buildings to the total urban earth flat-earth surface area, and the frontal area density (λ_f), which is the ratio of the total frontal area (facing wind) to the total urban earth flat-earth surface area. An urban area can be characterized with different types of land use, where each type may have different plan and frontal area densities, they can vary from high value values in industrial districts to low values associated with the land used for public transportation (Wong et al., 2010). Any Most development in an urban area could be associated with changing λ_p and λ_f, which can alter the local climate in different ways such as air and surface temperatures, building energy consumption, and thermal and wind comfort levels (Coutts et al., 2007; Emmanuel and Steemers, 2018).

~~Three case studies , , and with values of , , and , respectively,~~ Two case studies λ_p=0.36 and 0.56 are explored to assess the model and see how the urban microclimate changes when the plan area density increases ~~. The other parameters , which describe the cases, including the urban site (Guelph, Ontario, Canada), building dimensions, leaf area density profile, and the season that the VCWG was run, are listed in Table ??~~while keeping the other parameters unchanged. Figure 7 shows typical nighttime and daytime profiles of potential temperature and mean horizontal wind speed in the urban area associated with running the model for one day. Higher λ_p is associated with more urban surfaces allowing greater absorption of longwave and shortwave radiation and therefore higher level of building energy consumption for cooling ~~, particularly during the day~~(or heating). It is depicted in Fig. 7 that the case with higher λ_p shows higher potential temperature profiles during the day and night. During the nighttime, the temperature difference between the cases is not as much as the daytime, however, still higher temperatures can be obtained when plan area density is higher. Additionally, more urban surfaces impose more drag and consequently reduce wind speed (see Fig. 7).

Further investigations are performed for different frontal area densities λ_f= ~~0.42,~~ 0.55 ~~, and 0.69, equivalent to the average building heights of 15, 20, and 25 , respectively (see Table ??)~~and 0.84 by running the model for one day. At first glance, the cities with high-rise buildings are supposed to release more heat into the outdoor environment due to greater urban surfaces, but tall buildings can provide solar shading during the daytime and decrease temperature of the surfaces. As shown in Fig. 8, any increase in λ_f reduces potential temperature in the urban area during the day. However, due to the lack of shortwave radiation over nighttime and that urban surfaces are the main source of heat that can be released into the atmosphere, higher λ_f ~~does not necessarily result~~ results in higher potential temperatures at nighttime due to radiation trapping. Moreover, ~~increased~~ increasing frontal area density tends to increase surface roughness and consequently slow down wind speed within the canyon during daytime, which can also be depicted in Fig. 8.

The VCWG results are also consistent with previous studies in the literature (Coutts et al., 2007; Zajic et al., 2011; Santiago et al., 2014). The findings reported here highlight the careful considerations that need to be accounted for by city planners.

3.2.2 Leaf Area Density

Urban trees interact with the other urban elements by providing shade to reduce temperature of surfaces, removing the stored heat in the canyon substantially, and induce drag to reduce wind speed (Loughner et al., 2012; Krayenhoff et al., 2015; Redon et al., 2017). The capability of the VCWG to take into account these effects is assessed by investigating ~~three~~ two case studies with ~~, and~~ LAD representing trees with ~~low to high~~ average foliage densities of ~~0.039, 0.048, and 0.104~~ 0.08 and 0.14 $\mathrm{m^2 m^{-3}}$, respectively~~(see Table ??)~~, by running the model for one day. The result is shown in Fig. 9. The cooling effect of the trees is evident when the average LAD of tree foliage increases~~from to~~ , resulting in a decrease of potential temperature within the canyon, particularly during the day when the shading effect of trees lowers the surface temperatures. Such effects not only can improve thermal comfort at the pedestrian level, but also reduce the building energy consumption in the Summertime (Souch and Souch, 1993; Akbari et al., 2001). On the other hand, the urban trees are thought to be a sink of momentum and kinetic energy by exerting drag and damping the flow fluctuations (Giometto et al., 2017; Yuan et al., 2017). This effect cannot be ~~modelled~~ modeled very well by VCWG, which predicts the same level of wind speed within the canyon at ~~all~~ the two LAD

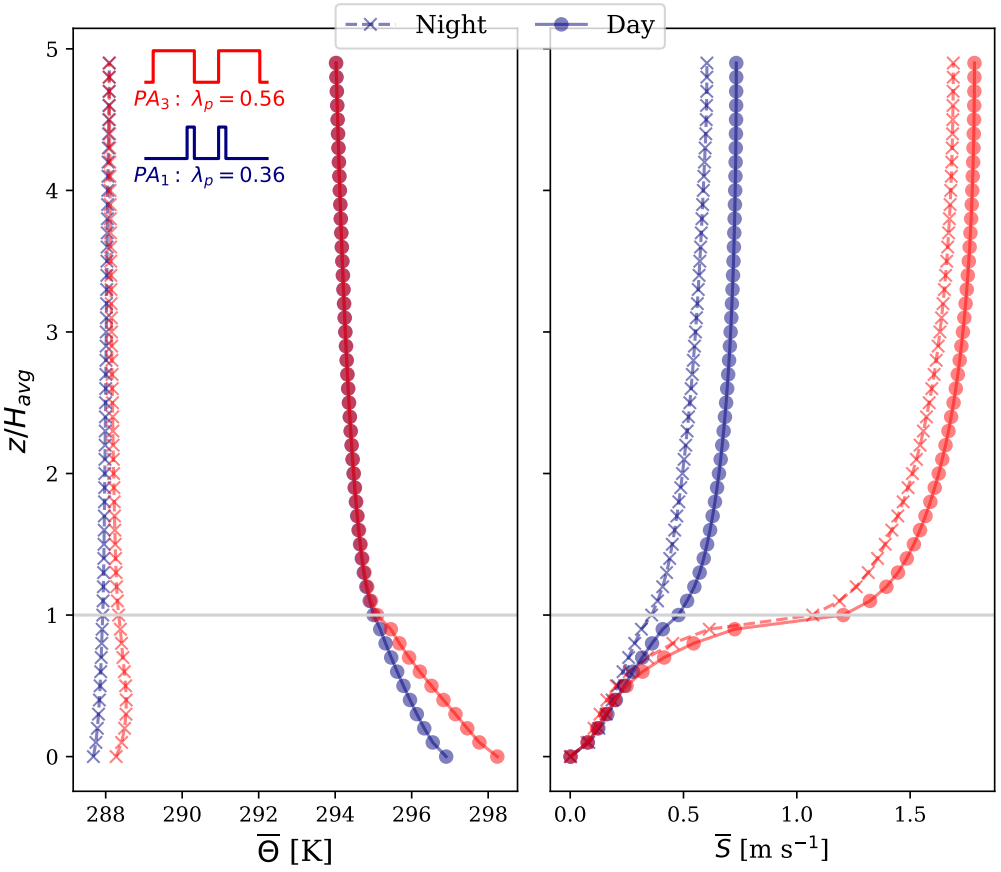

Figure 7. Effect of plan area density λ_p on the profiles of potential temperature and mean horizontal wind speed during nighttime (averaged from 0000 to 0400 LST) and daytime (averaged from 1200 to 1600 LST).

profiles. The analysis obtained from this exploration is in reasonable agreement with previous works (Souch and Souch, 1993; Loughner et al., 2012; Giometto et al., 2017; Yuan et al., 2017). Trees are recognized to be essential urban elements to moderate extreme wind speeds and heat waves, particularly during the warm season.

3.2.3 Building Energy Configuration

The building energy model within VCWG is explored by running VCWG under different building types, cooling system Coefficient Of Performance (COP), and heating system thermal efficiency η_{heat}. Two building types are considered, a school and a small office, with specifications provided in Table 2. It can be noted that the infiltration rate, ventilation rate, volumetric flow for water heating, and waste heat fluxes associated with gas combustion, electricity consumption, and lighting for a school are substantially greater than those for a small office. Note that construction material properties are also different for a

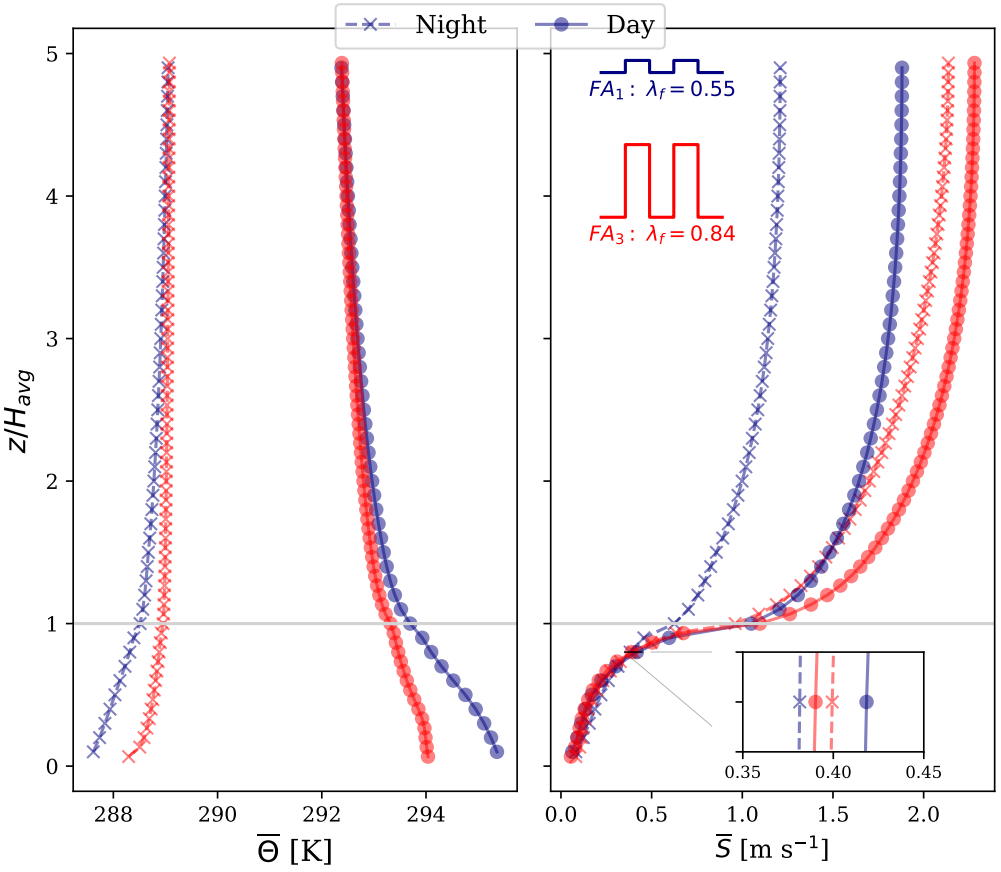

Figure 8. Effect of frontal area density λ_f on the profiles of potential temperature and mean horizontal wind speed during nighttime (averaged from 0000 to 0400 LST) and daytime (averaged from 1200 to 1600 LST).

school and small office within VCWG schedules, but the differences are not specified here for brevity. Two sets of COP and η_{heat} are considered for a small office. For an energy-efficient building values COP=3 and η_{heat}=0.8 are used, while for a low-energy-efficient building values COP=1 and η_{heat}=0.4 are used.

Figure 10 shows the effect of building type on hourly mean and standard deviation of cooling/heating waste heat, dehumidification waste heat, gas combustion waste heat, water heating waste heat, and UHI calculated for running the model for two weeks. The waste heat fluxes are reported per unit building footprint area. It can be noted that the building energy system operates under heating mode for a few hours around sunrise, while it runs under cooling mode for the majority of daytime period. It can be noted that a school results in higher values of waste heats and UHI, so the potential impact of an energy-intensive school on the urban climate may be higher than a small office. It is noted that a school generates substantial waste heat fluxes associated

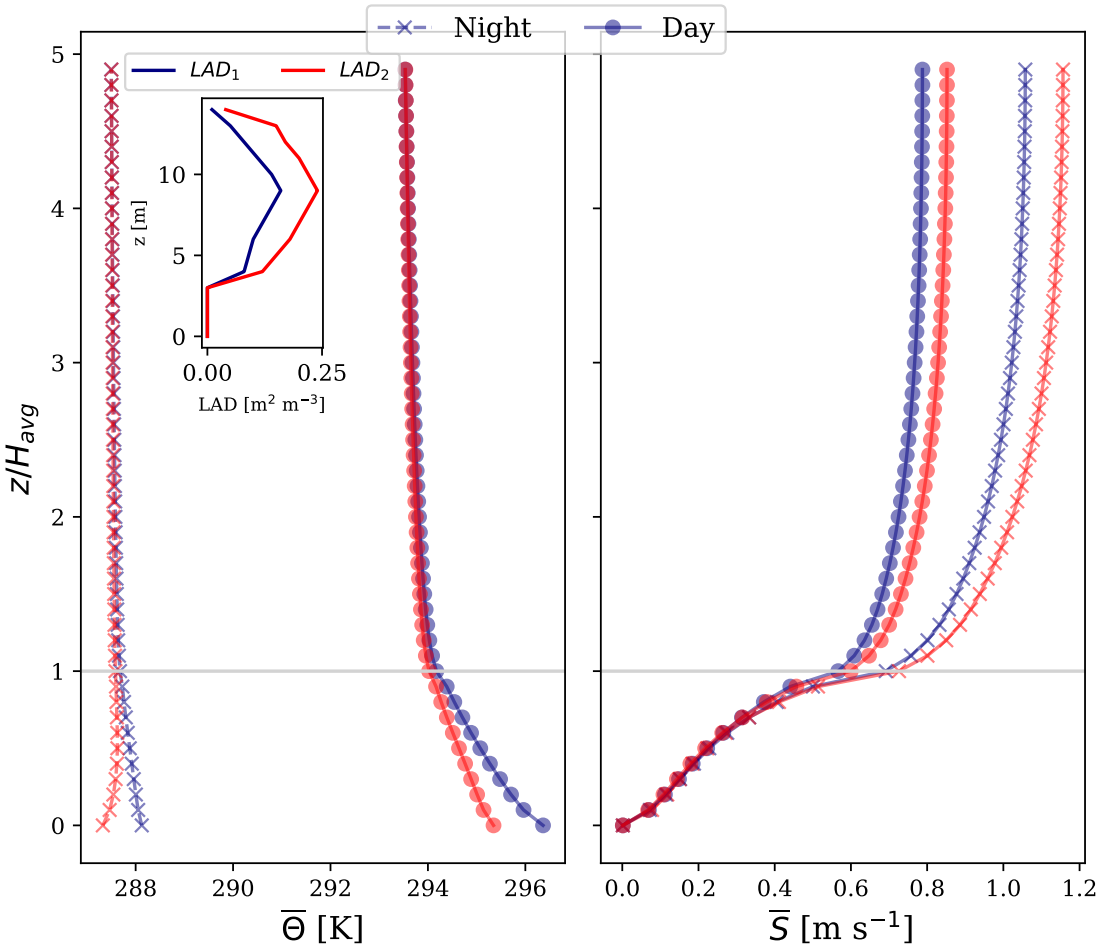

Figure 9. Effect of leaf area density profiles on the profiles of potential temperature and mean horizontal wind speed during nighttime (averaged from 0000 to 0400 LST) and daytime (averaged from 1200 to 1600 LST).

Table 2. Specifications of the building energy configuration for two building types. The infiltration unit is Air Changes per Hour [ACH].

Building type → Building specification ↓	Small Office	School
COP	3.07	3.2
η_{heat}	0.8	0.75
Infiltration [ACH]	0.2	0.7
Ventilation [Ls^{-1}]	275	55.583
Glazing ratio	0.21	0.34
Average volumetric flow for water heating [Lh^{-1}]	11.4	161
Average waste heat flux from gas combustion [Wm^{-2}]	0	0.617
Average waste heat flux from electricity consumption [Wm^{-2}]	4	10.3
Average waste heat flux from lighting [Wm^{-2}]	3.08	5.09

with gas combustion (due to cooking activities) and water heating (for domestic use) because of higher occupancy compared to a small office.

Figure 11 shows the effect of building cooling system Coefficient Of Performance (COP) and heating system thermal efficiency (η_{heat}) on hourly mean and standard deviation of waste heats and UHI calculated for running the model for two weeks. It can be noted that lower COP and thermal efficiency result in higher values of waste heats and UHI, so the potential impact of an energy-intensive building on the urban climate may be higher than an energy-efficient building. Most particularly, it can be noted that lower heating system thermal efficiency results in greater waste heat flux for water heating.

3.2.4 Radiation Configuration

The radiation model within VCWG is explored by running VCWG under different canyon aspect ratios $\mathrm{H_{avg}/w}$ and different street canyon axis angles θ_{can} with respect to the north axis to investigates the effects on direct solar radiation, diffuse solar radiation, and longwave fluxes. For exploring the effect of canyon aspect ratio on these fluxes values of $\mathrm{H_{avg}/w}$=3 and 2 are used with keeping θ_{can}=0 °, while for exploring the effect of street canyon axis angle on these fluxes values of θ_{can}=90 and 0 ° with respect to the north axis are used with keeping $\mathrm{H_{avg}/w}$=2. For these explorations VCWG is run for two weeks and hourly mean values for radiative fluxes are reported.

Figure 12 shows the radiative fluxes for different canyon aspect ratios. It can be seen that the direct solar radiation flux absorbed by the roof is not affected by the canyon aspect ratio, while the interior surfaces of the urban canyon absorb lower amounts of direct solar radiation flux for the higher canyon aspect ratio. This is expected since a higher canyon aspect ratio creates more shading effects on interior canyon surfaces compared to a lower canyon aspect ratio. Furthermore observe that the tree canopy receives slightly higher direct solar radiation flux compared to the road (consisting of ground and surface cover vegetation), for both canyon aspect ratios, because the tree canopy is at a higher elevation and more exposed to incoming

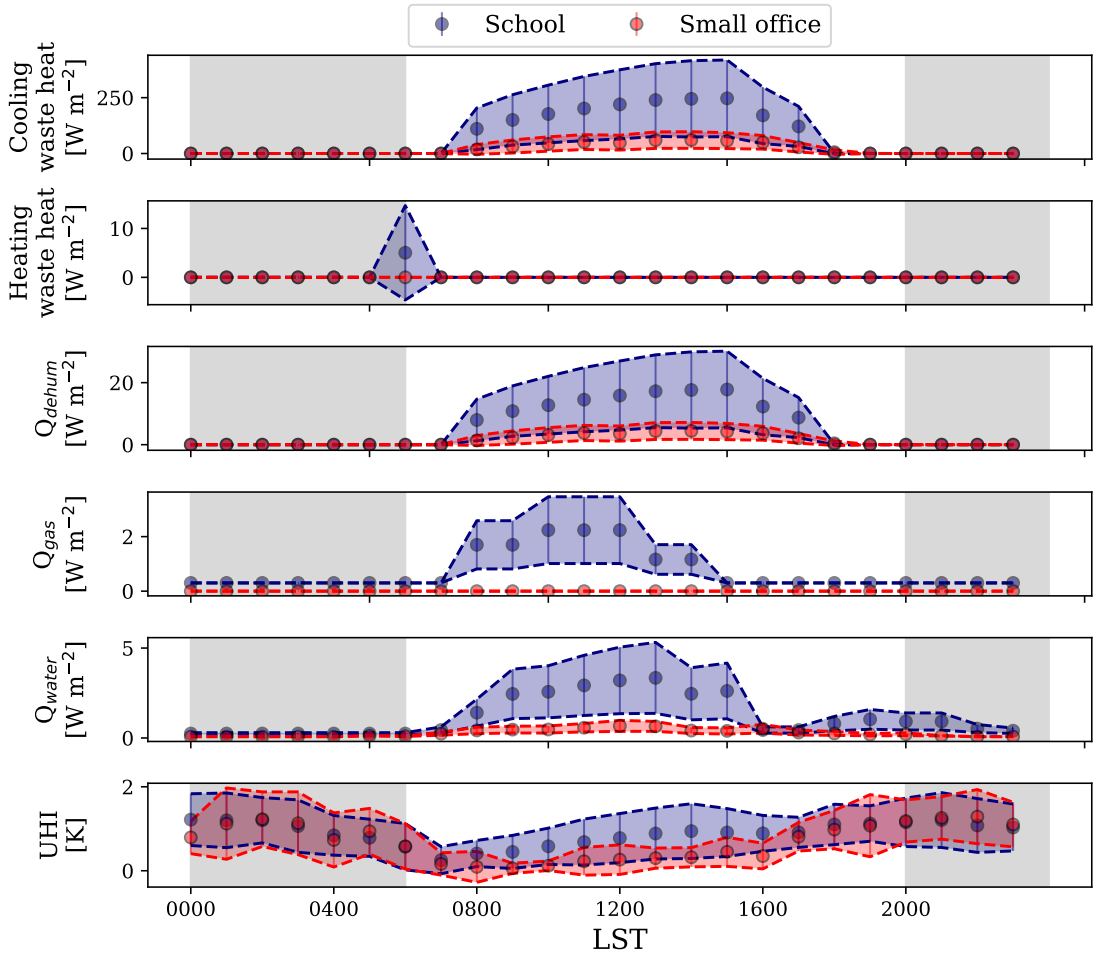

Figure 10. Effect of building type on cooling/heating waste heat, dehumidification waste heat, gas combustion waste heat, water heating waste heat, and UHI; diurnal variation of mean and standard variation (error bar) are shown using data obtained over a two-week period; nighttime is shown with shaded regions; times in Local Standard Time (LST).

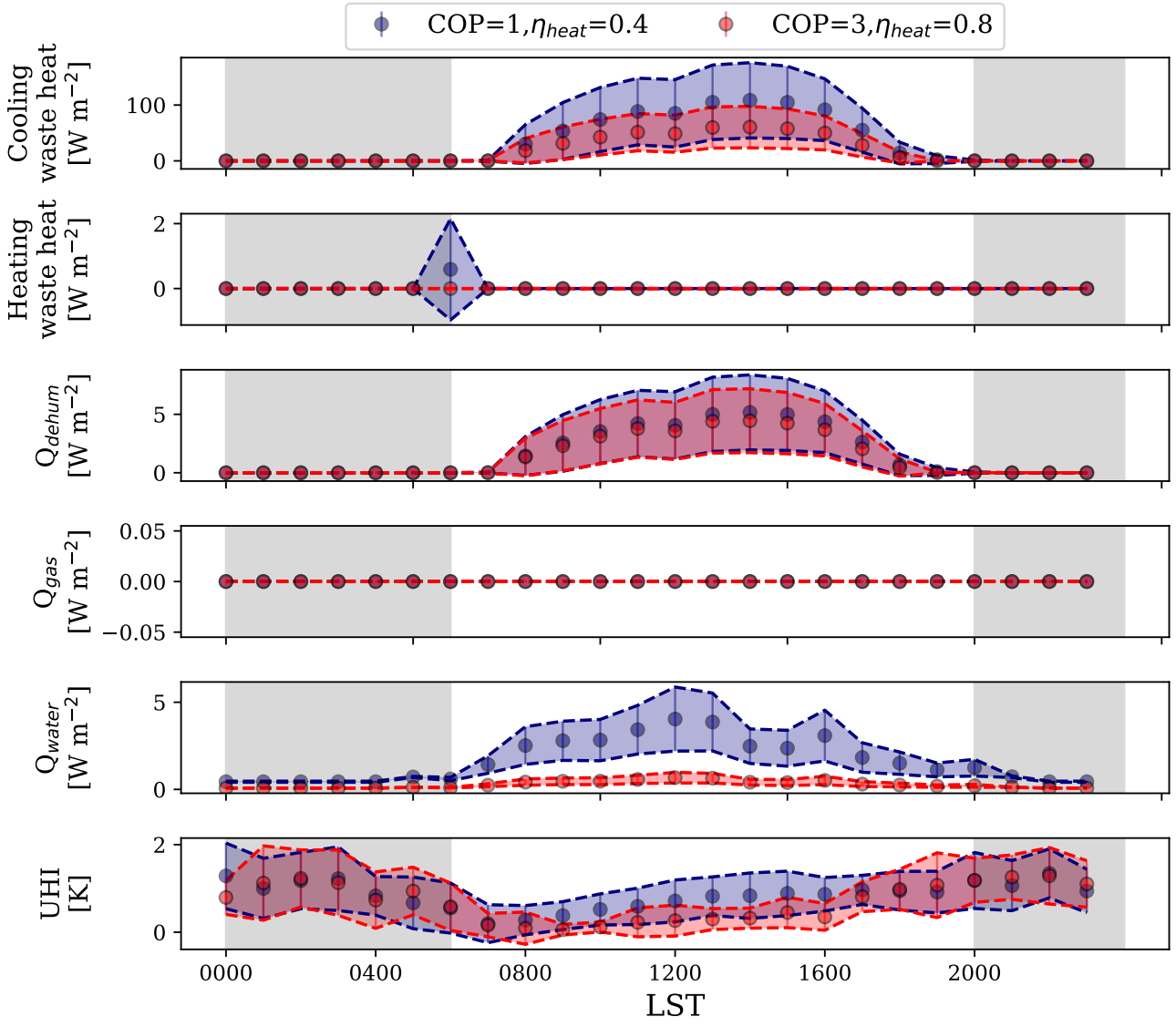

Figure 11. Effect of building cooling system Coefficient Of Performance (COP) and heating system thermal efficiency (η_{heat}) on cooling/heating waste heat, dehumidification waste heat, gas combustion waste heat, water heating waste heat, and UHI; diurnal variation of mean and standard variation (error bar) are shown using data obtained over a two-week period; nighttime is shown with shaded regions; times in Local Standard Time (LST).

direct solar radiation flux. Likewise, it can be seen that the diffuse solar radiation flux absorbed by the roof is not affected by the canyon aspect ratio, while the interior surfaces of the urban canyon absorb lower amounts of diffuse solar radiation flux for the higher canyon aspect ratio. Focusing on the net shortwave radiation flux components, i.e. the incoming shortwave radiation flux $S^{\downarrow}$ and the outgoing shortwave radiation flux $S^{\uparrow}$, it is noted that for the higher aspect ratio canyon the flux is more pronounced near noon Local Standard Time (LST), while for the lower aspect ratio canyon the flux is pronounced in more hours before and after noon LST. This expected since a higher aspect ratio canyon creates more shading effects on times before and after noon LST compared to a lower aspect ratio canyon. Focusing on the net longwave radiation flux components, i.e. the incoming longwave radiation flux $L^{\downarrow}$ and the outgoing longwave radiation flux $L^{\uparrow}$, it is noted that the canyon aspect ratio does not influence the radiation flux components substantially.

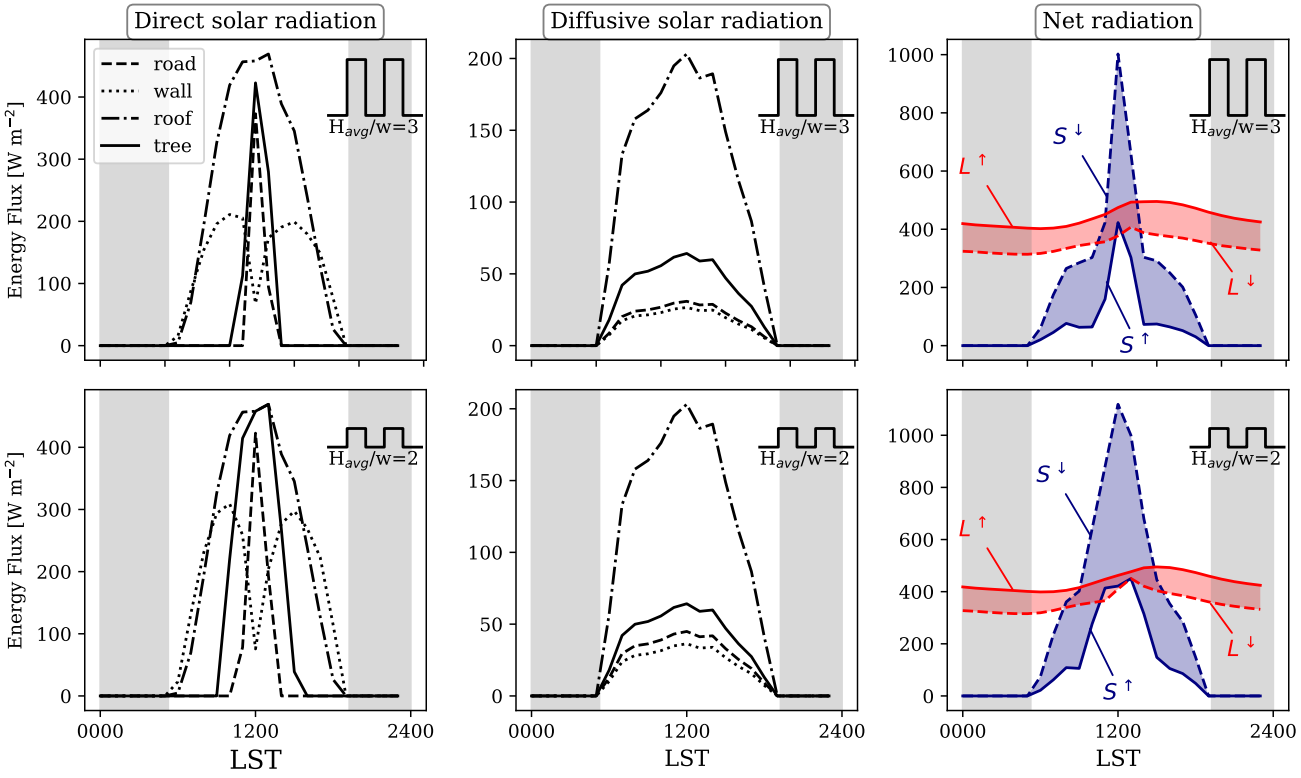

Figure 12. Effect of canyon aspect ratio H_{avg}/w on hourly mean direct solar radiation, diffuse solar radiation, and longwave radiation fluxes; diurnal variation of mean is shown using data obtained over a two-week period; nighttime is shown with shaded regions; times in Local Standard Time (LST).

Figure 13 shows the radiative fluxes for different street canyon axis angles. It can be seen that the direct solar radiation flux absorbed by the roof is not affected by the street canyon axis angle, while the interior surfaces of the urban canyon show

different responses to absorbing the direct solar radiation flux given the street canyon axis angle. With θ_{can}=90 ° the road surface absorbs the direct solar radiation flux in hours just after sunrise and before sunset, given that this flux reaches the road surface only at high solar zenith angles and solar azimuth angles from the east and west directions. On the other hand, with θ_{can}=0 ° the road surface absorbs the direct solar radiation flux in hours around noon LST, given that this flux reaches the road surface only at low solar zenith angles and solar azimuth angles from the north direction. Same trend can be observed for direct solar radiation flux absorbed by the tree canopy although the distribution is widened over more diurnal hours given the fact that the tree canopy is at a higher elevation and more exposed to incoming direct solar radiation flux compared to the road. With θ_{can}=90 ° the wall surface absorbs the direct solar radiation flux in most hours during midday, given that this flux reaches the wall surface with multiple combinations of solar zenith angles and solar azimuth angles. On the other hand, with θ_{can}=0 ° the wall surface absorbs little direct solar radiation flux in hours around noon LST, given that this flux does not reach the wall surface when the solar azimuth angle is from the north direction. In contrast, it can be seen that the diffuse solar radiation flux absorbed by all urban surfaces is not affected by the street canyon axis angle appreciably. Focusing on the net shortwave radiation flux components, the most notable difference is that the flux components are widened over a large range of diurnal hours when θ_{can}=90 ° due to the fact that multiple combinations of solar zenith and azimuth angles expose various urban surface to the incoming direct solar radiation flux. On the other hand when θ_{can}=0 ° the components of the shortwave radiation flux peak closer to noon LST and exhibit lower values after sunrise and before sunset hours since the combinations of solar zenith and azimuth angles do not expose interior canyon surfaces to the incoming direct solar radiation flux at those hours. Focusing on the net longwave radiation flux components, it is noted that the street canyon axis angle does not influence the radiation flux components substantially.

3.2.5 Seasonal Variations

In the context of urban development, there are no unique and pre-designed guidelines which can be extended to all built-up areas because careful considerations of geographical features and seasonal variations are required. For example, the type of urban vegetation, which is well suited for both warm and cold seasons in fulfilling thermal and wind comfort standards, can be climate specific (Jamei et al., 2016). Winter is characterized by larger zenith angles and lower solar radiation received by the surfaces compared to the other seasons. In Winter, the temperature difference between indoor and outdoor environment is higher than the Summer, thus, seasonal variations can alter building energy consumption and UHI effects substantially (Bueno et al., 2011).

~~Figure ??~~ Figure 14 shows the VCWG results for the ~~diurnal variations of potential temperature profiles in both rural and urban areas and the UHI for the Wintertime in Guelph~~hourly mean values of UHI in each month of the year 2011 in Vancouver, Canada. In ~~the Winter, the urban boundary layer is almost always unstable, while the rural boundary layer is almost always stable or weakly stable due to the lack of significantly positive or negative heat flux at the surface in such cold weather. On the other hand, due to the dominance of building waste heat and the anthropogenic activities in the Wintertime, there is always heating in the urban area, which creates an unstable boundary layer coupled to a weakly stable rural boundary layer most of the time. The VCWG predicted positive UHI for~~ this exploration LAD is kept constant for all the months of the ~~whole day, which is~~

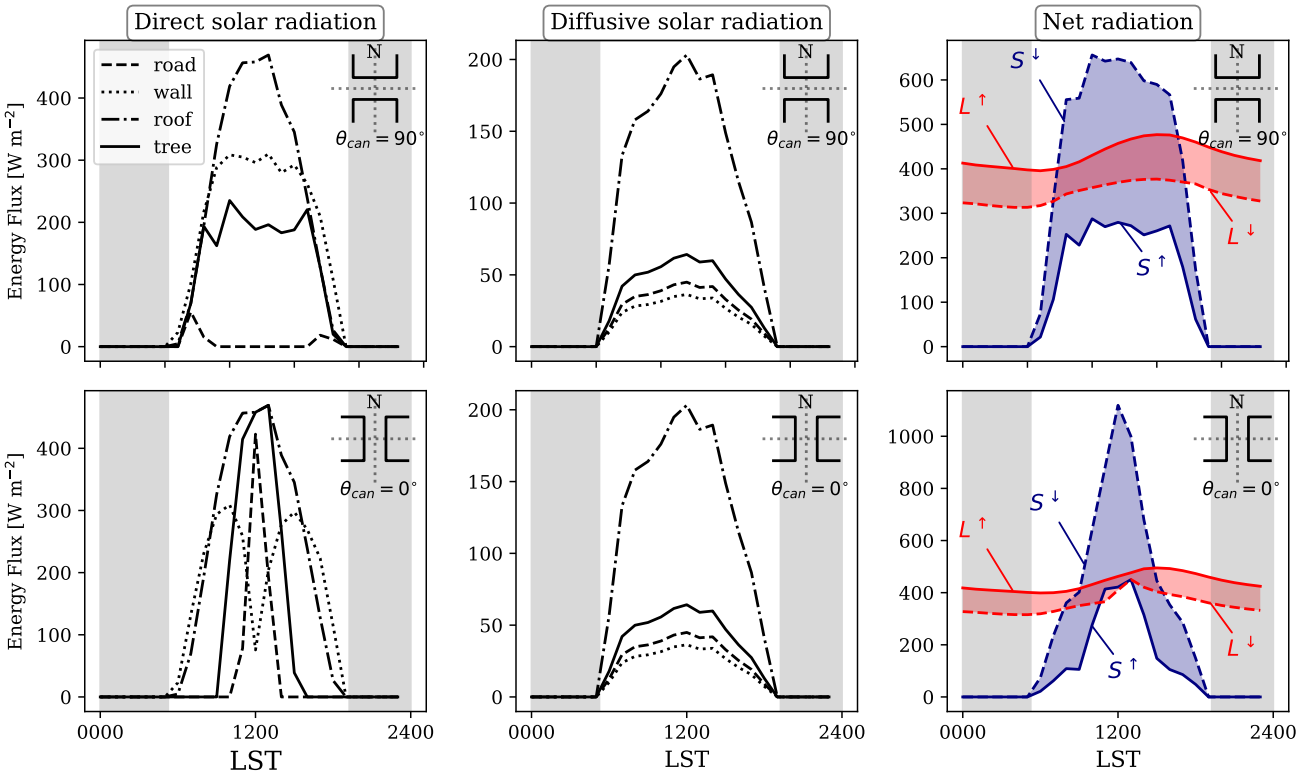

Figure 13. Effect of street canyon axis angle θ_{can} on hourly mean direct solar radiation, diffuse solar radiation, and longwave radiation fluxes; diurnal variation of mean is shown using data obtained over a two-week period; nighttime is shown with shaded regions; times in Local Standard Time (LST).

~~often observed during cold seasons depending on the climate zone (Cui and De Foy, 2012; Rasul et al., 2016; Yang and Bou-Zeid, 2018) . The thermal comfort and energy savings advantages of UHI is now revealed in the Winter for cold climate zones, which creates warmer cities and makes buildings less exposed to cold and consequently reduced building energy demand for heating (Santamouris et al., 2001; Oikonomou et al., 2012)~~year. It can be noted that in general daytime UHI values are lower than nighttime values, as expected. Given the moderate climate of Vancouver, other than diurnal timing of UHI, no substantial change in the magnitude of UHI is predicted for different months of the year. The seasonal variation of UHI as predicted by VCWG is in agreement with a similar map reported by Oke et al. (2017).

3.2.6 Other Climates

~~Generation of UHI is mainly attributed to the building material and geometry, sky view factor, cyclic factors, and anthropogenic heat. The process of urbanization increases heat storage in the city by trapping longwave radiation in the canyon by limiting~~

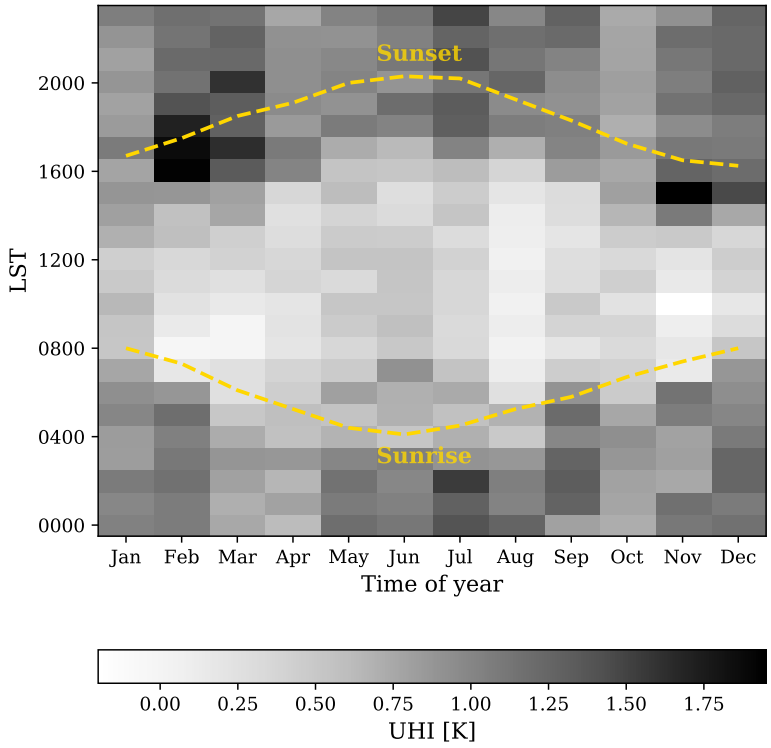

Figure 14. ~~Diurnal variation~~ Hourly mean values of ~~potential temperature profiles~~ UHI in ~~the urban and rural areas~~ each month in ~~the Winter at Guelph~~Vancouver, Canada, as predicted by VCWG; sunrise and sunset times are denoted by dashed lines.

~~the sky view factor, increasing anthropogenic heat fluxes, increasing absorption of shortwave radiation, and decreasing natural cooling due to removal of green spaces (Coutts et al., 2007; Rizwan et al., 2008). Thus, urban configuration, the Universal Transverse Mercator (UTM) zones, where each are exposed to a different solar path, and land use types mainly control intensity of UHI in different seasons. UHI could be observed during the daytime or nighttime, depending on the wind speed and seasonal time (Klysik and Fortuniak, 1999) or types of urban land use (Siu and Hart, 2013), which signify spatial variation and temporal variation of UHI in a city.~~

The VCWG was further explored by predicting UHI in different cities with different climate zones including Buenos Aires ~~in December 1983~~in January 1988, a city in the southern hemisphere with hot and humid climate, ~~Tucson in August 1967~~Phoenix in August 1980, which has a dry desert climate, Vancouver in August 2011, representing a moderate oceanic climate, Osaka in August 1996, with subtropical climate, and Copenhagen in August 1999, representing cold and temperate climate. ~~Input parameters for each case are detailed in Table ??.~~ All simulations were conducted for ~~one day of the month~~ two weeks and then mean and standard variation of diurnal variations in UHI were calculated (see Fig. 15).

The result shows ~~about~~ a diurnally-averaged value of +1.0 K for UHI for Buenos Aires~~during the night~~, which is consistent with a previous study measuring ~~an average UHI of~~ a diurnally-averaged UHI of +1.3 K (Bejarán and Camilloni, 2003). The temperature difference between rural and urban areas in a dry and hot climate like ~~Tucson~~ Phoenix is relatively higher with the ~~average~~ diurnally-averaged UHI value of +2.4 K, in agreement with a ~~measured average UHI of~~ study measuring a diurnally-averaged UHI of +2.5 K ~~(Comrie, 2000; Wang et al., 2016)~~(Hawkins et al., 2004; Fast et al., 2005). In case of Vancouver, the VCWG predicted ~~UHI from the afternoon to~~ a diurnally-averaged value of +0.7 K for UHI and showed high intensity ~~in the late afternoon~~before sunrise. VCWG predicted a maximum UHI of +1.9 K in Vancouver, in agreement with ~~measured~~ a measured maximum value of +1.4 K before sunrise (Runnalls, 1995; Lesnikowski, 2014; Ho et al., 2016). Case studies in Japan have reportedly obtained urban warming in large and developed cities such as Osaka, which is the interest in this study, and Tokyo in the afternoon (Leal Filho et al., 2017). This effect is also predicted by VCWG that showed the ~~average UHI of~~ diurnally-averaged UHI of +0.8 K, which is consistent with other studies measuring ~~an average UHI of~~ a diurnally-averaged UHI of +1.2 K (Kusaka et al., 2012; Leal Filho et al., 2017). UHI in Copenhagen is reported to change between +0.5 and +1.5 K depending on the wind speed, which agrees reasonably well with the VCWG prediction of UHI varying from slightly negative values during the daytime to +1.6 K ~~, as well as intensifying in the afternoon~~ during the nighttime (Mahura et al., 2009).

~~List of input parameters for the simulations designed to explore various climate zones. The aerodynamic roughness length scale, albedos, emissivities, building type, vertical resolution, and canyon axis orientation for these explorations are the same as in Table **??**. Case Studies → Input Parameters ↓ Latitude — 34.82 32.12 49.20 34.78 55.63 Longitude 58.53 110.93 123.18 — 135.45 — 12.67 Season Summer Summer Summer Summer Summer 0.44 0.44 0.44 0.44 0.44 0.82 0.55 0.55 0.55 0.55 30 20 20 20 20 Average of Leaf Area Density (LAD) profile 0.048 0.048 0.048 0.048 0.048~~

3.2.7 Time Series Analysis

The VCWG was run for two weeks ~~starting from 11 August 1967 in Tucson, where the EPW weather file is continuously available for two weeks~~in August 2011 in Vancouver, Canada, to observe the day-to-day prediction of the temperature. Hourly time series of VCWG-predicted urban and rural temperatures with the corresponding EPW relative humidity, incoming direct and diffusive solar radiation~~from sky~~, and mean horizontal wind speed in the rural area are shown in Fig. **??**16. The model can capture the cyclic pattern of temperature (and UHI) that is affected by the other ~~meteorological quantities~~forcing meteorological variables. For example, high UHI is mainly ~~obtained during nighttime~~ predicted during nighttime with preceding days dominated by high direct and diffuse incoming solar radiation and ~~urban cool island during daytime. In a mostly-cloudy day of 13 August 1967, less incoming radiation is associated with lower temperatures and a lower UHI compared to the other days. In a mostly-quiescent day of 21 August 1967 where wind speeds are lower, there is less turbulence mixing, and consequently more heat is trapped in the urban area that results in higher UHI~~low wind speed. On the other hand, low UHI is mainly predicted during nighttime with preceding days dominated by attenuated incoming solar radiation and high wind speed.

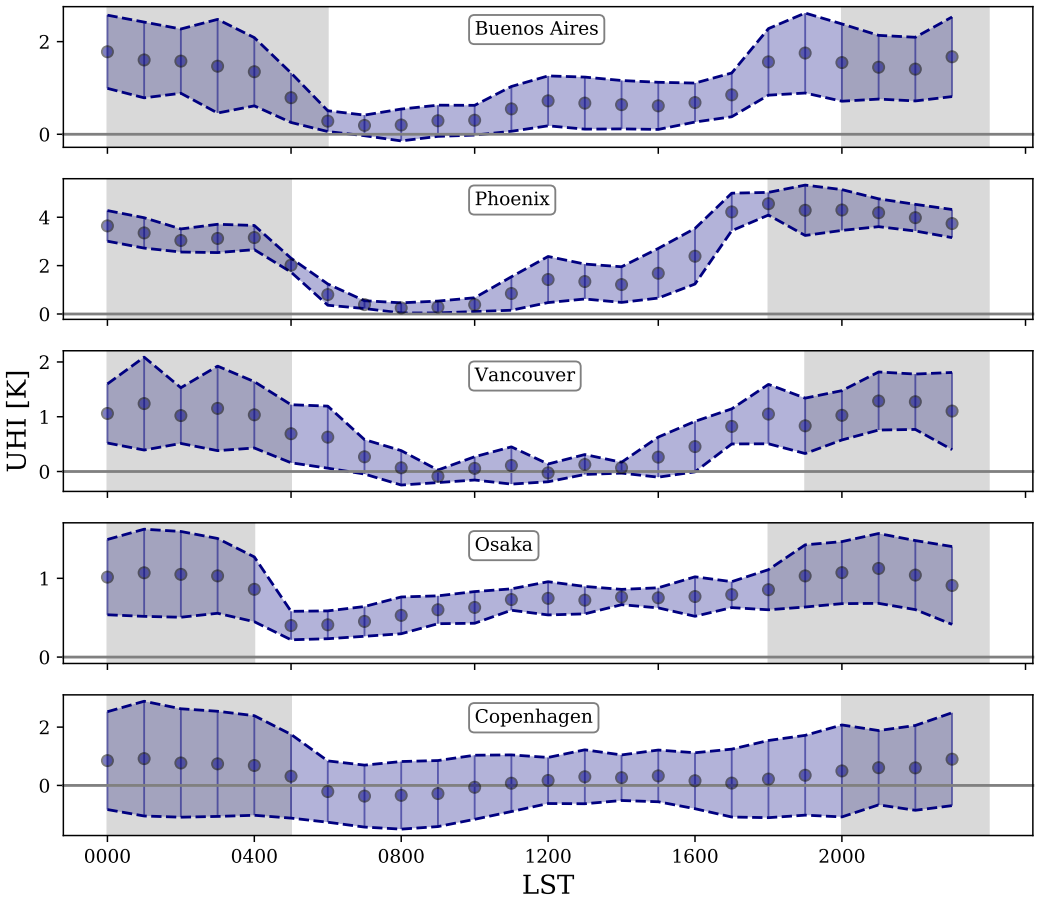

Figure 15. Diurnal variation of the ~~average urban and rural temperatures~~ UHIs in Buenos Aires, ~~Tucson~~ Phoenix, Vancouver, Osaka, and Copenhagen~~for a single day in Summer. Positive~~ ; diurnal variation of mean and ~~negative UHIs~~ standard deviation (error bar) are shown ~~by red and blue~~ using data obtained over a two-week period; nighttime is shown with shaded regions~~, respectively~~; times in Local Standard Time (LST).

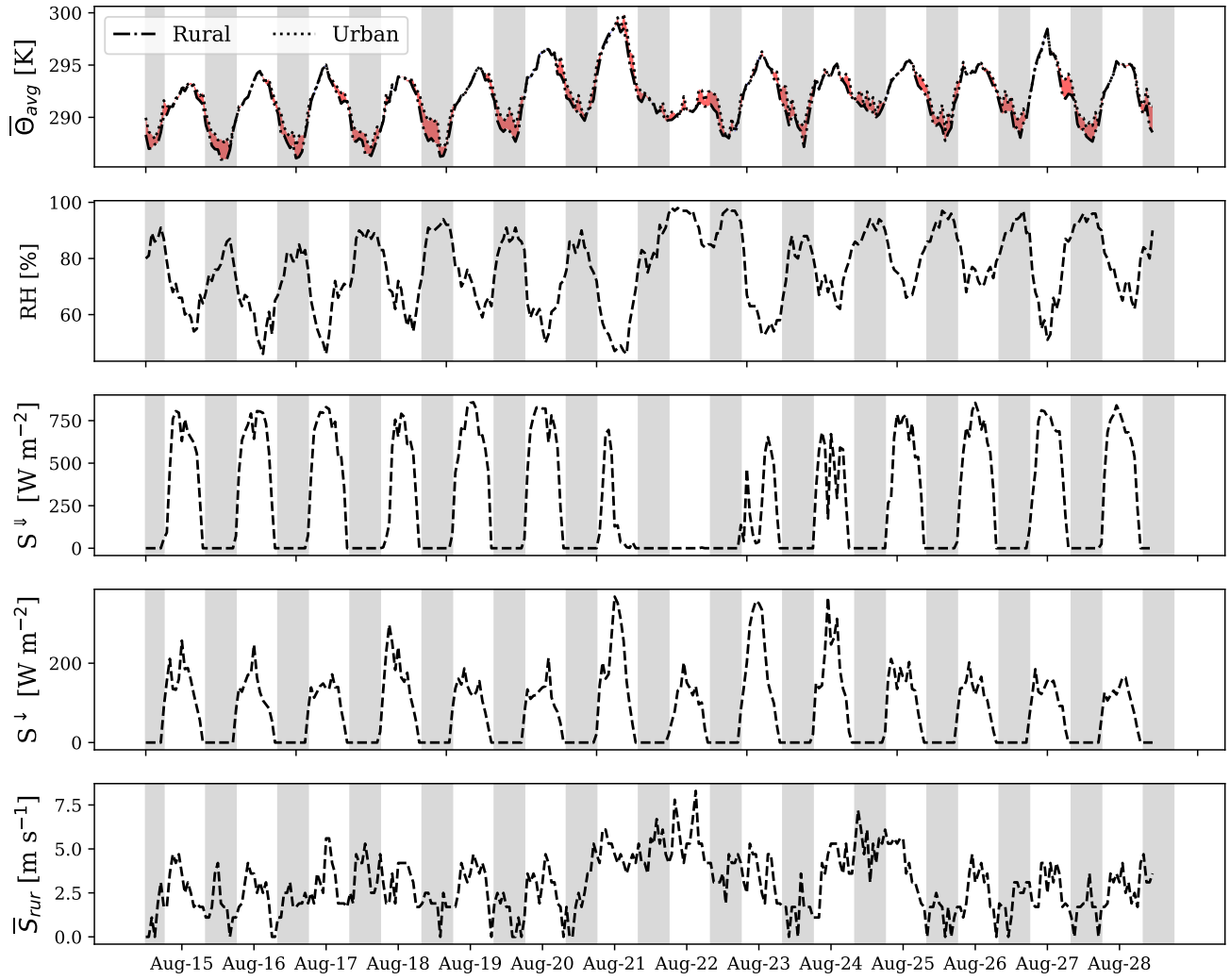

Figure 16. Hourly time series of rural and urban temperatures, rural relative humidity, rural incoming solar radiation, and rural mean horizontal wind speed ~~from 11~~ in August ~~1967~~ 2011 in ~~Tucson~~Vancouver, ~~Arizona, USA~~Canada; the shaded areas represent nighttime; positive UHI represented by shading the area between the temperature curves with red, while negative UHI represented by shading the area between the temperature curves with blue.

4 Conclusions and Future Work

The Vertical City Weather Generator (VCWG) is an urban microclimate model designed to calculate vertical profiles of meteorological variables including potential temperature, wind speed, specific humidity, and turbulence kinetic energy in an urban area. The VCWG is composed of sub models for ingestion of urban parameters and meteorological variables in a rural area as boundary conditions and prediction of the meteorological variables in a nearby urban area, the building energy performance variables, and the short and longwave radiation transfer processes. VCWG combines elements of several previous models developed by ~~Lee and Park (2008)~~Loughner et al. (2012), Santiago and Martilli (2010), Bueno et al. (2014), ~~Krayenhoff et al. (2014)~~ Krayenhoff (2014), Krayenhoff et al. (2015), and Redon et al. (2017) to generate a model with the ability to predict vertical profiles of urban meteorological variables, forced by rural measurements, and with feedback interaction with both building energy and radiation models.

To evaluate VCWG, a microclimate field campaign was held from 15 July 2018 to 5 September 2018, in Guelph, Canada. The data was collected at the University of Guelph main campus representing an urban site and in the Guelph Turfgrass Institute, which is an open space to be considered as a nearby rural site. In the urban site, temperature, wind velocity components, relative humidity, and solar radiation were measured. In the rural site, the temperature and relative humidity at 2 m as well as wind speed and direction at 10 m were provided from a weather station by the World Meteorological Organization (WMO) dataset. The results obtained from VCWG agreed reasonably well with the measurements and predicted a $+1.2$ and 1.53 K mean and standard deviation, respectively, for Urban Heat Island (UHI) with reasonable agreement to ~~a measured value of~~ observations reporting mean and standard deviation for UHI of $+1.8$ and 1.23 K~~in the previous year. Nevertheless, the before-sunrise UHI is not exactly reproduced, which is a current limitation of the model~~, respectively. The error analysis showed overall ~~a Normalized Mean Square Error () of , , and and overall a Fractional Bias () of , , and~~ BIAS of -1.43 K, 1.06 ms^{-1}, and 0.005 kgkg^{-1} for potential temperature, wind speed, and specific humidity, respectively. The analysis also showed overall RMSE of 1.56 K, 1.32 ms^{-1}, and 0.006 kgkg^{-1} for the same variables respectively.

The performance of the VCWG was further assessed by conducting ~~five~~ seven types of explorations for both nighttime and daytime urban microclimate. First, we investigated how the urban geometry, which is characterized by plan area density λ_p and frontal area density λ_f, could affect the urban microclimate. Any increase in λ_p was associated with higher air temperatures and reduced wind speeds within the urban canyon. On the other hand, a configuration with higher λ_f increased shading effects and consequently reduced daytime temperatures, but it increased nighttime temperatures due to more heat released from urban surfaces that was trapped in the canyon. The cooling effect of the urban vegetation was also evaluated by changing the Leaf Area Density (LAD) profiles within the canyon. Increasing the average LAD showed heat removal from the canyon alongside with lower wind speeds due to the drag induced by trees. The VCWG was also run for different building types (a school and a small office), cooling system Coefficient of Performance (COP), and heating thermal efficiency. The results showed that a school generates more waste heat fluxes associated with gas consumption and water heating, which causes higher impact on the urban climate. The analysis of different cooling system also revealed that less-efficient system (lower COP and heating efficiency) resulted in more waste heat emission. The radiation model was assessed by running the VCWG for different canyon

axis angles and canyon aspect ratio. The direct and diffusive solar radiation fluxes at the urban surfaces, and net longwave and shortwave solar radiation fluxes were compared. Net shortwave radiation flux was pronounced in less hours for the higher aspect ratio canyon, due to more shading effects on times before and after local noon. When the street canyon axis angle was perpendicular to the north axis, the net shortwave radiation fluxes were widened over a larger range of diurnal hours. Another exploration made ~~in the Wintertime~~ for all months of the year justified the ability of the VCWG to predict the urban microclimate in ~~both cold and warm~~ different seasons. The result showed the expected diurnal variation of temperature profile in the urban site. The ability of the model to predict UHI in different cities with different climate zones was assessed. The case studies were Buenos Aires, ~~Tucson~~Phoenix, Vancouver, Osaka, and Copenhagen. Finally, VCWG was able to produce realistic urban temperatures when it was run continuously for two weeks in ~~Tucson~~Vancouver. All exploration results obtained from the VCWG were reasonably consistent with the previous studies in the literature~~, except for occasional underprediction of UHI in the early morning~~.

In this study, it was shown that the urban microclimate model VCWG can successfully extend the spatial dimension of the preexisting bulk flow (single-layer) urban microclimate models to one-dimension in the vertical direction, while it also considers the relationship of the urban microclimate model to the rural meteorological measurements and the building energy conditions. The effect of the key urban elements such as building configuration, building energy systems, and vegetation were considered, but there is still opportunity to improve VCWG further. The urban site is simplified as blocks of buildings with symmetric and regular dimensions, which can be more realistically represented if more considerations were to be taken into account about nonuniform distribution of ~~buildings~~ building dimensions. Future studies can also focus on improvement of ~~flow field~~ flow-field parameterization or including additional source/sink terms in the transport equations to model horizontal motions, eddies, and flow fluctuations in the urban area, which is realistically very three-dimensional and ~~heterogenous~~heterogeneous. VCWG development can account for the spatial variation of urban microclimate in a computationally efficient manner independent of an auxiliary mesoscale model. This advantage is really important for urban planners, architects, and consulting engineers, to run VCWG operationally fast for many projects.

Code and data availability. The VCWG v1.1.0 is developed at the Atmospheric Innovations Research (AIR) Laboratory at the University of Guelph: http://www.aaa-scientists.com. The source code and the supporting environmental field monitoring data are available under GPL 3.0 licence: https://opensource.org/licenses/GPL-3.0 (last access: May 2019) and can be downloaded from https://www.zenodo.org/ with DOI: 10.5281/zenodo.3698344.

Appendix A

A1 Heat flux in the rural area

The net sensible heat fluxes at the surface level in the rural area can be decomposed into heat flux caused by vegetation, radiation flux absorbed by the surface, and the heat convection flux between the outer layer of soil and the atmosphere (see Eq.

6). The sensible heat flux from vegetation can be calculated as

$$Q_{Hveg,rur} = F_{veg}F(1 - F_{lat,grass})(1 - \alpha_V)Q^{rec}_{rad,rur} \tag{A1}$$

where F_{veg} is the fraction of the rural area covered by vegetation, $F_{lat,grass}$ is fraction of absorbed heat that is converted to an emitted latent heat flux, α_V is the albedo of the vegetation, and $Q^{rec}_{rad,rur}$ is the solar radiation flux (direct plus diffuse components) received at the rural surface given in the weather file. The net solar radiation flux absorbed at the surface can be calculated from

$$Q_{rad,rur} = ((1 - F_{veg})(1 - \alpha_{rur}) + F_{veg}(1 - \alpha_V))Q^{rec}_{rad,rur}, \tag{A2}$$

where α_{rur} is overall albedo of the rural area. The albedos of the rural area are input parameters in VCWG.

A2 Source/Sink Term in the 1-D Model

The pressure and skin drags exerted on the flow in Eq.s 8 and 9 are formulated as ~~follow (Krayenhoff et al., 2015)~~ follows (Santiago and Martilli, 2010; Krayenhoff, 2014; Krayenhoff et al., 2015; Simón-Moral et al., 2017; Nazarian et al., 2019; Krayenhoff et al

$$D_x = \underbrace{\frac{1}{\rho}\frac{\partial \tilde{P}}{\partial x}}_{I} - \underbrace{\nu(\nabla^2 \tilde{U})}_{II}, \tag{A3}$$

$$D_y = \underbrace{\frac{1}{\rho}\frac{\partial \tilde{P}}{\partial y}}_{I} - \underbrace{\nu(\nabla^2 \tilde{V})}_{II}, \tag{A4}$$

where term I represents dispersive pressure variation (form drag) induced by vegetation and building and term II represents the dispersive viscous dissipation (skin drag) induced by horizontal surfaces. The former can be parameterized as below

$$\frac{1}{\rho}\frac{\partial \tilde{P}}{\partial x} = -\left(B_D C_{DBv} + LAD\Omega C_{DV}\right)\overline{U}_{expl}\overline{U}, \tag{A5}$$

$$\frac{1}{\rho}\frac{\partial \tilde{P}}{\partial y} = -\left(B_D C_{DBv} + LAD\Omega C_{DV}\right)\overline{V}_{expl}\overline{V}, \tag{A6}$$

where B_D is sectional building area density, C_{DBv} is sectional drag coefficient in the presence of trees, LAD is leaf area density in the canyon, Ω is clumping factor, C_{DV} is the drag coefficient for tree foliage, and $\overline{U}_{expl}$ and $\overline{V}_{expl}$ are wind velocity components in x and y directions from a previous numerical solution, respectively, which are assumed explicitly as constants to linearize the system of equations to be solved. The skin drag can be parameterized as follow

$$\nu(\nabla^2 \tilde{U}) = -c c_d f_m \overline{U}_{expl}\overline{U}, \tag{A7}$$

$$\nu(\nabla^2 \tilde{V}) = -c c_d f_m \overline{V}_{expl}\overline{V}, \tag{A8}$$

where c_d is skin drag coefficient and f_m is a function of stability from Louis (1979).

The terms related to wake production S_{wake} and dissipation rate ε in Eq. 11 can be parameterized as

$$S_{wake} = \left(B_D C_{DBv} + LAD\Omega C_{DV}\right)\overline{U}^3_{expl}, \tag{A9}$$

$$\varepsilon = C_\varepsilon \frac{k^{\frac{3}{2}}}{\ell_{\varepsilon,dissip}}, \tag{A10}$$

where Ω is clumping factor, C_ε is a model constant and $\ell_{\varepsilon,\mathrm{dissip}}$ is a dissipation length scale ~~optimized using CFD~~ obtained by sensitivity study using CFD (Nazarian et al., 2019).

The heat source/sink terms, terms in Eq. 12, caused by roof ($S_{\Theta R}$) and ground ($S_{\Theta G}$) are calculated based on the study by Louis (1979) and the heat flux from the wall ($S_{\Theta W}$) is formulated in Martilli et al. (2002). The two other heat terms can be parameterized as below

$$S_{\Theta A} = \frac{4\rho_{abs}k_{air}}{\rho C_p v_L}\left[(1-\lambda_p)L_A\right], \tag{A11}$$

$$S_{\Theta V} = \frac{2g_{Ha}c_{PM}}{\rho C_p v_L}\left[LAD(1-\lambda_p)(\overline{\Theta}_V - \overline{\Theta})\right], \tag{A12}$$

where L_A is the absorbed flux density of longwave radiation in the canyon, ρ_{abs} is the density of absorbing molecules, k_{air} is their mass extinction cross section, $v_L{=}(1{-}\lambda_p)$ is the fraction of total volume that is outdoor air, g_{Ha} is conductance for heat, c_{PM} is the molar heat capacity for the air, and $\overline{\Theta}_V$ is the temperature of tree foliage.

In the specific humidity equation, the source/sink term can be calculated using the following equation

$$S_{QV} = \frac{\Lambda_M g_v \Omega}{\rho \Lambda v_L}\left[LAD(1-\lambda_p)(s[\overline{\Theta}_V - \overline{\Theta}]) + \frac{D}{P}\right] \tag{A13}$$

where Λ_M is molar latent heat of vaporization, g_v is the average surface and boundary-layer conductance for humidity for the whole leaf, D is the vapour deficit of the atmosphere, and P is atmospheric pressure.

A3 Building Heat Exchanges

The heat fluxes in Eq. 17 can be parameterized as bellow

$$\Sigma Q_{cv,isurf} = \Sigma h_i A_i (T_{si} - T_{in}) \tag{A14}$$

$$Q_{inf/exfinf} = \dot{m}_{inf/exfinf} C_p (T_{out} - T_{in}) \tag{A15}$$

$$Q_{sysvent} = \dot{m}_{sysvent} C_p (T_{supp} - T_{in}) \tag{A16}$$

where h_i and A_i are ~~heat convection coefficient~~ convective heat transfer coefficient (or u-value) and surface area of indoor elements such as ~~windows and ceiling~~ceiling, walls, floor, building mass, and windows. T_{si} is the temperature of inner layer of elements, T_{in} is indoor temperature, T_{out} is the outdoor temperature averaged over building height, T_{supp} is supply temperature, $\dot{m}_{inf}$ is mass flow rate of infiltration ~~/exfiltration, and~~ (exfiltration), and $\dot{m}_{vent}$ is mass flow rate of ventilated air in the HVAC system.

A4 Longwave and Shortwave Radiation

For shortwave radiation ~~, infinite~~ fluxes, multiple reflections are considered. The total absorbed shortwave radiation flux by each urban element can be calculated by adding the first absorption of shortwave radiation flux before any reflection to the radiation flux received as a result of ~~infinite~~ multiple reflections with the other elements. The following equations have been developed by Redon et al. (2017)

$$S_S = \Psi_{SG}\tau_{SG}(1-\delta_s)G_\infty + \Psi_{SV}\tau_{SV}\delta_s V_\infty + \Psi_{SW}\tau_{SW}W_\infty + \Psi_{ST}\delta_{Tt}T_\infty \tag{A17}$$

$$S_G = S^0_G + (1-\alpha_G)\left[\Psi_{GW}\tau_{GW}W_\infty + c_{GT}\Psi_{GT}\delta_t T_\infty\right] \tag{A18}$$

$$S_{W_i V} = S^0{}_V + (1-\alpha_V)\left[\Psi_{VW}\tau_{VW}W_\infty + c_{VT}\Psi_{VT}\delta_t T_\infty\right] \tag{A19}$$

$$S_W = S^0_W + (1-\alpha_W)\left[\Psi_{WG}\tau_{WG}(1-\delta_s)G_\infty + \Psi_{WV}\tau_{WV}\delta_s V_\infty + \Psi_{WW}\tau_{WW}S_{W_j}\frac{W_\infty}{2} + c_{WT}\Psi_{WT}\delta_{Tt}T_\infty\right] \tag{A20}$$

$$S_T = \frac{1}{\delta_T}\frac{1}{\delta_t}\left[(S^{\Downarrow}+S^{\downarrow}) - (S_S + (1-\delta_s)S_G + \delta_s S_V + \frac{2H_{avg}}{w}S_W)\right] \tag{A21}$$

where the subscripts 'S', 'G', 'V', 'W', and 'T' represent sky, ground, ground vegetation cover, wall, and tree, respectively. The superscript '0' signifies the before-reflection absorption of shortwave radiation (described in detail in Redon et al. (2017)). The view factor between two urban elements is shown by Ψ_{ij} with the suitable subscripts (e.g., i=G and j=W). For example Ψ_{GW} ~~represent~~ represents the view factor between ground and wall~~).~~. Note that ground and ground vegetation cover have the same view factors with other surfaces, e.g. $\Psi_{GW}=\Psi_{VW}$. The total shortwave radiation reflected by ground, ground vegetation cover, wall, and trees are shown by G_∞, V_∞, W_∞, and T_∞, respectively (described in detail in Redon et al. (2017)). $S^{\Downarrow}$ is direct incoming solar radiation, $S^{\downarrow}$ is ~~diffusive~~ diffuse incoming solar radiation ($S^{\Downarrow}$ and $S^{\downarrow}$ are both obtained from the input weather file), c_{GT} ~~is a model constant~~and c_{VT} are model constants, τ_{ij} is radiative transmissivity between two elements (e.g. i=G and j=W), w is street width, H_{avg} is average building height, ~~and is fraction of road surface~~ δ_t is cover fraction of tree canopy, and δ_s is surface fraction covered by vegetation. The shading effect of trees are considered in the formulation of transmissivity (Lee and Park, 2008). Note that ground and ground vegetation cover have the same transmissivity with other surfaces, e.g. $\tau_{GW}=\tau_{VW}$.

For longwave radiation ~~, only one reflection is~~ fluxes, multiple reflections are considered. The net longwave radiation fluxes received by the urban surfaces can be computed as ~~(Lee and Park, 2008)~~ (Loughner et al., 2012)

$$\begin{aligned}
L_W = \varepsilon_W \Big\{ & \tau_{WS}\Psi_{WS}L_S + \tau_{WG}((1-\delta_s)\varepsilon_G\Psi_{WG}\sigma T_G^4 + \delta_s\varepsilon_V\Psi_{WV}\sigma T_V^4) + \tau_{WW}\varepsilon_W\Psi_{WW}\sigma T_W^4 + L_{T\uparrow}^W \\
& - \sigma T_W^4 + \tau_{WG}\left[(1-\delta_s)(1-\varepsilon_G)\Psi_{WG}L_{T\uparrow}^G\right] + \tau_{WW}(1-\varepsilon_W)\Psi_{WW}L_{T\uparrow}^W \\
& + \tau_{WG}\tau_{WS}\left[(1-\delta_s)(1-\varepsilon_G)\Psi_{WG}\Psi_{GS}L_S + \delta_s(1-\varepsilon_V)\Psi_{WV}\Psi_{VS}L_S\right] \\
& + \tau_{WG}\tau_{WG}\left[(1-\delta_s)(1-\varepsilon_G)\Psi_{WG}\Psi_{WG}\varepsilon_W\sigma T_W^4 + \delta_s(1-\varepsilon_V)\Psi_{WG}\Psi_{WG}\varepsilon_W\sigma T_W^4\right] \\
& + \tau_{WW}\tau_{WG}\left[(1-\delta_s)(1-\varepsilon_W)\Psi_{WW}\Psi_{WG}\varepsilon_G\sigma T_G^4 + \delta_s(1-\varepsilon_W)\Psi_{WW}\Psi_{WG}\varepsilon_V\sigma T_V^4\right] \\
& + \tau_{WW}\tau_{WS}(1-\varepsilon_W)\Psi_{WW}\Psi_{WS}L_S + \tau_{WW}\tau_{WW}(1-\varepsilon_W)\Psi_{WW}\Psi_{WW}\varepsilon_W\sigma T_W^4 \Big\}
\end{aligned} \tag{A22}$$

$$\begin{aligned}
L_G = (1-\delta_s)\varepsilon_G \Big\{ & \tau_{GS}L_S\Psi_{GS} + \tau_{WG}\varepsilon_W\Psi_{WG}\sigma T_W^4 + L_{T\uparrow}^G - \sigma T_G^4 + \tau_{WG}(1-\varepsilon_W)\Psi_{GW}L_{T\uparrow}^W \\
& + \tau_{WG}\tau_{WS}(1-\varepsilon_W)\Psi_{GW}\Psi_{WS}L_S + \tau_{WG}\tau_{WW}\Psi_{GW}\Psi_{WW}\varepsilon_W\sigma T_W^4 \\
& + \tau_{WG}\tau_{WG}\left[(1-\delta_s)(1-\varepsilon_W)\Psi_{GW}\Psi_{WG}\varepsilon_G\sigma T_G^4 + \delta_s(1-\varepsilon_W)\Psi_{GW}\Psi_{WG}\varepsilon_V T_V^4\right] \Big\}
\end{aligned} \tag{A23}$$

$$\begin{aligned}
L_V = \delta_s\varepsilon_V \Big\{ & \tau_{GS}L_S\Psi_{GS} + \tau_{WG}\varepsilon_W\Psi_{WG}\sigma T_W^4 + L_{T\uparrow}^G - \sigma T_V^4 + \tau_{WG}(1-\varepsilon_W)\Psi_{GW}L_{T\uparrow}^W \\
& + \tau_{WG}\tau_{WS}(1-\varepsilon_W)\Psi_{GW}\Psi_{WS}L_S + \tau_{WG}\tau_{WW}\Psi_{GW}\Psi_{WW}\varepsilon_W\sigma T_W^4 \\
& + \tau_{WG}\tau_{WG}\left[(1-\delta_s)(1-\varepsilon_W)\Psi_{GW}\Psi_{WG}\varepsilon_G\sigma T_G^4 + \delta_s(1-\varepsilon_W)\Psi_{GW}\Psi_{WG}\varepsilon_V T_V^4\right] \Big\}
\end{aligned} \tag{A24}$$

~~where the upward and downward arrows indicate emitted and absorbed longwave radiation from and by the surface of interest~~

$$L_T = L_S^T + L_T^T + L_G^T + L_V^T + L_W^T - L_{T\uparrow}, \tag{A25}$$

where the subscripts 'S', 'G', 'V', 'W', and 'T' represent sky, ground, ground vegetation cover, wall, and tree, respectively. L_S is radiative longwave flux emitted from the atmosphere/sky, T_i is surface temperature where i can be G, ~~is leaf aspect ratio, is wall temperature and is ground temperature. The readers are invited to refer to the study by Lee and Park (2008) for more details on the parameterization of longwave radiation~~ V, and W. $L_{i\uparrow}^j$ is the longwave radiation emitted from surface i that reaches surface j. L_S^T represents the downwelling longwave radiation from the atmosphere above the street canyon that is absorbed by the tree canopy and L_T^T, L_G^T, L_V^T, and L_W^T represent the longwave radiation emitted from the tree canopy, ground, ground vegetation cover, and walls, respectively, that is absorbed by the tree canopy. These terms account for multiple reflections from the walls, ground, and ground vegetation cover in the urban street canyon. $L_{T\uparrow}$ is total longwave radiation emitted from the tree canopy. A complete formulation of the terms in L_T is provided in detail in Loughner et al. (2012).

Author contributions. MM wrote the paper with significant conceptual input from ESK and AAA and critical feedback from all co-authors. BD, AN, MKN, and MRN operated the instruments in the field and partially analyzed resulting data. BB and LKN developed the base Urban

Weather Generator (UWG) program in MATLAB. CM and SV translated UWG from MATLAB to Python. NN and ESK provided their code for the one-dimensional vertical diffusion model for the urban climate that was integrated into VCWG. MM and AAA developed the Vertical City Weather Generator (VCWG) program in Python by integrating various modeling components developed by BB, LKN, CM, SV, ESK, and NN.

Competing interests. The authors declare that they have no conflict of interest.

Acknowledgements. The authors are indebted to Steve Nyman, Chris Duiker, Peter Purvis, Manuela Racki, Jeffrey Defoe, Joanne Ryks, Ryan Smith, James Bracken, and Samantha French at the University of Guelph, who helped with the campaign logistics. Special credit is directed toward Amanda Sawlor, Esra Mohamed, Di Cheng, Randy Regan, Margaret Love, Angela Vuk, and Carolyn Dowling-Osborn at the University of Guelph for administrative support. The computational platforms were set up with the assistance of Jeff Madge, Joel Best, and Matthew Kent at the University of Guelph. The authors thank Alberto Martilli at Centre for Energy, Environment and Technology (CIEMAT) in Madrid, Spain, who developed and shared an earlier version of the one-dimensional vertical diffusion model for the urban climate. The authors also thank William D. Lubitz for providing ~~a mini SOnic Detection And Ranging (SODAR) instrument and~~ three ultrasonic anemometers for the field campaign.

This work was supported by the University of Guelph through the International Graduate Tuition Scholarship (IGTS) for the lead author; Philanthropic contributions from Professor Edward McBeans's Foundation toward acquisition of experimental equipment; Discovery Grant program (401231) from the Natural Sciences and Engineering Research Council (NSERC) of Canada; Government of Ontario through the Ontario Centres of Excellence (OCE) under the Alberta-Ontario Innovation Program (AOIP) (053450); and Emission Reduction Alberta (ERA) (053498). OCE is a member of the Ontario Network of Entrepreneurs (ONE).

References

Adnot, J., Riviere, P., Marchio, D., Becirspahic, S., Lopes, C., Blanco, I., Perez-Lombard, L., Ortiz, J., Papakonstantnou, N., Doukas, P., et al.: Energy efficiency and certification of central air conditioners (EECCAC), Study for the DG Transportation-Energy (DGTREN) of the Commission of the EU, Paris, 2003.

Akbari, H.: Energy Saving Potentials and Air Quality Benefits of Urban Heat Island Mitigation, 2005.

Akbari, H., Pomerantz, M., and Taha, H.: Cool surfaces and shade trees to reduce energy use and improve air quality in urban areas, Sol. Energy, 70, 295–310, 2001.

Aliabadi, A. A., Staebler, R. M., de Grandpré, J., Zadra, A., and Vaillancourt, P. A.: Comparison of estimated atmospheric boundary layer mixing height in the Arctic and southern Great Plains under statically stable conditions: experimental and numerical aspects, Atmos.-Ocean, 54, 60–74, 2016a.

Aliabadi, A. A., Staebler, R. M., Liu, M., and Herber, A.: Characterization and parametrization of Reynolds stress and turbulent heat flux in the stably-stratified lower Arctic troposphere using aircraft measurements, Bound.-Layer Meteorol., 161, 99–126, 2016b.

Aliabadi, A. A., Krayenhoff, E. S., Nazarian, N., Chew, L. W., Armstrong, P. R., Afshari, A., and Norford, L. K.: Effects of roof-edge roughness on air temperature and pollutant concentration in urban canyons, Bound.-Lay. Meteorol., 164, 249–279, 2017.

Aliabadi, A. A., Veriotes, N., and Pedro, G.: A Very Large-Eddy Simulation (VLES) model for the investigation of the neutral atmospheric boundary layer, Journal of Wind Engineering and Industrial Aerodynamics, 183, 152–171, 2018.

Aliabadi, A. A., Moradi, M., Clement, D., Lubitz, W. D., and Gharabaghi, B.: Flow and temperature dynamics in an urban canyon under a comprehensive set of wind directions, wind speeds, and thermal stability conditions, Environ. Fluid Mech., 19, 81–109, 2019.

Armson, D., Stringer, P., and Ennos, A.: The effect of tree shade and grass on surface and globe temperatures in an urban area, Urban For. Urban Gree., 11, 245–255, 2012.

Balogun, A. A., Tomlin, A. S., Wood, C. R., Barlow, J. F., Belcher, S. E., Smalley, R. J., Lingard, J. J. N., Arnold, S. J., Dobre, A., Robins, A. G., Martin, D., and Shallcross, D. E.: In-street wind direction variability in the vicinity of a busy intersection in central London, Bound.-Lay. Meteorol., 136, 489–513, 2010.

Bejarán, R. and Camilloni, I.: Objective method for classifying air masses: an application to the analysis of Buenos Aires'(Argentina) urban heat island intensity, Theor. Appl. Climatol., 74, 93–103, 2003.

Blocken, B.: Computational Fluid Dynamics for urban physics: Importance, scales, possibilities, limitations and ten tips and tricks towards accurate and reliable simulations, Build. Environ., 91, 219–245, 2015.

Bornstein, R. D.: The Two-Dimensional URBMET Urban Boundary Layer Model, J. Appl. Meteorol., 14, 1459–1477, 1975.

Britter, R. E. and Hanna: Flow and Dispersion in Urban Areas, Annu. Rev. Fluid Mech, 35, 469–496, 2003.

Broadbent, A. M., Coutts, A. M., Nice, K. A., Demuzere, M., Krayenhoff, E. S., Tapper, N. J., and Wouters, H.: The Air-temperature Response to Green/blue-infrastructure Evaluation Tool (TARGET v1. 0): an efficient and user-friendly model of city cooling, Geosci. Model Dev., 12, 785–803, 2019.

Bueno, B., Norford, L. K., Pigeon, G., and Britter, R.: Combining a detailed building energy model with a physically-based urban canopy model, Bound.-Lay. Meteorol., 140, 471–489, 2011.

Bueno, B., Norford, L. K., Hidalgo, J., and Pigeon, G.: The urban weather generator, J. Build. Perf. Simulat., 6, 269–281, 2012a.

Bueno, B., Pigeon, G., Norford, L. K., Zibouche, K., and Marchadier, C.: Development and evaluation of a building energy model integrated in the TEB scheme, Geosci. Model Dev., pp. 433–448, 2012b.

Bueno, B., Roth, M., Norford, L. K., and Li, R.: Computationally efficient prediction of canopy level urban air temperature at the neighbourhood scale, Urban Climate, 9, 35–53, 2014.

Businger, J. A., Wyngaard, J. C., Izumi, Y., and Bradley, E. F.: Flux-profile relationships in the atmospheric surface layer, J. Atmos. Sci., 28, 181–189, 1971.

C. S. B. Grimmond, M. Best, J. B.: Urban Surface Energy Balance Models: Model Characteristics and Methodology for a Comparison Study. In: Baklanov A., Sue G., Alexander M., Athanassiadou M. (eds) Meteorological and Air Quality Models for Urban Areas, McGraw-Hill Inc., New York, 3rd edn., 2009.

Chen, F., Kusaka, H., Bornstein, R., Ching, J., Grimmond, C. S. B., Grossman-Clarke, S., Loridan, T., Manning, K. W., Martilli, A., Miao, S., Sailor, D., Salamanca, F. P., Taha, H., Tewari, M., Wang, X., Wyszogrodzki, A. A., and Zhang, C.: The integrated WRF/urban modelling system: development, evaluation, and applications to urban environmental problems, Int. J. Climatol., 31, 273–288, 2011.

Chin, H.-N. S., Leach, M. J., Sugiyama, G. A., Leone Jr, J. M., Walker, H., Nasstrom, J., and Brown, M. J.: Evaluation of an Urban Canopy Parameterization in a Mesoscale Model Using VTMX and URBAN 2000 Data, Mon. Weather Rev., 133, 2043–2068, 2005.

Ciccioli, P., Fabozzi, C., Brancaleoni, E., Cecinato, A., Frattoni, M., Cieslik, S., Kotzias, D., Seufert, G., Foster, P., and Steinbrecher, R.: Biogenic emission from the Mediterranean pseudosteppe ecosystem present in Castelporziano, Atmos. Environ., 31, 167–175, 1997.

Coceal, O. and Belcher, S.: A canopy model of mean winds through urban areas, Q. J. R. Meteorol. Soc., 130, 1349–1372, 2004.

Comrie, A. C.: Mapping a wind-modified urban heat island in Tucson, Arizona (with comments on integrating research and undergraduate learning), B. Am. Meteorol. Soc., 81, 2417–2432, 2000.

Conry, P., Fernando, H., Leo, L., Sharma, A., Potosnak, M., and Hellmann, J.: Multi-scale simulations of climate-change influence on Chicago Heat Island, in: ASME 2014 4th Joint US-European Fluids Engineering Division Summer Meeting collocated with the ASME 2014 12th International Conference on Nanochannels, Microchannels, and Minichannels, American Society of Mechanical Engineers, 2014.

Coutts, A. M., Beringer, J., and Tapper, N. J.: Impact of Increasing Urban Density on Local Climate: Spatial and Temporal Variations in the Surface Energy Balance in Melbourne, Australia, J. Appl. Meteorol. Clim., 46, 477–493, 2007.

Crank, P. J., Sailor, D. J., Ban-Weiss, G., and Taleghani, M.: Evaluating the ENVI-met microscale model for suitability in analysis of targeted urban heat mitigation strategies, Urban climate, 26, 188–197, 2018.

Cui, Y. Y. and De Foy, B.: Seasonal variations of the urban heat island at the surface and the near-surface and reductions due to urban vegetation in Mexico City, J. Appl. Meteorol. Clim., 51, 855–868, 2012.

De Munck, C., Pigeon, G., Masson, V., Meunier, F., Bousquet, P., Tréméac, B., Merchat, M., Poeuf, P., and Marchadier, C.: How much can air conditioning increase air temperatures for a city like Paris, France?, Int. J. Climatol., 33, 210–227, 2013.

Dupont, S., Otte, T. L., and Ching, J. K. S.: Simulation of Meteorological Fields Within and Above Urban and Rural Canopies with a Mesoscale Model, Bound.-Lay. Meteorol., 113, 111–158, 2004.

Dyer, A.: A review of flux-profile relationships, Bound.-Lay. Meteorol., 7, 363–372, 1974.

Emmanuel, R. and Steemers, K.: Connecting the realms of urban form, density and microclimate, Build. Res. Inf., 46, 804–808, 2018.

Erell, E. and Williamson, T.: Simulating air temperature in an urban street canyon in all weather conditions using measured data at a reference meteorological station, Int. J. Climatol., 26, 1671–1694, 2006.

Fast, J. D., Torcolini, J. C., and Redman, R.: Pseudovertical Temperature Profiles and the Urban Heat Island Measured by a Temperature Datalogger Network in Phoenix, Arizona, J. Appl. Meteorol., 44, 3–13, 2005.

Founda, D. and Santamouris, M.: Synergies between urban heat island and heat waves in Athens (Greece), during an extremely hot summer (2012), Sci. Rep., 7, 1–11, 2017.

Futcher, J. A.: 658-ICE TEA CITY, in: 25th Conference on Passve and Low Energy Architecture, 2008.

Giometto, M., Christen, A., Egli, P., Schmid, M., Tooke, R., Coops, N., and Parlange, M.: Effects of trees on mean wind, turbulence and momentum exchange within and above a real urban environment, Adv. Water Resour., 106, 154–168, 2017.

Giometto, M. G., Christen, A., Meneveau, C., Fang, J., Krafczyk, M., and Parlange, M. B.: Spatial Characteristics of Roughness Sublayer Mean Flow and Turbulence Over a Realistic Urban Surface, Bound.-Lay. Meteorol., 160, 425–452, 2016.

Gowardhan, A. A., Pardyjak, E. R., Senocak, I., and Brown, M. J.: A CFD-based wind solver for an urban fast response transport and dispersion model, Environ. Fluid Mech., 11, 439–464, 2011.

Grachev, A. A., Andreas, E. L., Fairall, C. W., Guest, P. S., and Persson, P. O. G.: On the turbulent Prandtl number in the stable atmospheric boundary layer, Bound.-Lay. Meteorol., 125, 329–341, 2007.

Grachev, A. A., Andreas, E. L., Fairall, C. W., Guest, P. S., and Persson, P. O. G.: The critical Richardson number and limits of applicability of local similarity theory in the stable boundary layer, Bound.-Lay. Meteorol., 147, 51–82, 2013.

Grimmond, C. S. B. and Oke, T. R.: Aerodynamic Properties of Urban Areas Derived from Analysis of Surface Form, J. Appl. Meteorol., 38, 1262–1292, 1999.

Grimmond, C. S. B., Souch, C., and Hubble, M. D.: Influence of tree cover on summertime surface energy balance fluxes, San Gabriel Valley, Los Angeles, Clim. Res., 6, 45–57, 1996.

Gros, A., Bozonnet, E., and Inard, C.: Cool materials impact at district scale: Coupling building energy and microclimate models, Sustain. Cities Soc., 13, 254–266, 2014.

Gryning, S.-E., Batchvarova, E., Brümmer, B., Jørgensen, H., and Larsen, S.: On the extension of the wind profile over homogeneous terrain beyond the surface boundary layer, Bound.-Lay. Meteorol., 124, 251–268, 2007.

Hamdi, R. and Masson, V.: Inclusion of a Drag Approach in the Town Energy Balance (TEB) Scheme: Offline 1D Evaluation in a Street Canyon, J. Appl. Meteorol. Clim., 47, 2627–2644, 2008.

Hawkins, T. W., Brazel, A. J., Stefanov, W. L., Bigler, W., and Saffell, E. M.: The Role of Rural Variability in Urban Heat Island Determination for Phoenix, Arizona, J. Appl. Meteorol., 43, 476–486, 2004.

Ho, H. C., Knudby, A., Xu, Y., Hodul, M., and Aminipouri, M.: A comparison of urban heat islands mapped using skin temperature, air temperature, and apparent temperature (Humidex), for the greater Vancouver area, Sci. Total Environ., 544, 929–938, 2016.

Jamei, E., Rajagopalan, P., Seyedmahmoudian, M., and Jamei, Y.: Review on the impact of urban geometry and pedestrian level greening on outdoor thermal comfort, Renew. Sust. Energ. Rev., 54, 1002–1017, 2016.

Joffre, S., Kangas, M., Heikinheimo, M., and Kitaigorodskii, S.: Variability of the Stable and Unstable Atmospheric Boundary-Layer Height and its Scales Over a Boreal Forest, Bound.-Lay. Meteorol., 99, 429–450, 2001.

Kang, W. and Sung, H. J.: Large-scale structures of turbulent flows over an open cavity, J. Fluid Struct., 25, 1318–1333, 2009.

Kastner-Klein, P., Berkowicz, R., and Britter, R.: The influence of street architecture on flow and dispersion in street canyons, Meteorol. Atmos. Phys, 87, 121–131, 2004.

Keck, R.-E., de Maré, M., Churchfield, M. J., Lee, S., Larsen, G., and Aagaard Madsen, H.: On atmospheric stability in the dynamic wake meandering model, Wind Energy, 17, 1689–1710, 2014.

Kikegawa, Y., Genchi, Y., Yoshikado, H., and Kondo, H.: Development of a numerical simulation system toward comprehensive assessments of urban warming countermeasures including their impacts upon the urban buildings' energy-demands, Appl. Energ., 76, 449–466, 2003.

Kleerekoper, L., van Esch, M., and Salcedo, T. B.: How to make a city climate-proof, addressing the urban heat island effect, Resour. Conserv. Recy., 64, 30–38, 2012.

Kłysik, K. and Fortuniak, K.: Temporal and spatial characteristics of the urban heat island of Łódź, Poland, Atmos. Environ., 33, 3885–3895, 1999.

Kochanski, A., Pardyjak, E., Stoll, R., Gowardhan, A., Brown, M., and Steenburgh, W.: One-Way Coupling of the WRF-QUIC Urban Dispersion Modeling System, J. Appl. Meteorol. Clim., 54, 2119–2139, 2015.

Kondo, H., Genchi, Y., Kikegawa, Y., Ohashi, Y., Yoshikado, H., and Komiyama, H.: Development of a Multi-Layer Urban Canopy Model for the Analysis of Energy Consumption in a Big City: Structure of the Urban Canopy Model and its Basic Performance, Bound.-Lay. Meteorol., 116, 395–421, 2005.

Kong, L., Lau, K. K.-L., Yuan, C., Chen, Y., Xu, Y., Ren, C., and Ng, E.: Regulation of outdoor thermal comfort by trees in Hong Kong, Sustain. Cities Soc., 31, 12–25, 2017.

Kono, T., Ashie, Y., and Tamura, T.: Mathematical Derivation of Spatially-Averaged Momentum Equations for an Urban Canopy Model Using Underlying Concepts of the Immersed Boundary Method, Bound.-Lay. Meteorol., 135, 185–207, 2010.

Krayenhoff, E., Christen, A., Martilli, A., and Oke, T.: A Multi-Layer Radiation Model for Urban Neighbourhoods with Trees, Bound.-Lay. Meteorol., 151, 139–178, 2014.

Krayenhoff, E. S.: A multi-layer urban canopy model for neighbourhoods with trees, Ph.D. thesis, University of British Columbia, 2014.

Krayenhoff, E. S. and Voogt, J. A.: A Microscale Three-Dimensional Urban Energy Balance Model for Studying Surface Temperatures, Bound.-Layer Meteorol., 123, 433–461, 2007.

Krayenhoff, E. S., Santiago, J.-L., Martilli, A., Christen, A., and Oke, T. R.: Parametrization of Drag and Turbulence for Urban Neighbourhoods with Trees, Bound.-Lay. Meteorol., 156, 157–189, 2015.

Krayenhoff, E. S., Jiang, T., Christen, A., Martilli, A., Oke, T. R., Bailey, B. N., Nazarian, N., Voogt, J. A., Giometto, M. G., Stastny, A., et al.: A multi-layer urban canopy meteorological model with trees (BEP-Tree): Street tree impacts on pedestrian-level climate, Urban Climate, 32, 100 590, 2020.

Kusaka, H., Kondo, H., Kikegawa, Y., and Kimura, F.: A Simple Single-Layer Urban Canopy Model for Atmospheric Models: Comparison with Multi-Layer and Slab Models, Bound.-Lay. Meteorol., 101, 329–358, 2001.

Kusaka, H., Hara, M., and Takane, Y.: Urban Climate Projection by the WRF Model at 3-km Horizontal Grid Increment: Dynamical Downscaling and Predicting Heat Stress in the 2070's August for Tokyo, Osaka, and Nagoya Metropolises, J. Meteorol. Soc. Jpn. Ser. II, 90, 47–63, 2012.

Leal Filho, W., Echevarria Icaza, L., Emanche, V., and Quasem Al-Amin, A.: An Evidence-Based Review of Impacts, Strategies and Tools to Mitigate Urban Heat Islands, Int. J. Env. Res. Pub. He., 14, 1600, 2017.

Lee, S.-H. and Park, S.-U.: A Vegetated Urban Canopy Model for Meteorological and Environmental Modelling, Bound.-Lay. Meteorol., 126, 73–102, 2008.

Lesnikowski, A.: Adaptation to urban heat island effect in Vancouver, BC: A case study in analyzing vulnerability and adaptation opportunities, Ph.D. thesis, University of British Columbia, 2014.

Li, D.: Turbulent Prandtl number in the atmospheric boundary layer-where are we now?, Atmos. Res., 216, 86–105, 2018.

Li, D. and Bou-Zeid, E.: Synergistic interaction between urban heat islands and heat waves: The impact in cities is larger than the sum of its parts, J. Appl. Meteorol. Climatol., 52, 2051–2064, 2013.

Loughner, C. P., Allen, D. J., Zhang, D.-L., Pickering, K. E., Dickerson, R. R., and Landry, L.: Roles of Urban Tree Canopy and Buildings in Urban Heat Island Effects: Parameterization and Preliminary Results, J. Appl. Meteorol. Clim., 51, 1775–1793, 2012.

Louis, J.-F.: A Parametric Model of Vertical Eddy Fluxes in the Atmosphere, Bound.-Lay. Meteorol., 17, 187–202, 1979.

Lundquist, K. A., Chow, F. K., and Lundquist, J. K.: An Immersed Boundary Method for the Weather Research and Forecasting Model, Mon. Weather Rev., 138, 796–817, 2010.

Mahura, A., Baklanov, A., Petersen, C., Nielsen, N. W., and Amstrup, B.: Verification and Case Studies for Urban Effects in HIRLAM Numerical Weather Forecasting, in: Meteorological and Air Quality Models for Urban Areas, pp. 143–150, Springer, 2009.

Maronga, B., Gryschka, M., Heinze, R., Hoffmann, F., Kanani-Sühring, F., Keck, M., Ketelsen, K., Letzel, M. O., Sühring, M., and Raasch, S.: The Parallelized Large-Eddy Simulation Model (PALM) version 4.0 for atmospheric and oceanic flows: model formulation, recent developments, and future perspectives, Geosci. Model Dev., 8, 2515–2551, 2015.

Martilli, A. and Santiago, J. L.: CFD simulation of airflow over a regular array of cubes. Part II: analysis of spatial average properties, Bound.-Lay. Meteorol., 122, 635–654, 2007.

Martilli, A., Clappier, A., and Rotach, M. W.: An Urban Surface Exchange Parameterisation for Mesoscale Models, Bound.-Lay. Meteorol., 104, 261–304, 2002.

Masson, V.: A Physically-Based Scheme for the Urban Energy Budget in Atmospheric Models, Bound.-Lay. Meteorol., 94, 357–397, 2000.

Masson, V., Grimmond, C. S. B., and Oke, T. R.: Evaluation of the Town Energy Balance (TEB) Scheme with Direct Measurements from Dry Districts in Two Cities, J. Appl. Meteorol., 41, 1011–1026, 2002.

Masson, V., Gomes, L., Pigeon, G., Liousse, C., Pont, V., Lagouarde, J. P., Voogt, J., Salmond, J., Oke, T. R., Hidalgo, J., Legain, D., Garrouste, O., Lac, C., Connan, O., Briottet, X., Lachérade, S., and Tulet, P.: The Canopy and Aerosol Particles Interactions in TOlouse Urban Layer (CAPITOUL) experiment, Meterol. Atmos. Phys., 102, 135–157, 2008.

Mauree, D., Blond, N., and Clappier, A.: Multi-scale modeling of the urban meteorology: Integration of a new canopy model in the WRF model, Urban Climate, 26, 60–75, 2018.

Mills, G.: An urban canopy-layer climate model, Theor. Appl. Climatol., 57, 229–244, 1997.

Moeng, C., Dudhia, J., Klemp, J., and Sullivan, P.: Examining Two-Way Grid Nesting for Large Eddy Simulation of the PBL Using the WRF Model, Mon. Weather Rev., 135, 2295–2311, 2007.

Monin, A. S. and Obukhov, A. M.: Basic regularity in turbulent mixing in the surface layer of the atmosphere, Tr. Akad. Nauk SSSR Geophiz. Inst., 1957.

Moninger, W. R., Benjamin, S. G., Jamison, B. D., Schlatter, T. W., Smith, T. L., and Szoke, E. J.: Evaluation of regional aircraft observations using TAMDAR, Weather and Forecasting, 25, 627–645, 2010.

Nazarian, N. and Kleissl, J.: Realistic solar heating in urban areas: air exchange and street-canyon ventilation, Build. Environ., 95, 75–93, 2016.

Nazarian, N., Martilli, A., and Kleissl, J.: Impacts of Realistic Urban Heating, Part I: Spatial Variability of Mean Flow, Turbulent Exchange and Pollutant Dispersion, Bound.-Lay. Meteorol., 166, 367–393, 2018.

Nazarian, N., Krayenhoff, E. S., and Martilli, A.: A One-Dimensional Model of Turbulent Flow Through 'Urban' Canopies: Updates Based on Large-Eddy Simulation, Geosci. Model Dev. Discussions, 2019, 1–24, 2019.

Oikonomou, E., Davies, M., Mavrogianni, A., Biddulph, P., Wilkinson, P., and Kolokotroni, M.: Modelling the relative importance of the urban heat island and the thermal quality of dwellings for overheating in London, Build. Environ., 57, 223–238, 2012.

Oke, T., Johnson, G., Steyn, D., and Watson, I.: Simulation of surface urban heat islands under 'ideal'conditions at night Part 2: Diagnosis of causation, Bound.-Lay. Meteorol., 56, 339–358, 1991.

Oke, T. R.: The energetic basis of the urban heat island, Q. J. Roy. Meteor. Soc., 108, 1–24, 1982.

Oke, T. R., Mills, G., Christen, A., and Voogt, J. A.: Urban Climates, Cambridge University Press, 2017.

Optis, M., Monahan, A., and Bosveld, F. C.: Limitations and breakdown of Monin–Obukhov similarity theory for wind profile extrapolation under stable stratification, Wind Energy, 19, 1053–1072, 2016.

Palyvos, J.: A survey of wind convection coefficient correlations for building envelope energy systems' modeling, Appl. Therm Eng., 28, 801–808, 2008.

Peña, A., Gryning, S.-E., and Mann, J.: On the length-scale of the wind profile, Q. J. Roy. Meteor. Soc., 136, 2119–2131, 2010.

Perret, L. and Savory, E.: Large-Scale Structures Over a Single Street Canyon Immersed in an Urban-Type Boundary Layer, Bound.-Lay. Meteorol., 148, 111–131, 2013.

Pope, S. B.: Turbulent flows, Cambridge University Press, Cambridge, U.K., 2000.

Rasul, A., Balzter, H., and Smith, C.: Diurnal and seasonal variation of surface urban cool and heat islands in the semi-arid city of Erbil, Iraq, Climate, 4, 42, 2016.

Raupach, M. R., Finnigan, J., and Brunet, Y.: Coherent eddies and turbulence in vegetation canopies: the mixing-layer analogy, in: Bound.-Lay. Meteorol. 25th Anniversary Volume, 1970-1995, pp. 351–382, Springer, 1996.

Redon, E. C., Lemonsu, A., Masson, V., Morille, B., and Musy, M.: Implementation of street trees within the solar radiative exchange parameterization of TEB in SURFEX v8. 0, Geosci. Model Dev., 10, 385–411, 2017.

Resler, J., Krč, P., Belda, M., Juruš, P., Benešová, N., Lopata, J., Vlček, O., Damašková, D., Eben, K., Derbek, P., Maronga, B., and Kanani-Sühring, F.: PALM-USM v1. 0: A new urban surface model integrated into the PALM large-eddy simulation model, Geosci. Model Dev., 10, 3635–3659, 2017.

Rizwan, A. M., Dennis, L. Y., and Chunho, L.: A review on the generation, determination and mitigation of Urban Heat Island, J. Environ. Sci., 20, 120–128, 2008.

Rotach, M. W., Vogt, R., Bernhofer, C., Batchvarova, E., Christen, A., Clappier, A., Feddersen, B., Gryning, S. E., Martucci, G., Mayer, H., Mitev, V., Oke, T. R., Parlow, E., Richner, H., Roth, M., Roulet, Y. A., Ruffieux, D., Salmond, J. A., Schatzmann, M., and Voogt, J. A.: BUBBLE–an Urban boundary layer meteorology project, Theor. Appl. Climatol., 81, 231–261, 2005.

Roth, M.: Review of atmospheric turbulence over cities, Q. J. R. Meteorol. Soc., 126, 941–990, 2000.

Roth, M., Inagaki, A., Sugawara, H., and Kanda, M.: Small-scale spatial variability of turbulence statistics,(co) spectra and turbulent kinetic energy measured over a regular array of cube roughness, Environ. Fluid Mech., 15, 329–348, 2015.

Runnalls, K. E.: Temporal dynamics of Vancouver's urban heat island, Ph.D. thesis, University of British Columbia, 1995.

Ryu, Y.-H., Baik, J.-J., and Lee, S.-H.: A New Single-Layer Urban Canopy Model for Use in Mesoscale Atmospheric Models, J. Appl. Meteorol. Clim., 50, 1773–1794, 2011.

Salamanca, F., Krpo, A., Martilli, A., and Clappier, A.: A new building energy model coupled with an urban canopy parameterization for urban climate simulations—part I. formulation, verification, and sensitivity analysis of the model, Theor. Appl. Climatol., 99, 331–344, 2010.

Salamanca, F., Georgescu, M., Mahalov, A., Moustaoui, M., and Wang, M.: Anthropogenic heating of the urban environment due to air conditioning, J. Geophys. Res.-Atmos., 119, 5949–5965, 2014.

Salizzoni, P., Marro, M., Soulhac, L., Grosjean, N., and Perkins, R. J.: Turbulent Transfer Between Street Canyons and the Overlying Atmospheric Boundary Layer, Bound.-Lay. Meteorol., 141, 393–414, 2011.

Saneinejad, S., Moonen, P., Defraeye, T., Derome, D., and Carmeliet, J.: Coupled CFD, radiation and porous media transport model for evaluating evaporative cooling in an urban environment, J. Wind. Eng. Ind. Aerodyn., 104, 455–463, 2012.

Santamouris, M., Papanikolaou, N., Livada, I., Koronakis, I., Georgakis, C., Argiriou, A., and Assimakopoulos, D.: On the impact of urban climate on the energy consumption of buildings, Solar energy, 70, 201–216, 2001.

Santiago, J. L. and Martilli, A.: A Dynamic Urban Canopy Parameterization for Mesoscale Models Based on Computational Fluid Dynamics Reynolds-Averaged Navier-Stokes Microscale Simulations, Bound.-Lay. Meteorol., 137, 417–439, 2010.

Santiago, J. L., Krayenhoff, E. S., and Martilli, A.: Flow simulations for simplified urban configurations with microscale distributions of surface thermal forcing, Urban Climate, 9, 115–133, 2014.

Schoetter, R., Masson, V., Bourgeois, A., Pellegrino, M., and Lévy, J.-P.: Parametrisation of the variety of human behaviour related to building energy consumption in the Town Energy Balance (SURFEX-TEB v. 8.2), Geosci. Model Dev., 10, 2801–2831, 2017.

Simón-Moral, A., Santiago, J. L., and Martilli, A.: Effects of Unstable Thermal Stratification on Vertical Fluxes of Heat and Momentum in Urban Areas, Bound.-Lay. Meteorol., 163, 103–121, 2017.

Siu, L. W. and Hart, M. A.: Quantifying urban heat island intensity in Hong Kong SAR, China, Environ. Monit. Assess., 185, 4383–4398, 2013.

Souch, C. and Souch, C.: The effect of trees on summertime below canopy urban climates: a case study Bloomington, Indiana, J. Arboriculture, 19, 303–312, 1993.

Soulhac, L., Salizzoni, P., Cierco, F.-X., and Perkins, R.: The model SIRANE for atmospheric urban pollutant dispersion; part I, presentation of the model, Atmos. Environ., 45, 7379–7395, 2011.

Stull, R.: Practical meteorology: an algebra based survey of atmospheric science, BC Campus, 2016.

Stull, R. B.: An Introduction to Boundary Layer Meteorology, Kluwer Academic Publishers, Dordrecht, The Netherlands, 1988.

Sun, J.: Vertical variations of mixing lengths under neutral and stable conditions during CASES-99, J. Appl. Meteorol. Clim., 50, 2030–2041, 2011.

Sun, J., Lenschow, D. H., LeMone, M. A., and Mahrt, L.: The role of large-coherent-eddy transport in the atmospheric surface layer based on CASES-99 observations, Bound.-Lay. Meteorol., 160, 83–111, 2016.

Talbot, C., Bou-Zeid, E., and Smith, J.: Nested mesoscale large-eddy simulations with WRF: performance in real test cases, J. Hydrometeorol., 13, 1421–1441, 2012.

Tseng, Y.-H., Meneveau, C., and Parlange, M. B.: Modeling flow around bluff bodies and predicting urban dispersion using large eddy simulation, Environ. Sci. Technol., 40, 2653–2662, 2006.

van der Kooi, C. J., Kevan, P. G., and Koski, M. H.: The thermal ecology of flowers, Ann. Bot-London, 124, 343–353, 2019.

Wang, C., Myint, S., Wang, Z., and Song, J.: Spatio-temporal modeling of the urban heat island in the Phoenix metropolitan area: Land use change implications, Remote Sensing, 8, 185, 2016.

Wang, H., Skamarock, W. C., and Feingold, G.: Evaluation of Scalar Advection Schemes in the Advanced Research WRF Model Using Large-Eddy Simulations of Aerosol-Cloud Interactions, Mon. Weather Rev., 137, 2547–2558, 2009.

WMO: Aircraft Meteorological Data Relay (AMDAR) Reference Manual, Secretariat of the World Meteorological Organization, 2003.

Wong, M. S., Nichol, J. E., To, P. H., and Wang, J.: A simple method for designation of urban ventilation corridors and its application to urban heat island analysis, Build. Environ., 45, 1880–1889, 2010.

Yaghoobian, N. and Kleissl, J.: Effect of reflective pavements on building energy use, Urban Climate, 2, 25–42, 2012.

Yang, J. and Bou-Zeid, E.: Should Cities Embrace Their Heat Islands as Shields from Extreme Cold?, J. Appl. Meteorol. Clim., 57, 1309–1320, 2018.

Yang, X. and Li, Y.: The impact of building density and building height heterogeneity on average urban albedo and street surface temperature, Build. Environ., 90, 146–156, 2015.

Yang, X., Li, Y., Luo, Z., and Chan, P. W.: The urban cool island phenomenon in a high-rise high-density city and its mechanisms, Int. J. Climatol., 37, 890–904, 2017.

Yuan, C., Norford, L. K., and Ng, E.: A semi-empirical model for the effect of trees on the urban wind environment, Landscape Urban Plan., 168, 84–93, 2017.

Zajic, D., Fernando, H. J. S., Calhoun, R., Princevac, M., Brown, M. J., and Pardyjak, E. R.: Flow and Turbulence in an Urban Canyon, J. Appl. Meteorol. Clim., 50, 203–223, 2011.

Zhang, Y., Li, D., Lin, Z., Santanello Jr, J. A., and Gao, Z.: Development and Evaluation of a Long-Term Data Record of Planetary Boundary Layer Profiles From Aircraft Meteorological Reports, Journal of Geophysical Research: Atmospheres, 124, 2008–2030, 2019.